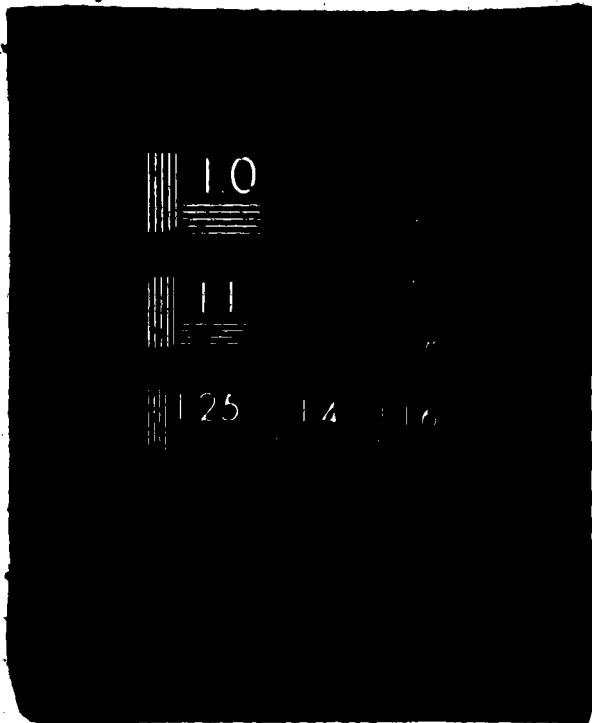


1 OF 2

N77 30474

UNCLAS



(NASA-CR-153411) BALL TO SEPARATOR CONTACT
FORCES IN ANGULAR CONTACT BALL BEARINGS
UNDER THRUST AND RADIAL LOADS Status Report
(California State Univ., Northridge.) 110 p
HC AC6/MF A01

N77-30474

CSCL 13I G3/37

Unclassified
42008

**Study of Rolling Element Dynamic Interactions
With Separators and Raceway Paths**

**Ball to Separator Contact Forces
in
Angular Contact Ball Bearings Under Thrust and Radial Loads**

**California State University, Northridge
School of Engineering and Computer Science
Northridge, California 91330**

Prepared by Lester J. Nypan

July 30, 1977

**Status Report NSG 3065
Prepared for NASA Lewis Research Center
Cleveland, Ohio 44135**

Table of Contents

	Page
I Abstract	1
II Introduction	2
III Separator Study Machine	3
IV Test Bearings	6
V Separator Force Transducer	6
VI Force Transducer Calibration	8
VII Experimental Procedure	8
VIII Data Analysis	9
IX Results and Discussion	12
X Conclusion	17
XI References	19
Appendix I Computer Program	103

List of Figures

Figure	Page
1 Separator Study Machine	19
2 Test Bearing in Separator Study Machine	22
3 Ball Contact Force Transducer	23
4 Sample Force Transducer Calibration	24
5 Example of Photographs Taken	25
6 Ball Contact Forces at 4000 rpm	26
7 Ball Contact Forces at 8000 rpm	44
8 Ball Contact Forces at 12000 rpm	65
9 Variation of Magnitude of Cage Forces with Speed-Radial Loads	74
10 Variation of Location of Cage Forces with Speed-Radial Loads	78
11 Variation of Magnitude of Cage Forces w/ Speed-Thrust Loads	83
12 Cage to Inner Race Land Contact Force	86
13 Cage to Inner Race Land Clearance Variation with Location	88
14 Cage to Shaft Speed Ratios	93

List of Tables

Table		Page
1	Test Bearing Specifications	99
2	Speed, Load and Spring Constants	100
3	Spring Constants and Bearings Used	101
4	Calculated Number of Shaft Revolutions Between Photographs	102

Abstract

Experimental data is reported on ball to cage contact forces in a 110 mm bore ball bearing operating at speeds to 12000 rpm under radial and thrust loads. Information is also reported on cage to inner race land contact force, cage to inner race land clearance, and cage to shaft speed ratios.

II Introduction

Current developments in jet engine technology are placing more stringent demands on gas turbine design. There is a constantly increasing requirement for engines to develop greater thrust outputs. In addition to this increased loading the need to raise the thrust/weight ratio of engines and to improve the fuel consumption has led to higher rotor speeds and operating temperatures, lighter components and correspondingly increased structural flexibility. In anticipation of tomorrow's requirements, further advanced knowledge of engine component technology must be obtained.(1)*

In the case of rolling contact bearings there is a need for a better understanding of cage and rolling element dynamics, particularly in ultra-high speed applications.(2,3,4,5)

Recently developed, advanced bearing theories have resulted in computerized optimization of rolling element bearing designs and in some cases accurate prediction of bearing performance. These developments and advances by no means substitute for testing of rolling element bearings which for many years was the basis for bearing development. To the contrary, the need for more refined data gathering methods has become obvious. Tests are needed to verify the theories which form the foundation of these computer programs. Also, performance tests and studies will always be needed to refine bearing designs for critical applications.

The interaction between the rolling elements of a bearing with the raceways and separators is particularly difficult to measure due

*Numbers in parentheses designate references at end of report.

to the rapidity of their motion. The kinematic behavior and the resulting forces acting on a rolling element/separator/raceway assembly could in the past be measured only by tests where the operating conditions were drastically simplified.

III Separator Study Machine

An optical bearing test rig has been constructed to operate the bearing and make photographic records of the rolling elements and separator behavior. Figure 1a shows an overall view of the machine as it is presently installed in the Dynamics Laboratory of the Engineering Building at California State University, Northridge. The machine was originally assembled by Industrial Tectonics, Inc., Compton, Calif., and has been used in industrial bearing research, and in a ball motion study reported in (6).

The bearing test rig is basically a shaft supported by a pair of preloaded ball bearings at one end and the test bearing at the other end. One face of the test bearing is exposed to allow free view of the balls and the separator. Radial load was applied to the test bearing by a hydraulic actuator through a cable loop over the bearing housing. The shaft was driven by a 75 hp hydraulic motor through a geared belt drive, giving speeds infinitely variable from 100 to 15,000 rpm. Figure 1b is a schematic of the shaft assembly.

Lubricating oil for under race cooling and test bearing lubrication is supplied through a series of orifices from the rear of the test bearing.

Due to the high tangential velocities present when a bearing is rotated at shaft speeds up to 15,000 rpm, conventional photograph techniques are inadequate. The difficulty lies in obtaining photo-

graphs having sufficient resolution for analysis when very short exposures are required to freeze the motion of the bearing elements. This problem has been overcome by eliminating the gross rotational motion using a derotation prism. The resulting image thus presents the differential motion between the separator and the rolling element, enabling observation and photographs to be made of an individual separator pocket. Derotation is accomplished by synchronizing the rotation of a Pechan prism at half-speed with the rotation of the ball separator, thus causing the apparent image rotation and the true separator rotation to coincide. This results in the derotated image of the area of interest being imaged on the film plane of a camera. Light rays from the illuminated bearing are collected through the front window of the instrument. This window is optically coated to reject ultraviolet energy produced by ultraviolet lamps, serving the circuit for the prism speed control. From the window, the rays travel through collimator lenses and the Pechan prism before they travel through the exit lenses. Their path is then deflected by mirrors which fold the image in different directions. Figure 1c shows light paths through the scanner.

One light trace travels to a beam splitter where approximately 15 % of the light is reflected to the eyepiece optics to provide an image observable to the operator. The balance of light enters the aperture of the pulse camera.

Alignment and positioning of the optical elements ensure that the eyepiece observes the same image quality and format as that which the film sees.

Another image is folded and demagnified in the transfer lens assembly before it enters the camera.

A derotated image of the luminous painted segment of the test bearing separator is optically folded out and directed toward an

image splitting mirror surface wedge which proportions the light entering two photomultiplier tube photocathodes. The electronic signals from these tubes are used by the tracking system to control the prism speed.

A tracking system holds the image of a selected point at the test bearing separator in the field of view. It will accommodate a variation of up to 10% of a fixed ratio of separator-to-shaft speed without loss of the ability to lock onto the proper position within one revolution of the bearing retainer.

It is necessary to sense the tracking error in angular position of the derotation prism to provide an input for the servo system. This error signal is provided in the form of the difference in output of two multiplier phototubes.

A sector on the bearing retainer is coated with fluorescent paint and illuminated with ultraviolet light. An image of the sector of arc is formed in a plane containing the apex of a mirror surface wedge. The light striking the two surfaces of the wedge is reflected and illuminates the photocathode of the photomultiplier tubes. Rotation of the prism results in a displacement of the image and a consequent increase in the output of one tube and decrease in the output of the other.

Electronic filtering is provided to discriminate between the steady signal due to the ultraviolet excitation of the phosphor and any intermittent excitation due to strobe lamps to reduce any interaction between the level of light striking the phosphor and the error signal produced by the photomultipliers.

Four Chadwick-Helmuth Strobex lamps are flashed at the 16-frames-per-second camera rate to illuminate the separator and to stop the images of the protractors on the inner and outer races of the bearing so that angular position information is recorded on the photographs.

Four mercury vapor spot lamps with ultraviolet filters illuminate the fluorescent patch for the tracking system.

The camera used was a Neyhard Enterprises model G-4. The camera film magazine accepts 100 or 200 foot reels of 35 mm film. The camera has a data box, the image of which is projected onto each film frame.

IV Test Bearings

The bearings used in the ball to separator contact force investigation were mainshaft thrust bearings used in the Pratt and Whitney TF 30 gas turbine engine, part numbers PWA 506110 and PWA 506111. Dimensions and other characteristics of these bearings are given in Table 1.

V Separator Force Transducer

A ball contact force transducer was constructed on the bearing separator by introducing a cantilever beam between two of the bearing balls. The cantilever beam replaced a rigid separating element so that cantilever beam deflection would give an indication of the ball contact force. A hole was drilled through one of the side rails of the separator to hold the fixed end of the cantilever beam. A notch to frame the deflected end of the cantilever was cut in the other side rail opposite the hole. Various beam cross sections were used depending on contact forces and deflections encountered. A Teflon

rubbing block was cemented to the center portion of the beam to make up the normal ball spacing dimension of the rigid separator element replaced by the ball force indicating beam. A duplicate modification was installed at 180° to the first to maintain separator balance.

With the shaft and test bearing operating at a speed and load condition to be investigated, the derotation prism was synchronized with the separator to produce a stationary image of the deflecting end of the cantilever beam as the balls and separator repeatedly moved through loaded and unloaded regions of the bearing. The 16 frame per second 35 mm instrumentation camera photographed the motions of the cantilever beam deflections relative to the notch in the separator. As ball contact forces may be expected to be a repetitive event from revolution to revolution the relatively slow framing rate can be extended to a very high effective framing rate by taking a large number of photographs over many revolutions of the bearing. This gives frames covering 0 to 360° to the applied load. The angle to the applied load was indicated by the position of the cantilever beam relative to a fixed protractor on the bearing outer race. Radial loads were applied vertically at the 360 (0) degree mark on the protractor. Static photographs with the cantilever beam at 90, 180, and 270 degrees to the vertical clearly indicated positive, zero, and negative deflections consistent with the weight of 19.05 mm (0.750 in) steel balls.

Figure 3 shows one of the ball contact force transducers as constructed.

VI Force Transducer Calibration

The force transducing cantilever beam was assembled into the separator with epoxy resin with the Teflon spacing element also epoxied in place. The separator was held in a small vise and loaded with a wire hook positioned at the estimated ball contact location. A small weight pan and 6.35 mm (0.250 in.) balls were used to load the cantilever beam. Cantilever deflections were photographed.

Figure 4 gives the force-deflection relation for the stiffest cantilever beam used (61.8 N/mm). The permanent deformation evident in Fig. 4 did not affect ball force measurements as forces encountered did not exceed 27.5 N (6.2lb.). Table 3 gives values of spring constant and bearings used in the course of investigation.

VII Experimental Procedure

The lubricating oil used throughout the tests was a 5-centistoke neopentyl polyol (tetra) ester. This is a type II oil which conforms to specification MIL-L-23699. Test bearing inlet oil was heated and controlled to 485° K ($150 \pm 2^{\circ}$ F).

The Separator Study Machine bearing rig was started with a 500 lb thrust load and brought up to speed, the desired load condition applied, the prism synchronized with the separator and 100 to 200 photographs taken. Film used was Kodak 2475 Recording Film. It was cut into lengths fitting stainless steel reels and developed in a small tank with HC 110 developer, dilution A, for 30 minutes at laboratory room temperature. This seemed to give images of adequate contrast, with background fog just beginning to be noticeable on fresh film.

VIII Data Analysis

After chemical processing of the film was completed the film was respliced and each frame was numbered.

The film was read with a Benson-Lechner model N-2 film reader capable of indicating 4 digits with the least digit representing 0.005 mm (0.0002 in.) in the film image. The film images, however, varied in density and sharpness from frame to frame due to variation in Xeno flash intensity, duration, and jitter in flash initiation among the four Xenon flash tubes, as well as from oil splash in the bearing chamber and on the bearing chamber window.

Readings were taken by aligning a cross-hair onto the lowest edge of the notch for R1, the bottom of the beam end for R2, the top of the beam end for R3, and the top of the notch for R4. The computer program listed in Appendix I was used to calculate differences R2-R1, R3-R1, R4-R1, R3-R2, R4-R3, and R4-R2. From R4-R1 and R3-R2 a consistency check was available to pull out or correct obviously defective readings as the notch dimension and beam height should always be of constant value. After subtraction of undeflected (zero) readings, the other four differences give four separate indications of the beam deflection in that film frame.

The computer program also calculated average values of notch size for the photo set and normalized the deflection indications on the average notch size to compensate for image size variation with focus setting. It then scales the deflections to the lineal measured notch dimension. The deflection indications are then multiplied by the spring constant determined in the force transducer calibration, and are listed and plotted by a Calcomp plotter.

Figure 5 is representative of photographs obtained.

It was possible to determine cage to shaft speed ratio with some accuracy over 10 successive photographs of multiple shaft revolutions from the following considerations.

The derotating prism is synchronized to rotate at half the separator speed thus producing a stationary image of the separator to be photographed. Protractors which are mounted on the stationary outer race and on the rotating inner race are visible in the photographs. Four Xenon flash tubes with a flash duration of 50 microseconds permit clear instantaneous photographs of the stationary separator and stop the motion of the protractor images. Typically 100 to 200 photographs were taken at a cine frame rate of 16 per second for each case investigated.

In these photographs the angle turned through by the separator (cage) can be determined from the difference in angle on the stationary outer race protractor between two consecutive frames. Thus,

$$2\Delta\theta_p = \Delta\theta_c = \Delta\theta_o = \left(\frac{W_c}{W_s}\right) W_s \Delta t \quad (1)$$

where:

$\Delta\theta_p$ = true prism angle turned through

$\Delta\theta_c$ = true cage angle turned through

$\Delta\theta_o$ = angle difference $+360^\circ$ x number of revolutions
between photographs

$\frac{W_c}{W_s}$ = separator to shaft speed ratio in the operating bearing

W_s = shaft speed

Δt = time between photographs

The protractors are engraved with angle increasing in the direction of shaft rotation. The shaft turns through a greater angle than does the separator; consequently, the cage photographs centered on the transducer in the cage show the inner race angles decreasing. The

true angle that the shaft has turned through in the 1/16 second between successive frames may be determined from the protractor angles photographed by

$$\Delta\theta_s = \Delta\theta_o - \Delta\theta_{st} = \left(\frac{W_c}{W_s}\right) W_s \Delta t - W_s \Delta t \quad (2)$$

where:

$\Delta\theta_s$ = angle difference on inner race protractor between photographs

$(\theta_{s_{i+1}} - \theta_{s_i}$ with i being the frame number)

$\Delta\theta_{st}$ = true angle turned through by the shaft in time Δt

From equation 2, then $\Delta\theta_{st} = \Delta\theta_o - \Delta\theta_s$, and $W_c \Delta t = \Delta\theta_o$,

$W_s \Delta t = \Delta\theta_{st}$ so:

$$\frac{W_c}{W_s} = \frac{\Delta\theta_o}{\Delta\theta_o - \Delta\theta_s} \quad (3)$$

where $\Delta\theta_s$ is a negative number.

Care must be taken in calculating angle differences $\Delta\theta_o$ and $\Delta\theta_s$ between photographs and in using equation (3). Multiple revolutions of shaft and separator occur without this being apparent in the photographs. At 16 frames per second with a nominal value of 0.441 for W_c/W_s the ranges of angle differences given in Table 4 may be anticipated.

To obtain the true angle of rotation of the cage between successive frames, it is necessary to:

1. Subtract the angle read from the reference point of the separator in the photograph from that read in the i-1 frame.
2. Determine the number of full rotations between frames using Table 4.
3. Add the number of full rotations to the difference found in step 1.

These considerations led to the cage/shaft speed ratios that appear on the cage force figure captions and in the cage/shaft speed ratio versus load figures.

IX Results and Discussion

This investigation was undertaken to experimentally evaluate ball to cage contact forces. It was subsequently noted that information on cage to inner race land contact force, cage to inner race land operating clearance, and cage to shaft speed ratios could also be extracted from the data obtained.

A. Ball to Cage Contact Forces

The principal results of this investigation are the ball to cage contact forces shown in Figures 6-8. These show the ball force on the cage as a function of ball location in the bearing. Ball location is measured clockwise from the centerline of the radial load at 0° (360°). Table 2 summarizes the shaft speeds, loads, spring constants, figure identification system, and loads used in the investigation.

Different spring constants were necessary as the investigation progressed from 1000 to 4000 rpm and to higher speeds. Larger forces were

encountered and cantilever deflections approaching the ball to cage pocket clearance were observed.

Data was obtained at 1000 rpm with a spring constant of 1.49 N/mm (8.51 lb/in). These forces were small and of similar nature to those at higher speeds. The 1000 rpm results are not presented as they are too small to be visible on the scales used to present the higher speed results. Centrifugal force at 12000 rpm deflected the 17.2 N/mm (98.2 lb/in) beam out to contact the cage so that friction limited the motion of the cantilever.

All the data at 12000 rpm was taken with the 61.8 N/mm (353 lb/in) spring constant cantilever. Some lower speed cases were also run with the larger spring constant cantilevers.

Positive forces in the figures are those exerted by balls tending to accelerate the cage. Negative forces are those exerted by balls tending to retard or decelerate the cage. In general the stiffer cantilever beam deflecting elements indicate greater forces, with more scatter in the film readings.

The force indicated by a cantilever deflection is created by a ball advancing into the cantilever located on the cage. A ball's advance relative to the cage, which moves with average ball speed, is determined by ball kinematics such as ball location on the raceway path, deflections, etc. The motion of the ball relative to the average ball will deflect the cantilever until the ball begins to recede from the cantilever due to ball kinematics, provided limiting traction forces are not exceeded. Thus the cantilever is deflected as much as necessary to accomodate the ball advance relative to the cage. For a given ball advance, the stiffer cantilever's deflection indicates larger force. The stiffer cantilever deflecting elements will also have smaller deflections. Errors in measuring their deflection will produce

larger variation in the force measurements. All of the variation in the figures may not be due to errors in cantilever deflection. It is possible that there is some variation in the balls' motion as they traverse various portions of raceway surfaces with possible cage motions of oscillation, rocking and impacting on balls and inner race land surfaces.

Figures 9 and 10 summarize the variation of magnitude and location of cage forces with speed for radially loaded bearings. Figure 11 summarizes the variation of magnitude of cage forces with speed for thrust loaded bearings. As might be expected the equally loaded balls in thrust loaded cases do not show much variation in cage force with ball location within the bearing.

The approximately 1 lb. negative force in pure thrust loaded cases indicates the balls are decelerating (retarding) the cage uniformly. This is consistent with the cage being driven by the higher speed shaft surface on which the cage is guided.

Centrifugal force moves the tip of the cantilever beam out by a noticeable amount in photographs taken at 12000 rpm. It is felt that the radial centrifugal deflections do not affect the deflection characteristics of the beam in the tangential direction. It was reasoned that the portion of the beam that is bent by the ball is only that part extending from a fixed end in one rail of the cage to the center of the ball pocket where contact with the ball takes place. The larger portion of the beam extends from the center of the ball pocket and through the other rail of the cage. It is acting as a straight pointer to magnify the deflection at the center of the cage pocket. Over the part of the beam stressed in bending the radial deflection is small compared to beam dimensions.

B. Cage to Inner Race Land Contact Force

From the data of Figures 6, 7, and 8 it was possible to derive the force between the cage and its guiding contact with the inner race land. This was obtained by taking horizontal and vertical components of each force point as plotted in Figures 6, 7, and 8. Adding vertical and horizontal forces in an 18 degree sector, and dividing by the number of forces in the sector gave the average force one of the 20 balls would exert on the cage. The sum of the 20 ball forces should equal the resultant force that the inner race must exert on the cage. The angular location of the resultant force was obtained by taking the arc tangent of the ratio of horizontal to vertical force components. Figure 12 summarizes the magnitude and direction of the cage to inner race land force due to ball contact forces for various speeds and loads. It should be noted that this did not include the 3.5N (0.78 lb) weight of the cage.

C. Cage to Inner Race Land Operating Clearance

Figure 13 shows the separation between the cage and the inner race as a function of location from the zero degree index on the stationary outer race protractor. What appears in Figure 13 to be cage to inner race contact may actually be a close approach or small clearance that was shadowed by the optical angle and projection of the inner race image onto the cage image in the film plane. It appears that cage motion is somewhat erratic in the 12000 rpm speed case. The thrust loaded condition indicated an almost constant cage to inner race clearance. A clearance was visible in every one of the photographs read for the thrust loaded case.

The location of the cage to shaft contact indicated in Fig. 13a seems to agree with that of Fig. 12g. Figure 13c likewise agrees with

Fig. 12b. Figure 13b, however, indicates cage to shaft contact somewhere between 45 and 190 degrees, possibly centered at 120 degrees much of the time, while the corresponding point in Fig. 12b was found to be located at 40 degrees. It would seem that there are uncertainties in the cage force measurements and their locations that are not always averaged away by the simple device of calculating an average force per ball and adding the 20 ball to cage forces vectorially to arrive at a cage to shaft resultant force.

D. Cage to Shaft Speed Ratios

Figure 14 shows the cage to shaft speed ratios calculated by the method described in Section VIII Data Analysis. It may be noted that data taken before January 12, 1977 (also identified by the spring constant of 4.7 N/mm) were taken with a PWA 506111 bearing while the balance of the data was taken with a PWA 506110 bearing. The different spring constants used may have influenced the cage motion through their effect on cage forces. It is also possible that internal bearing clearances changed due to changes in temperatures of bearing components. The bearings used were of split inner race construction with presumably some gothic arch to the inner race surfaces to prevent ball contact with radial oil passages between the races.

All data obtained fell between cage to shaft speed ratios of 0.465 and 0.433. There was a general trend for cage to shaft speed ratio to decrease with load. It would seem that the loads employed did not encourage skidding, and that the cage to shaft speed ratio variations observed were due to deflections of bearing components due to load and temperature.

X Conclusion

Ball to cage contact forces were evaluated experimentally. They appear to be greatest in radially loaded bearings operating at high speed, and are of the order of 25 N (5 lb) at the maximum. Resultant cage to inner race land forces vary in a similar manner with values up to 20 N (4 lb). Resultant force as used here is the vector sum around the bearing of the average forces on each ball, and is equal to the vector sum of cage to shaft normal and tangential force components. Cage to shaft speed ratios indicated that the load conditions employed did not encourage skidding.

XI References

1. Brown, P.F., "Bearings and Dampers for Advanced Jet Engines", Paper 700318 SAE National Air Transportation Meeting, New York, New York, April 20-23, 1970.
2. Gupta, P.K., Transient Ball Motion and Skid in Ball Bearings
3. Harris, T.A., "An Analytical Method to Predict Skidding in Thrust Loaded Angular Contact Ball Bearings", Journal of Lubrication Technology, Trans. ASME, Series F, Vol. 73, 1971, pp. 17-24.
4. Poplawski, J.V., "Slip and Cage Forces in A High Speed Roller Bearing", Journal of Lubrication Technology, Trans. ASME, Series F, Vol. 72, pp.
5. Walters, C.T., "The Dynamics of Ball Bearings", Journal of Lubrication Technology, Trans. ASME, Series F, Vol. 93, 1971, pp. 1-10.
6. Signer, H.R., "Experimental Ball Bearing Dynamics Study", NASA CR 1345 28, October 1973.

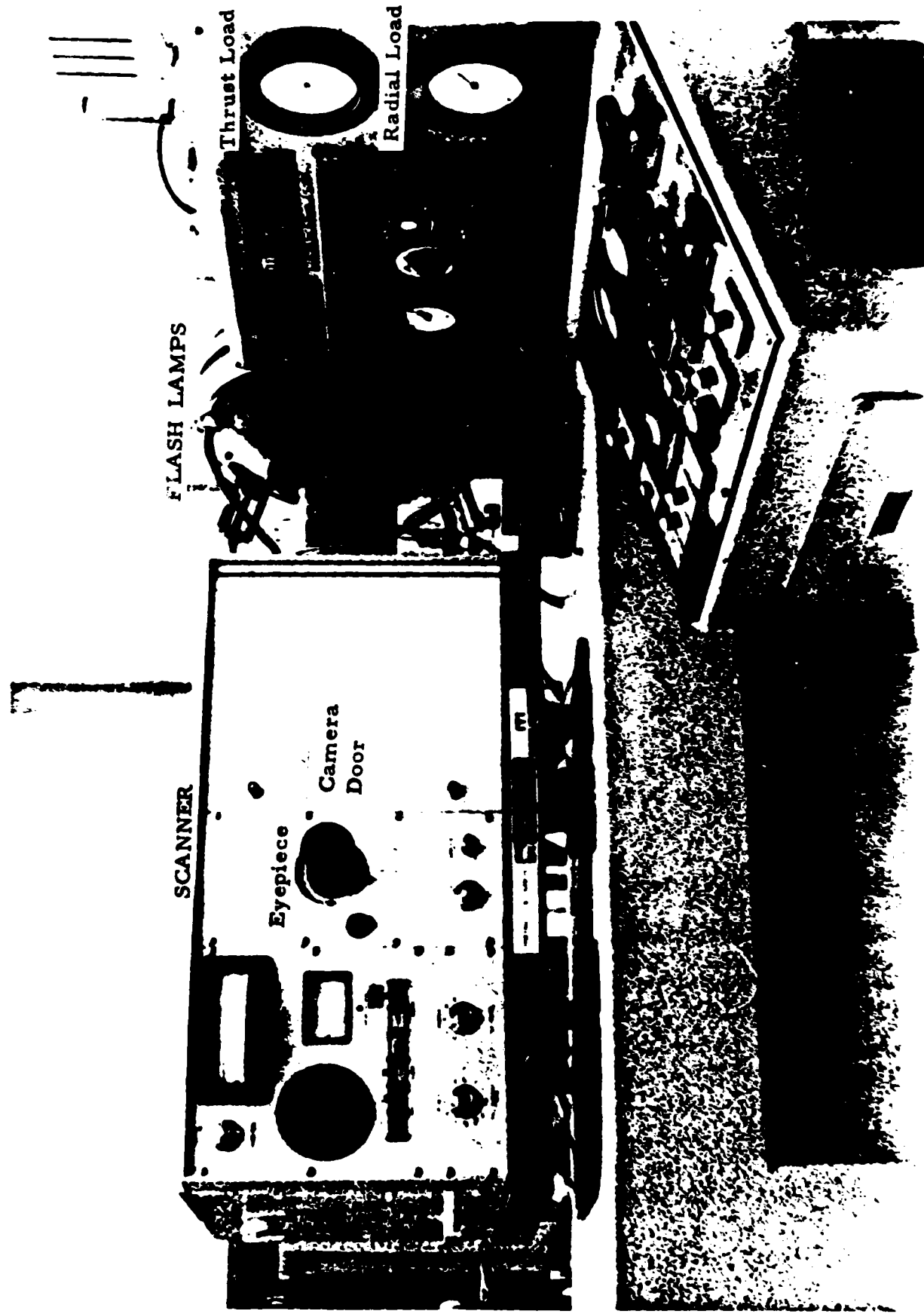


FIG. 1-A SEPARATOR
STUDY MACHINE

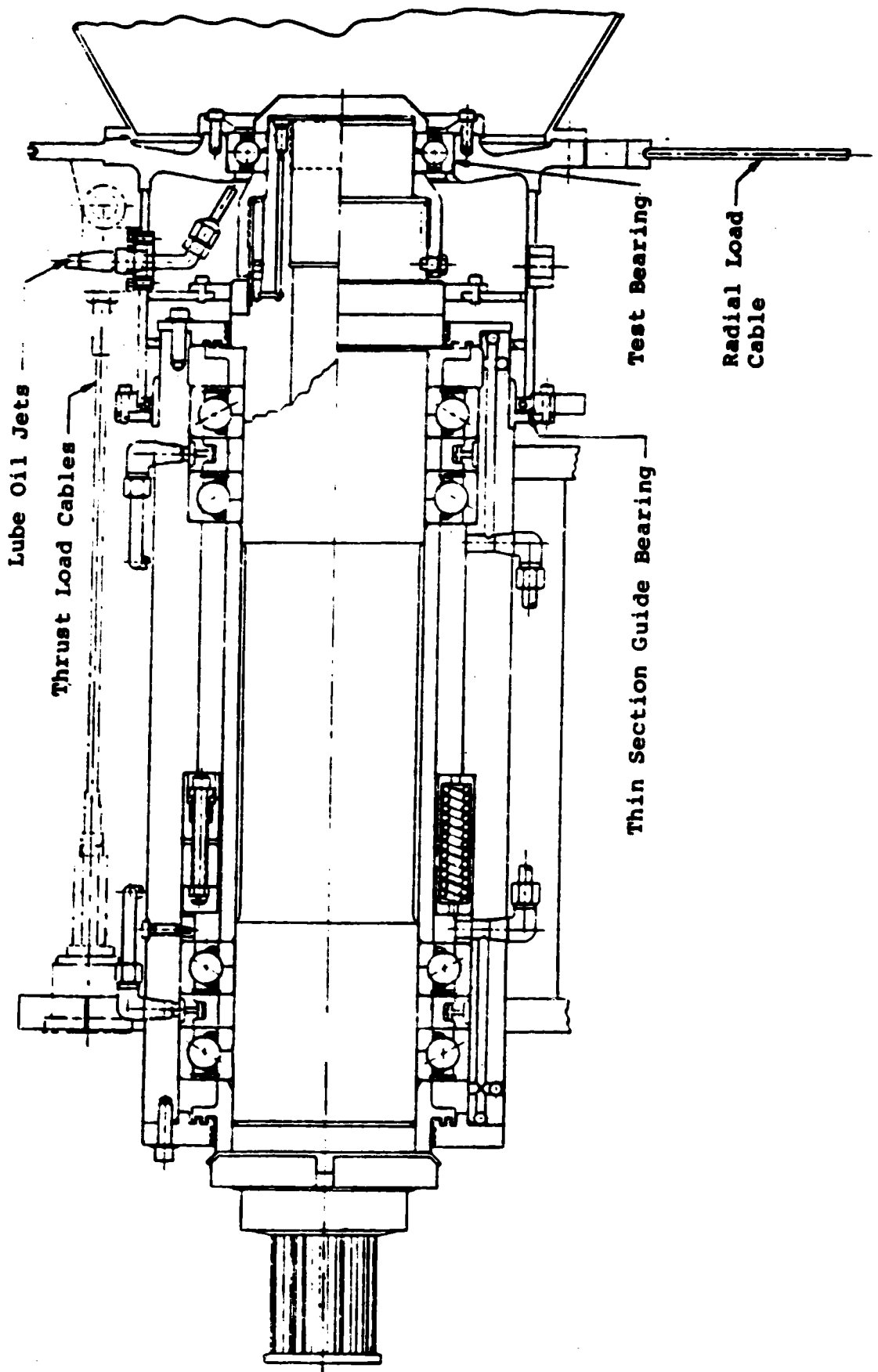


FIG. 1b SCHEMATIC OF SHAFT ASSEMBLY

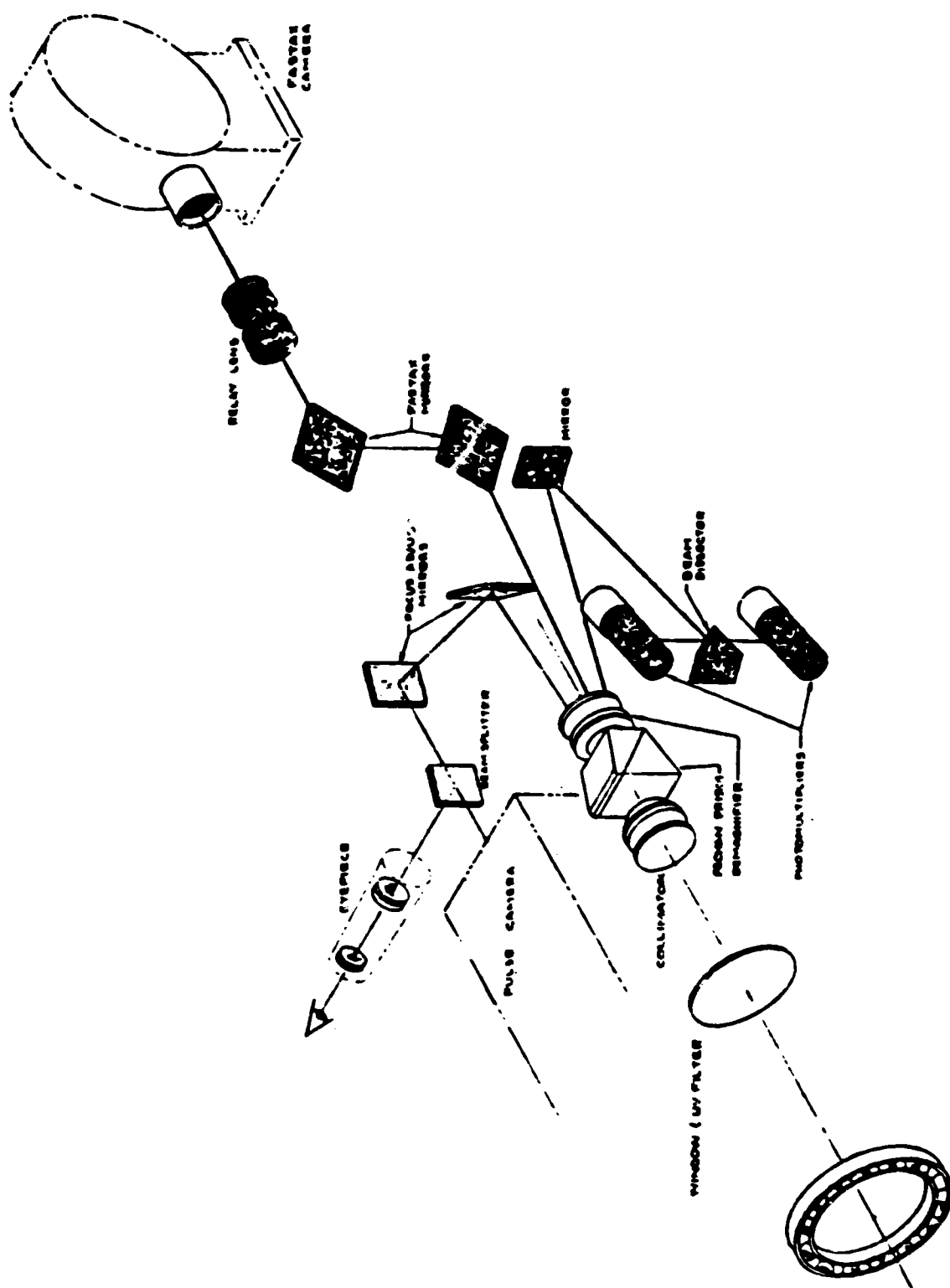


FIG. 1c OPTICAL PATHS THROUGH THE BEARING SCANNER

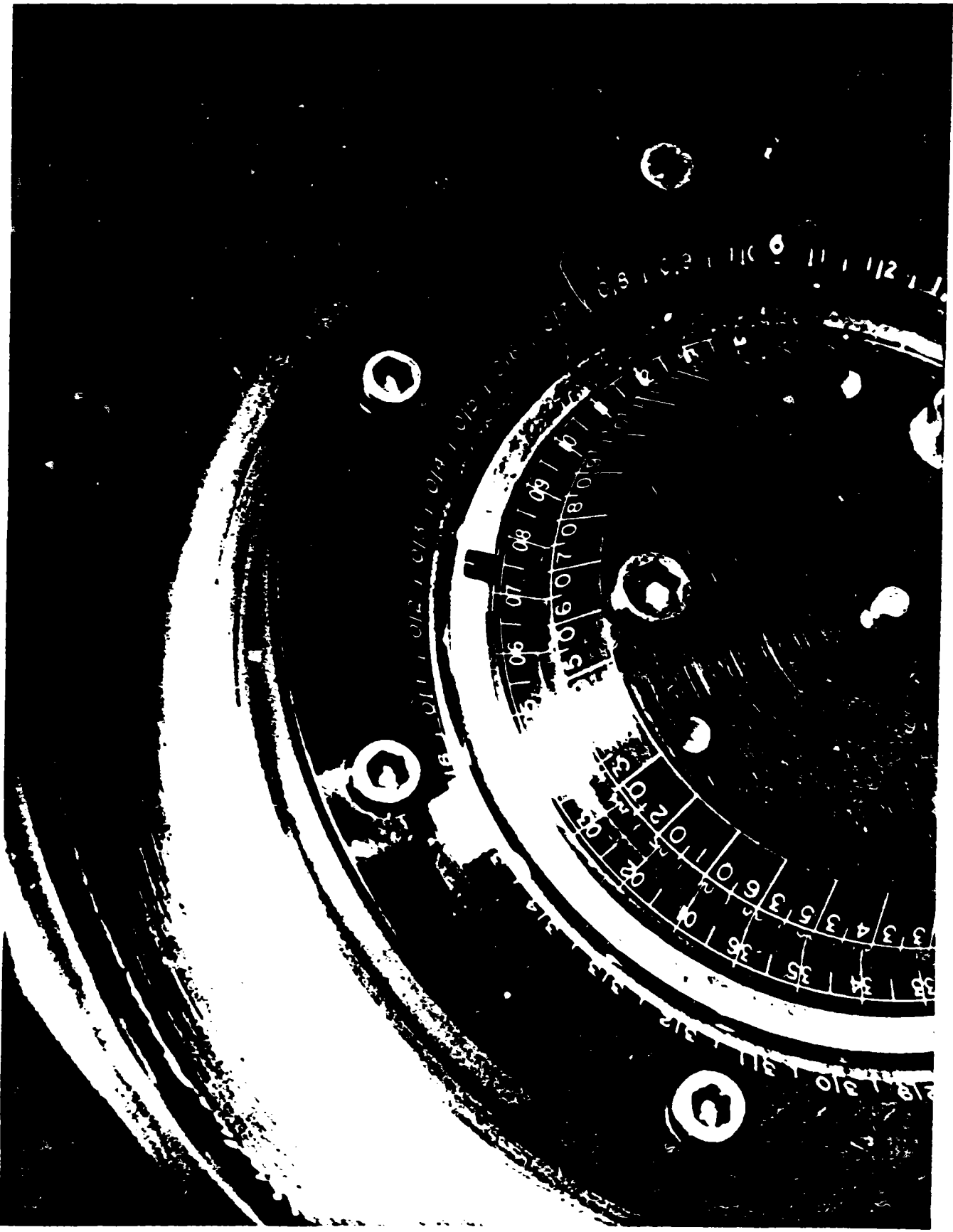


FIG. 2 TEST BEARING
IN SEPARATOR STUDY
MACHINE

THE QUALITY OF THE
IMAGE IS POOR



FIG. 3 BALL CONTACT
FORCE TRANSDUCER

GGG0119INIFAN 1 - 07/14/

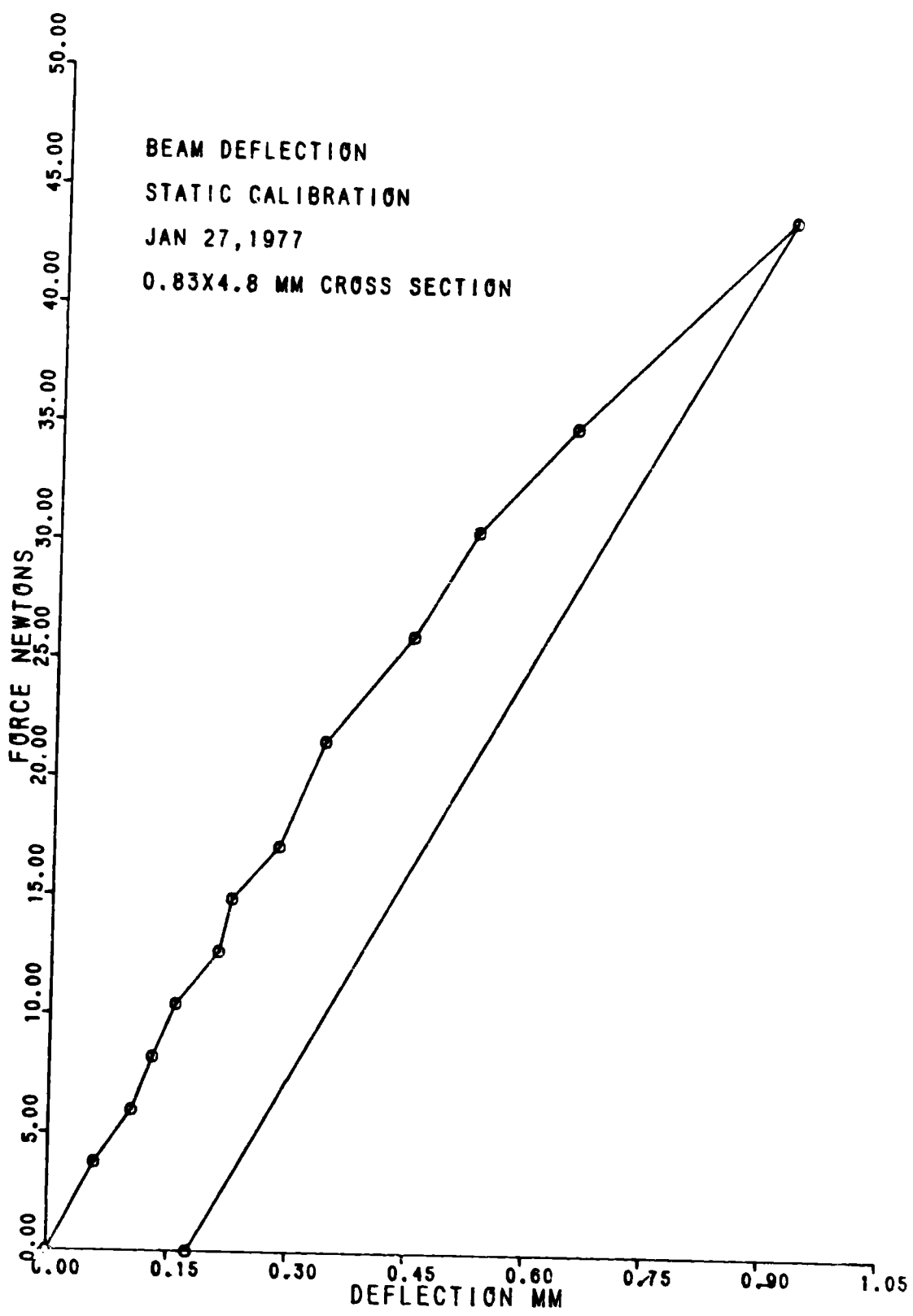


FIG. 4 SAMPLE FORCE
TRANSDUCER CALIBRATION
(61.8 N/mm BEAM)

REPRODUCIBILITY OF THE
ORIGINAL PAGE IS POOR

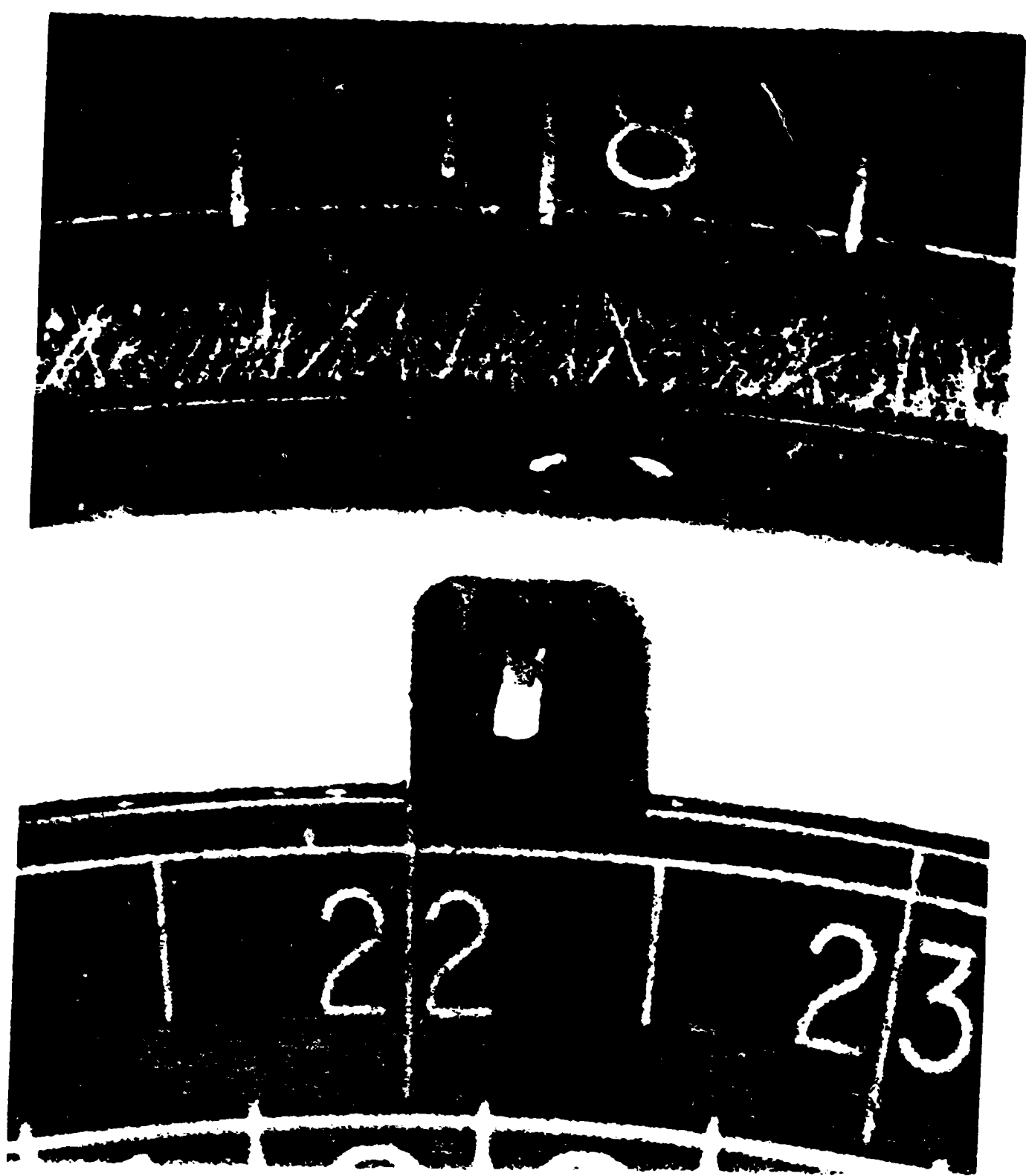


FIG. 5 EXAMPLE OF
PHOTOGRAPHS TAKEN

REPRODUCIBILITY OF THE
ORIGINAL PAGE IS POOR

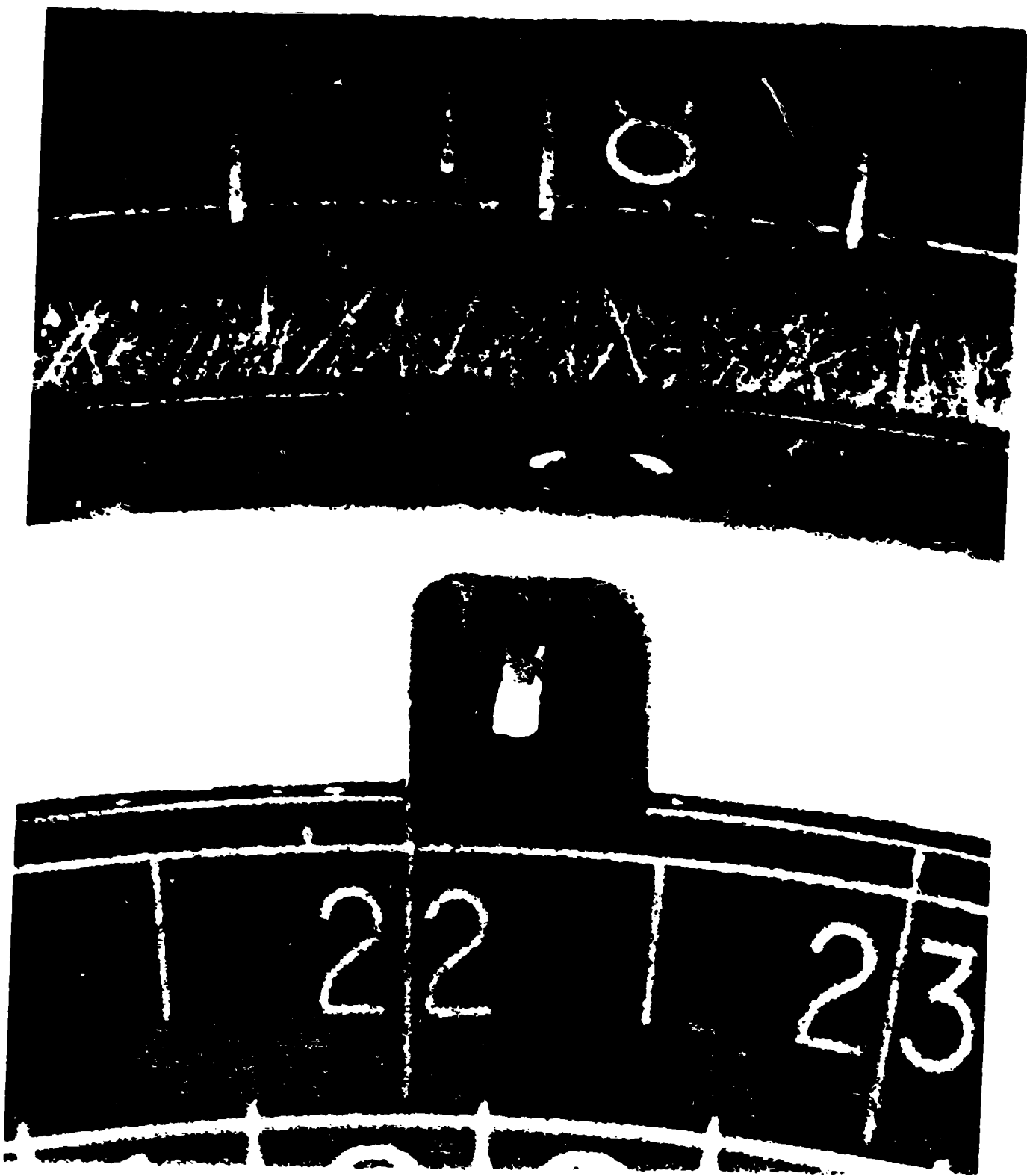


FIG. 5 EXAMPLE OF
PHOTOGRAPHS TAKEN

70011945-15/06/77

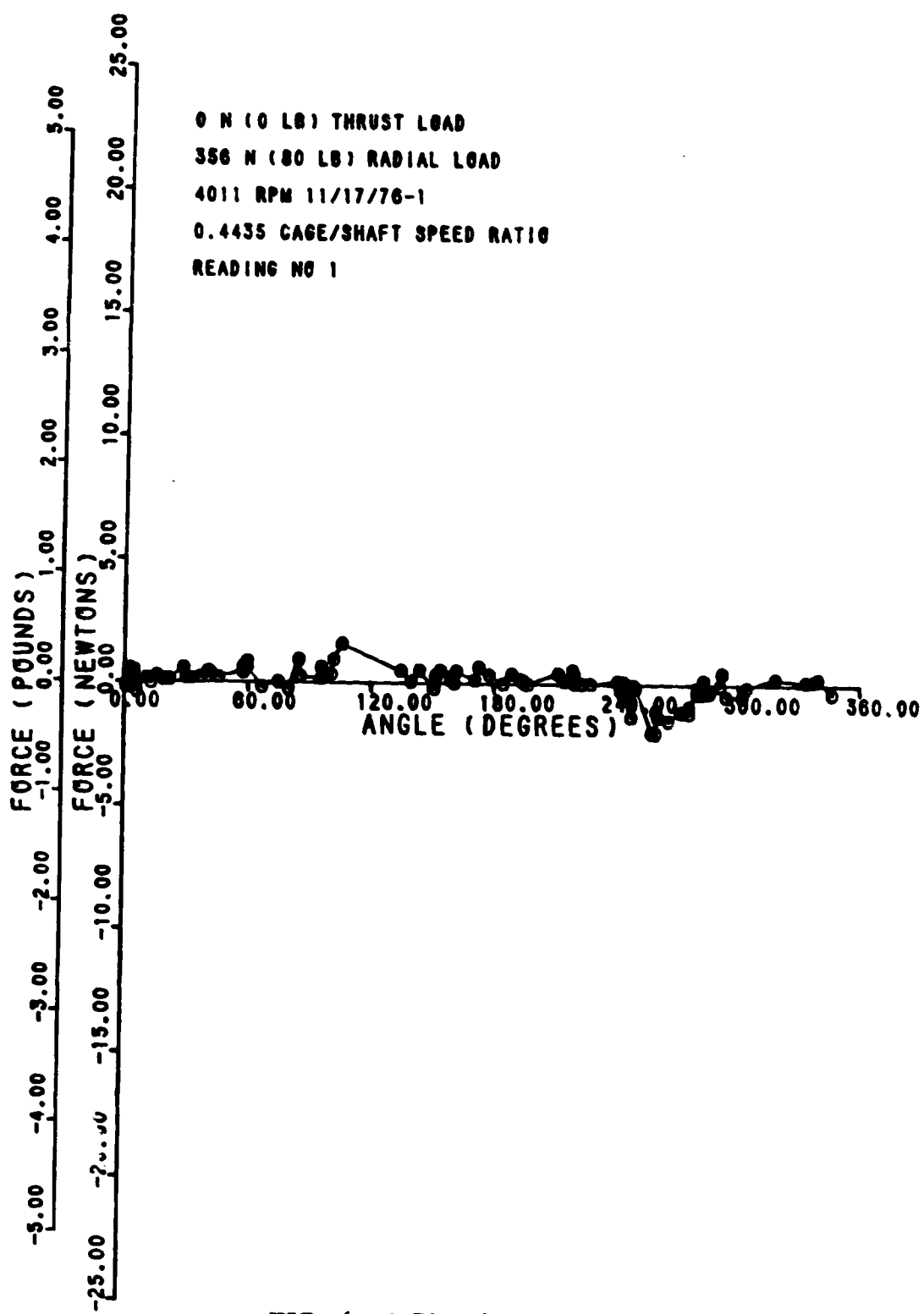


FIG. 6a-4. 73 N/mm

02/23/77

7009011090

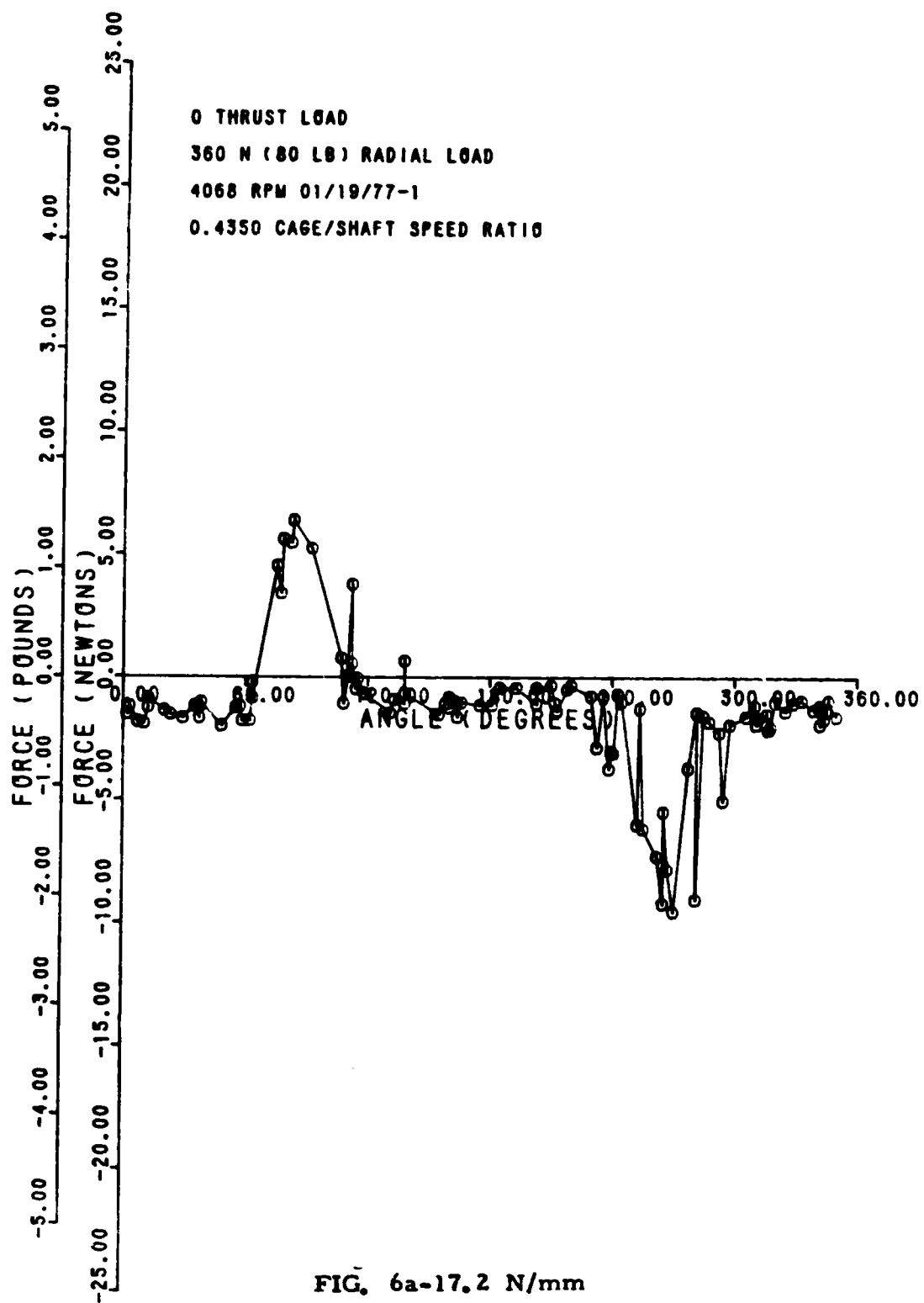
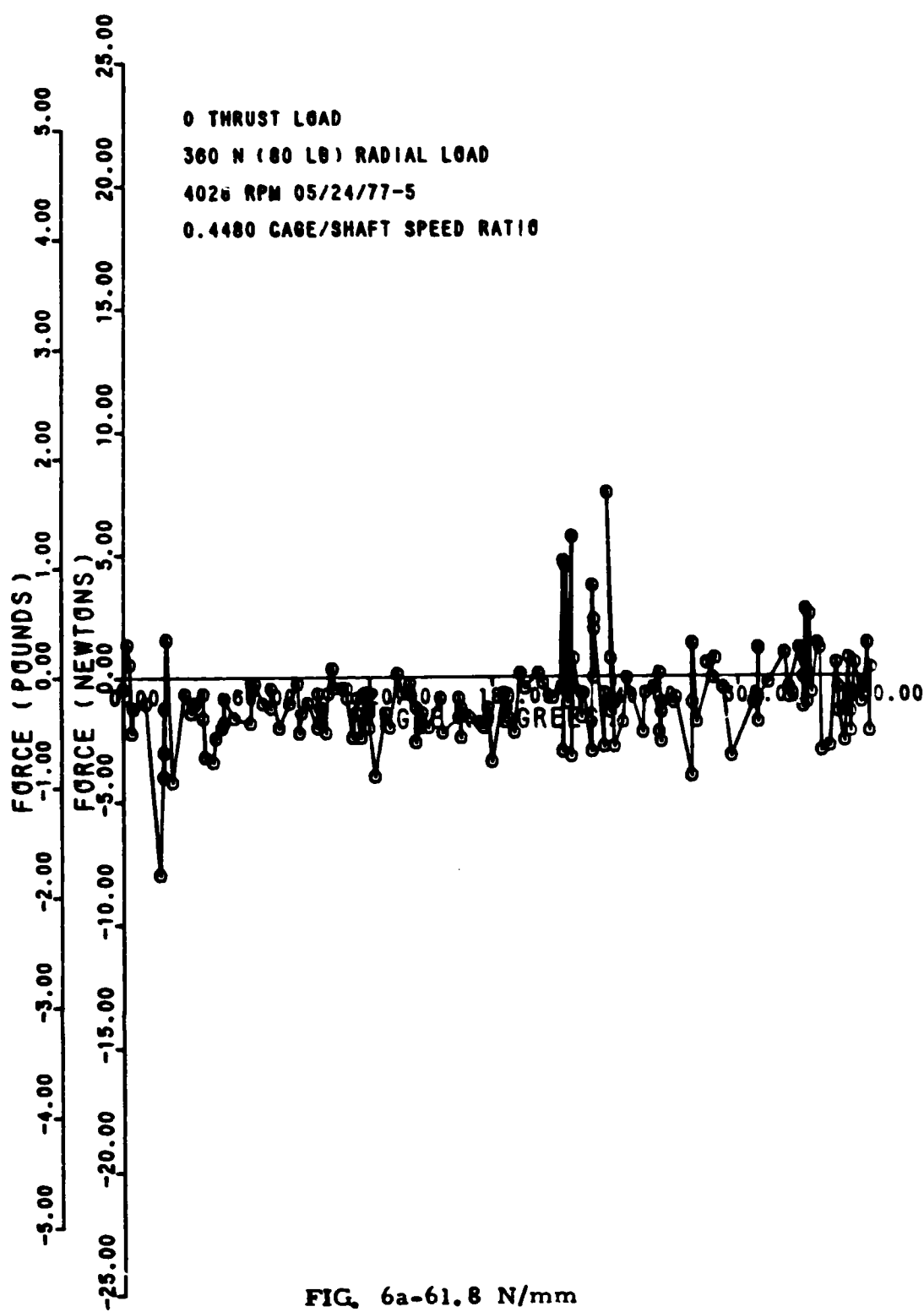


FIG. 6a-17.2 N/mm

0090115 NY AN8

06/02/77



70060139155

06/15/77

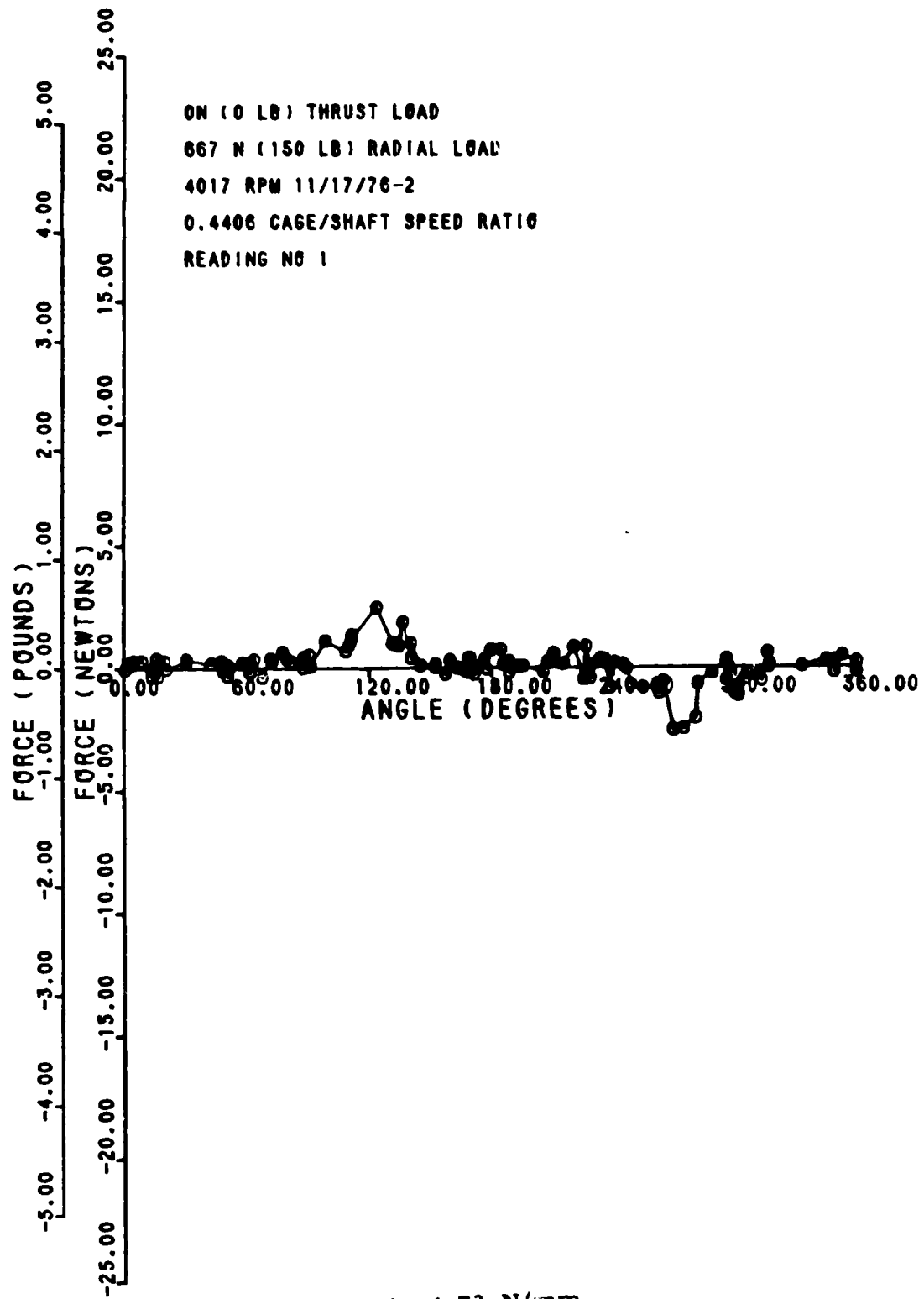


FIG. 6b-4.73 N/mm

7 0 0 E 0 : 1 9 N Y I P H A N I

R D6, # 2
05/06/77

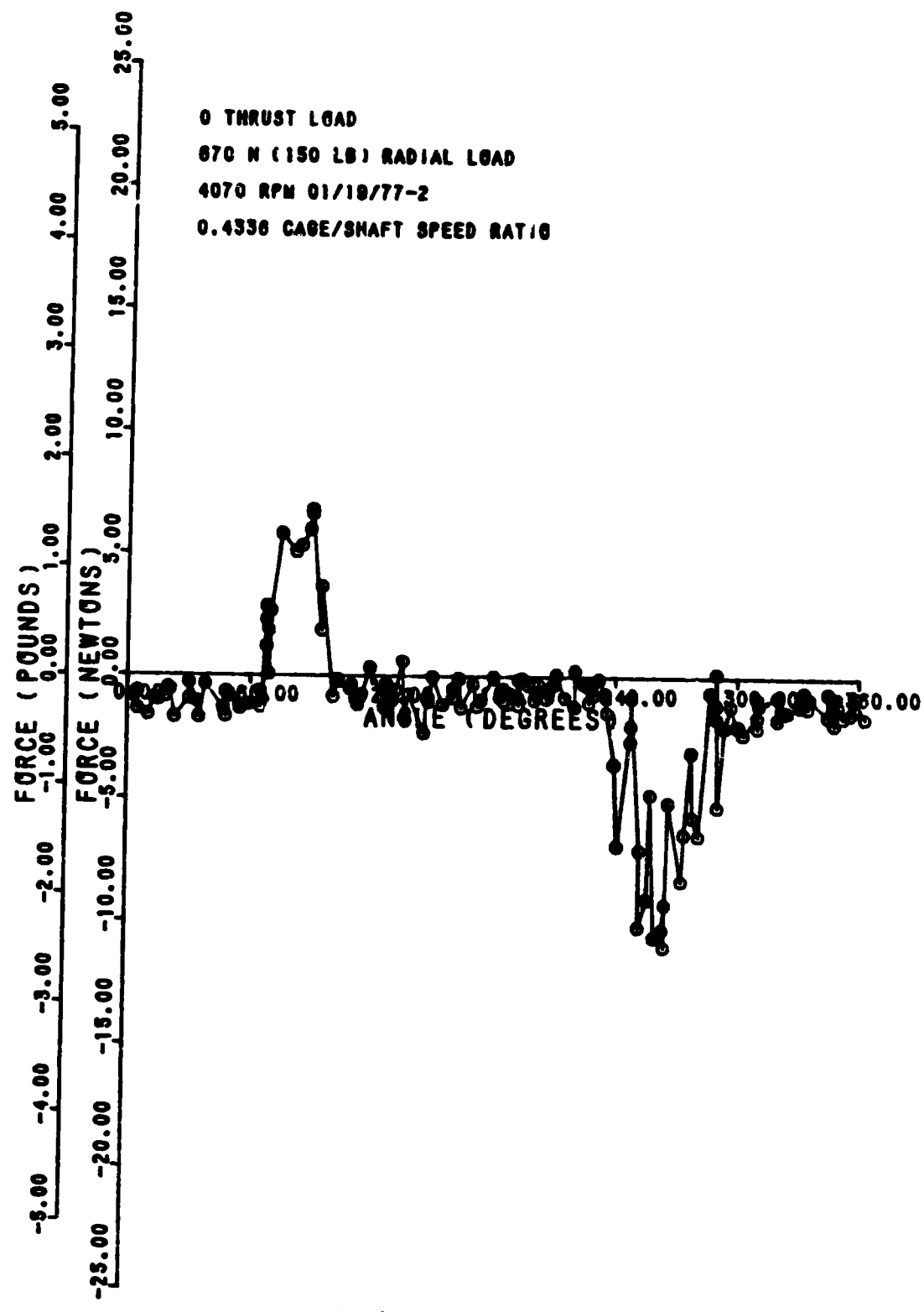


FIG. 6b-17.2 N/mm

70090115NYPAN12 06/02/77

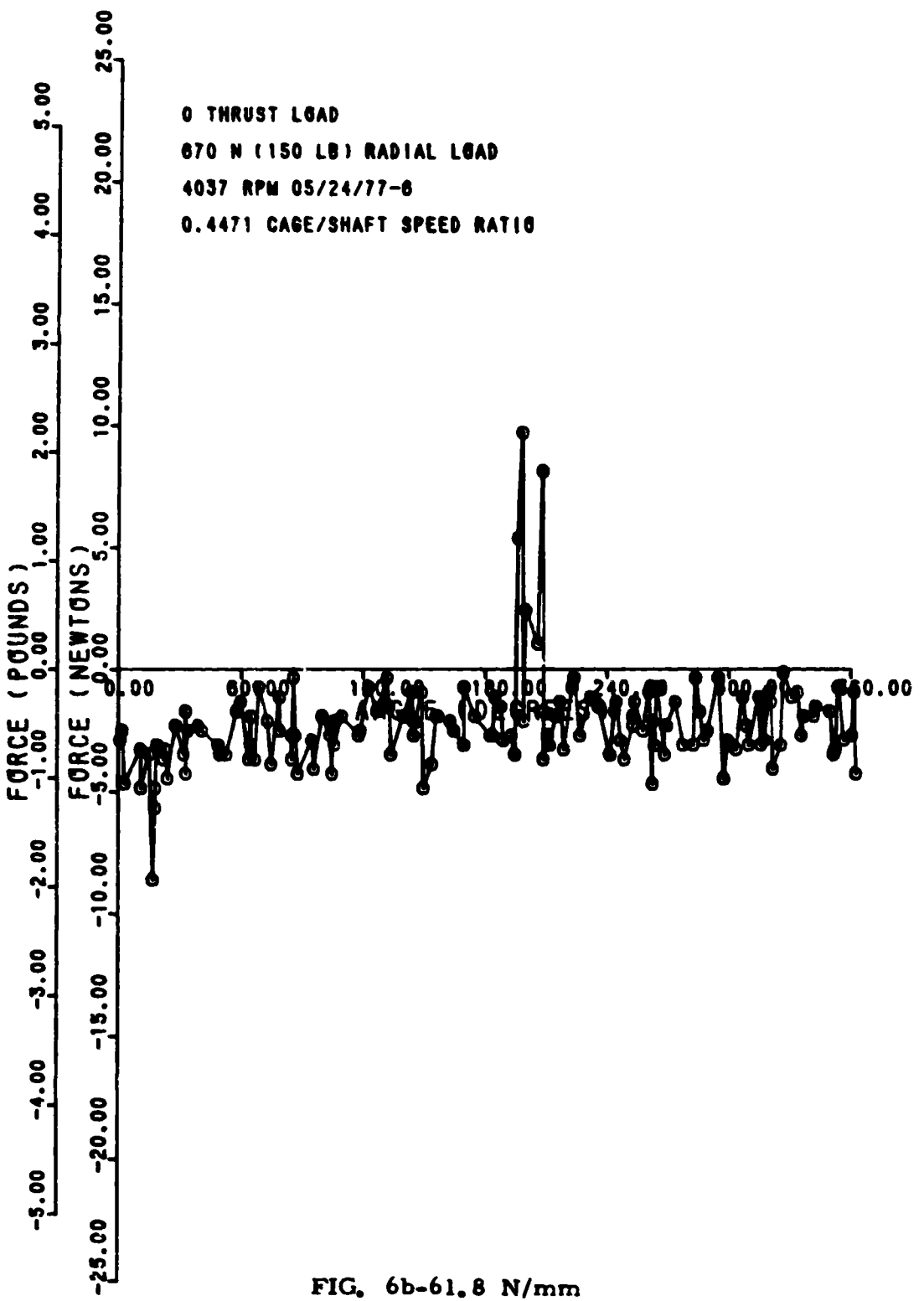


FIG. 6b-61.8 N/mm

06/16/77

700G-119N-17PAN5

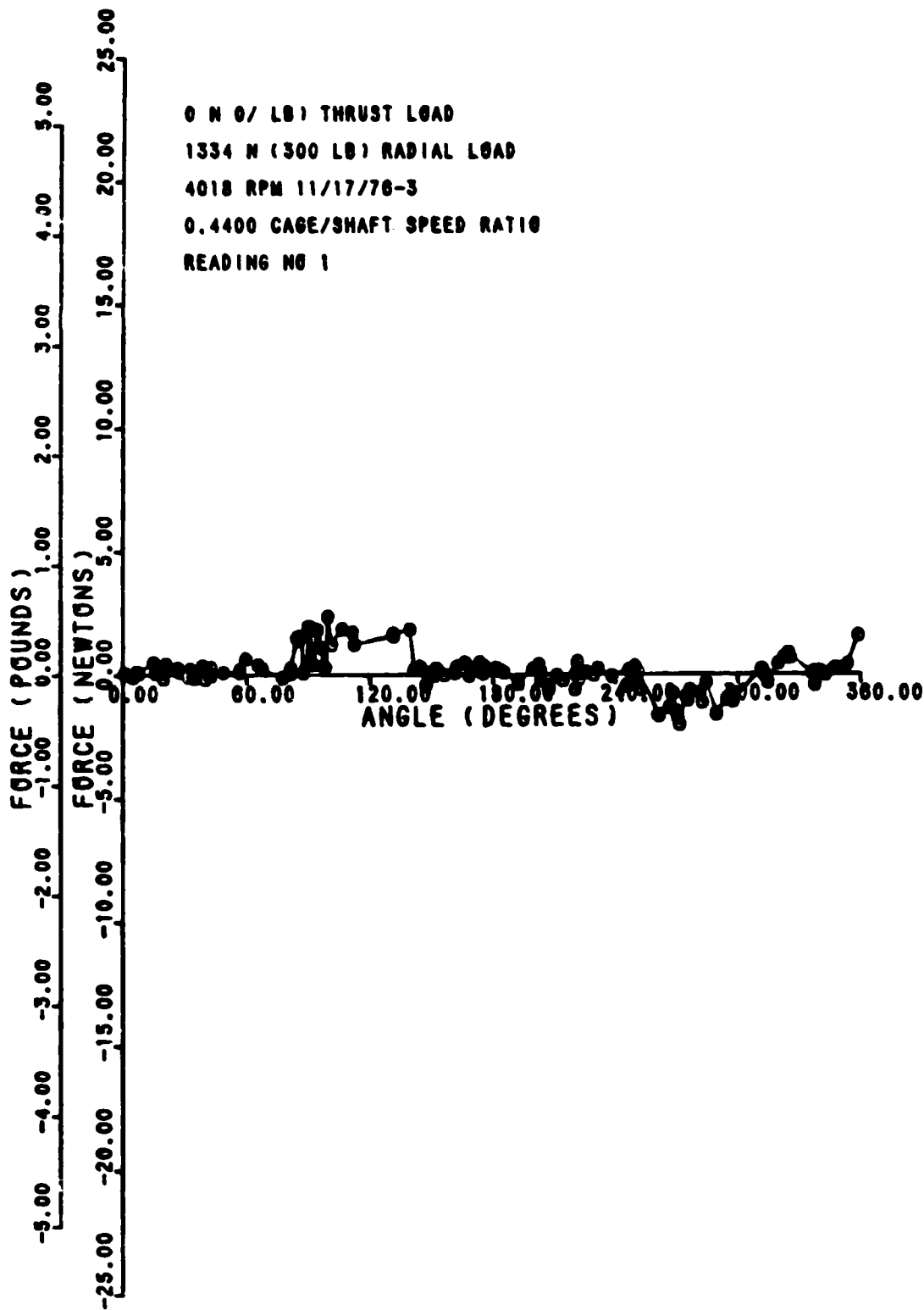
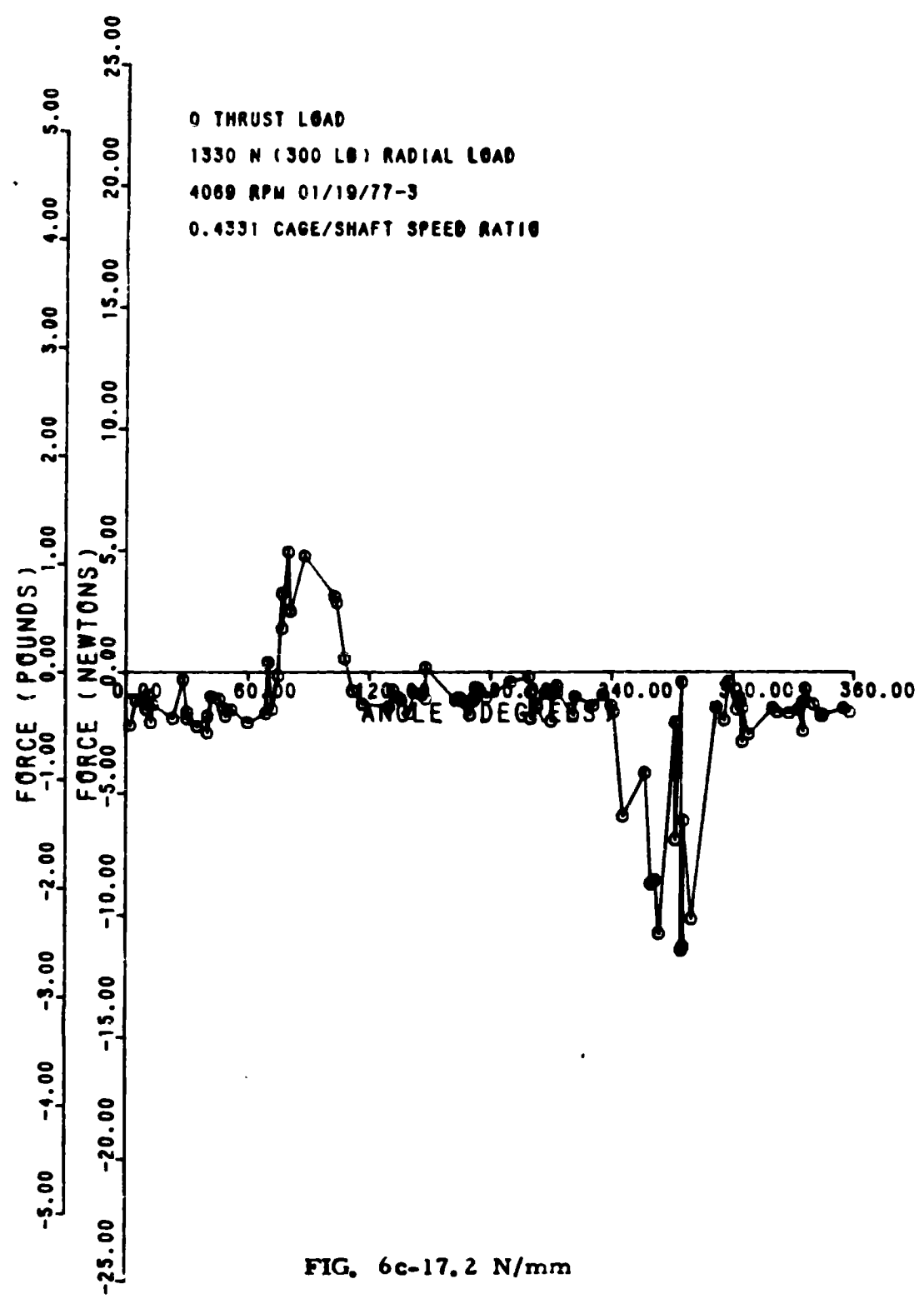


FIG. 6c-4. 73 N/mm

7-000139:00 11 05 1977 PAINI

04/30/77



70090115 JAN 16

06/02/77

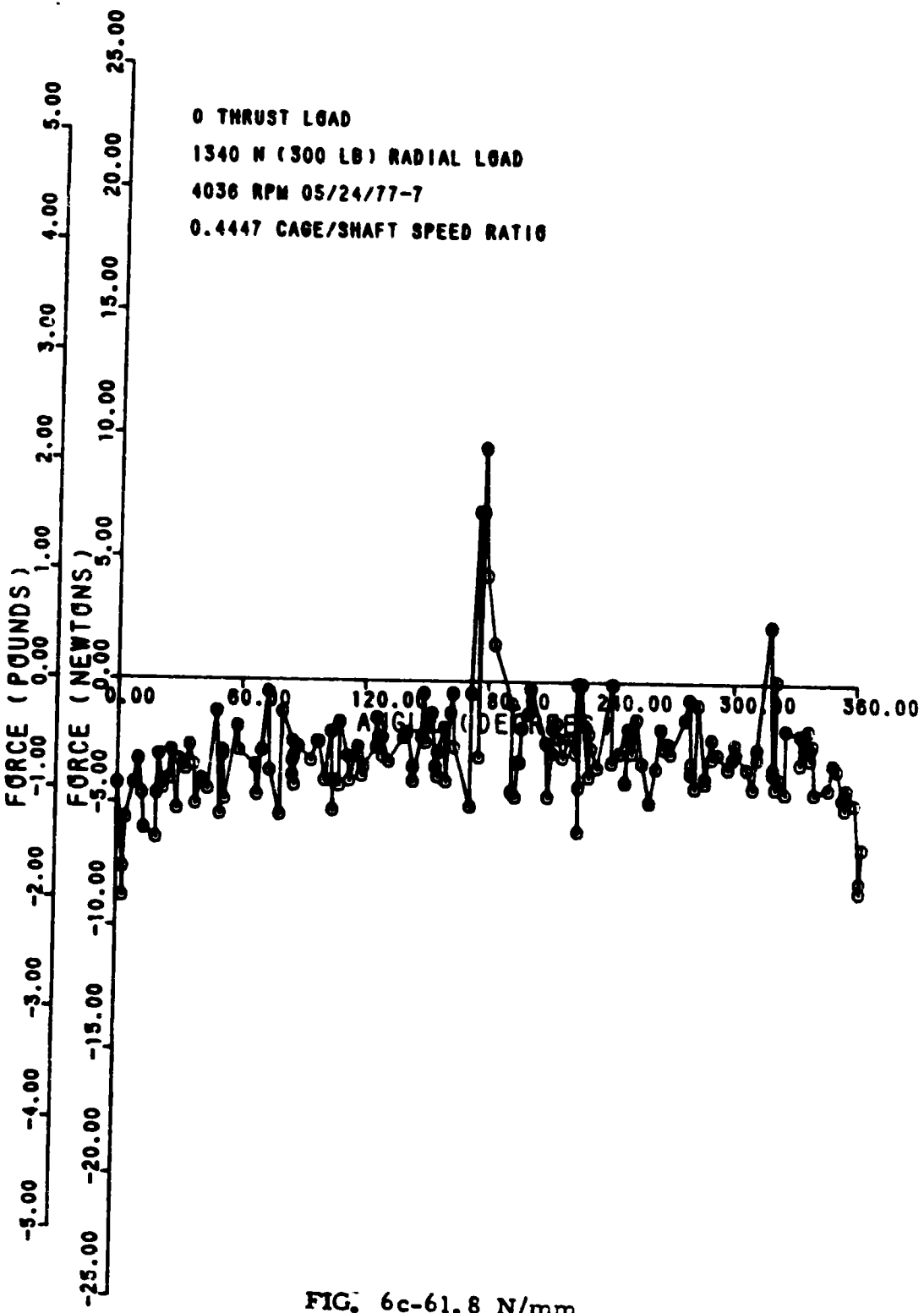


FIG. 6c-61.8 N/mm

70090119NYPAN3 03/11/77

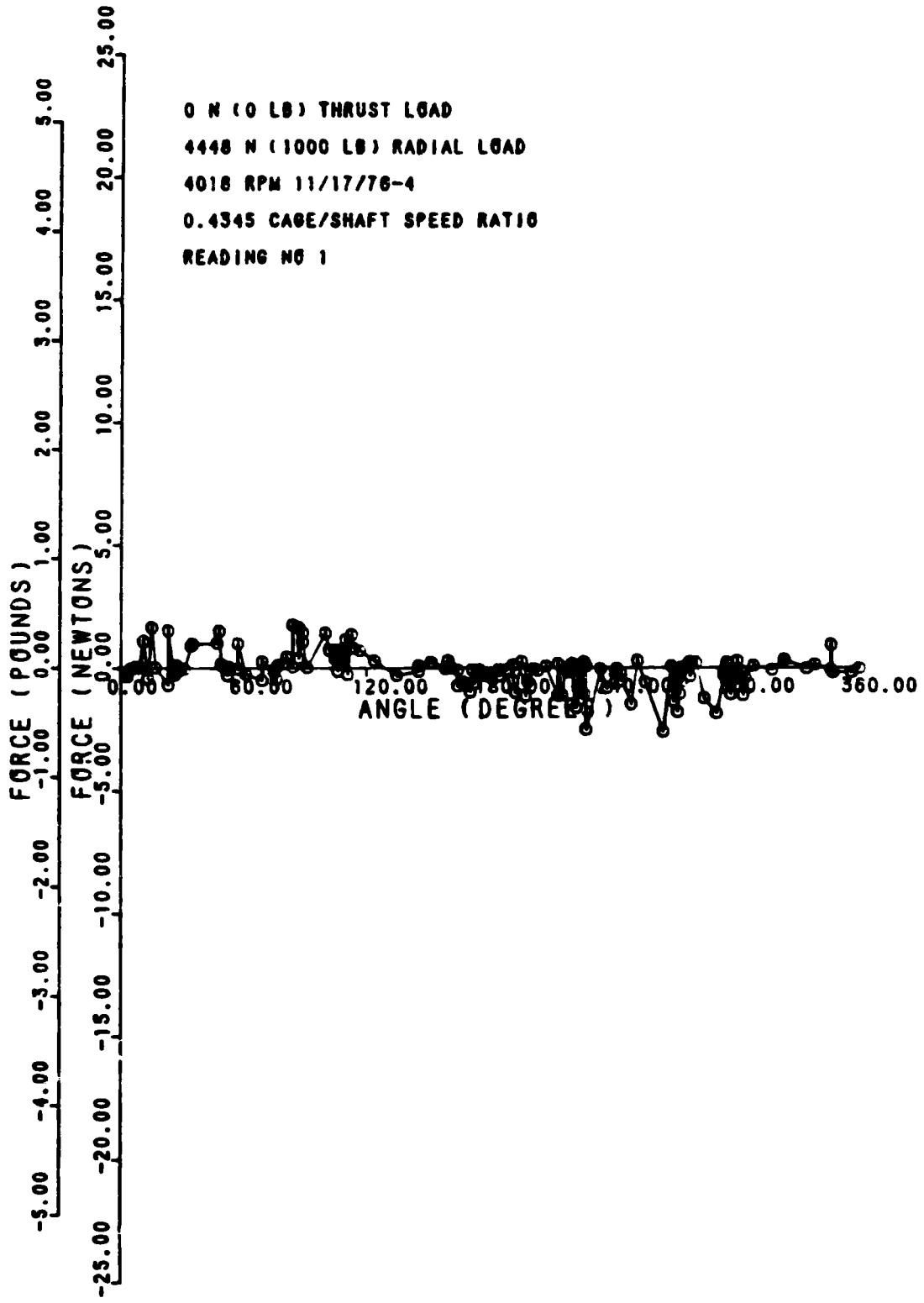


FIG. 6d-4.73 N/mm

70-090-1 FIG NY-PANN 12 - 02/23/77

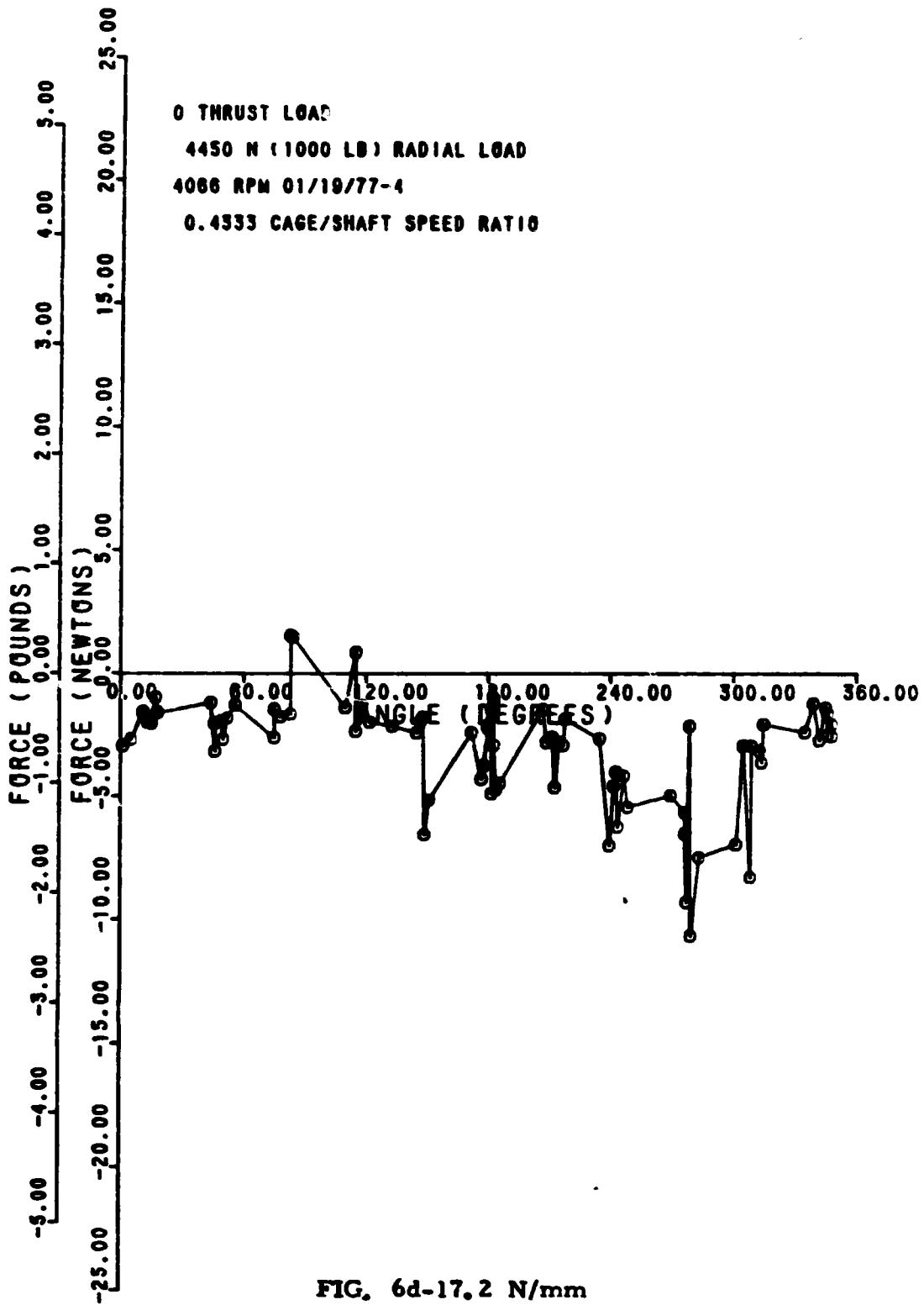
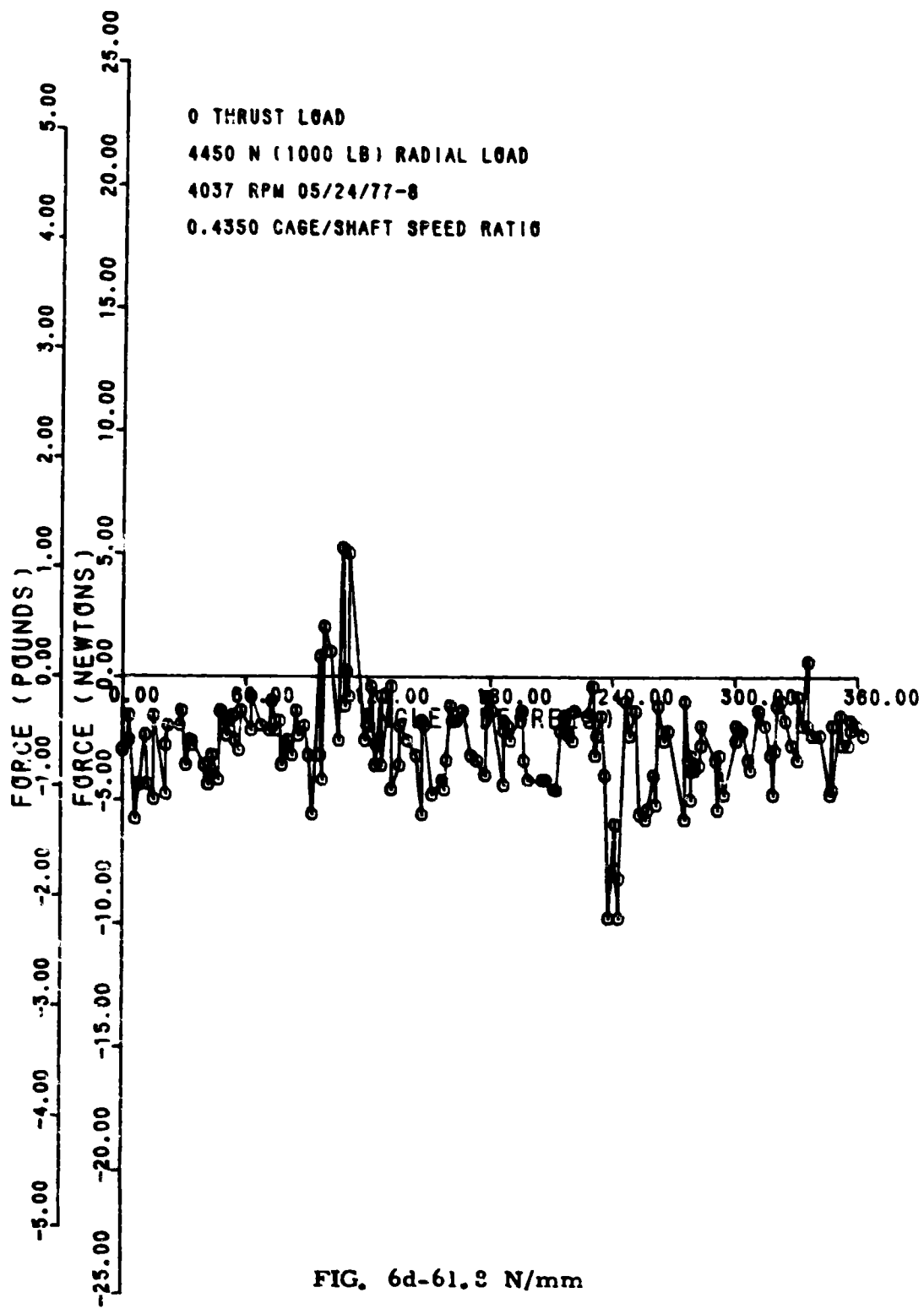


FIG. 6d-17.2 N/mm

06/07/77

COGENT INC.



70090119NYPAN4

-
05/03/77

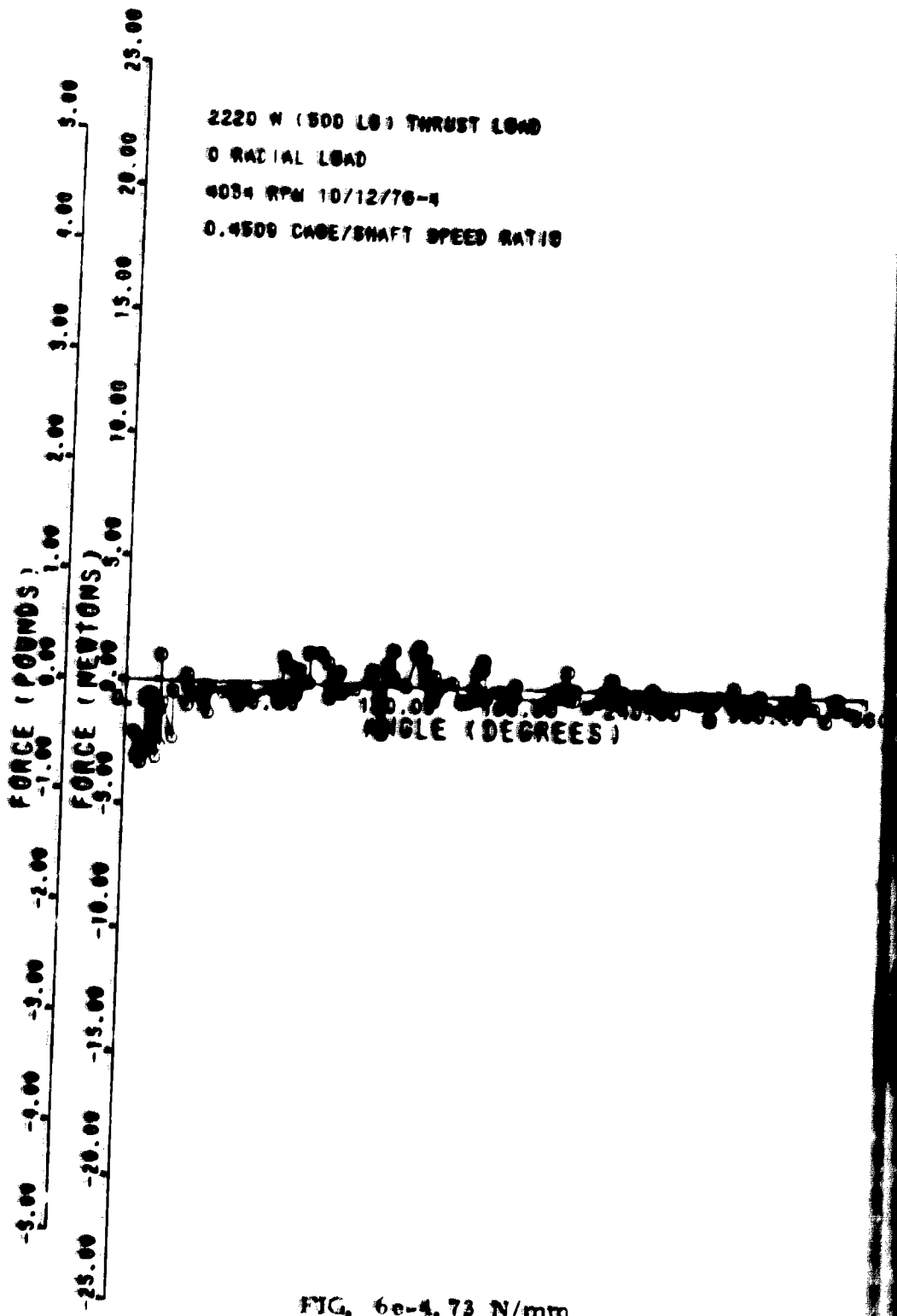


FIG. 6e-4. 73 N/mm

7000-09-01-11512-A1N2-1-02-28/77

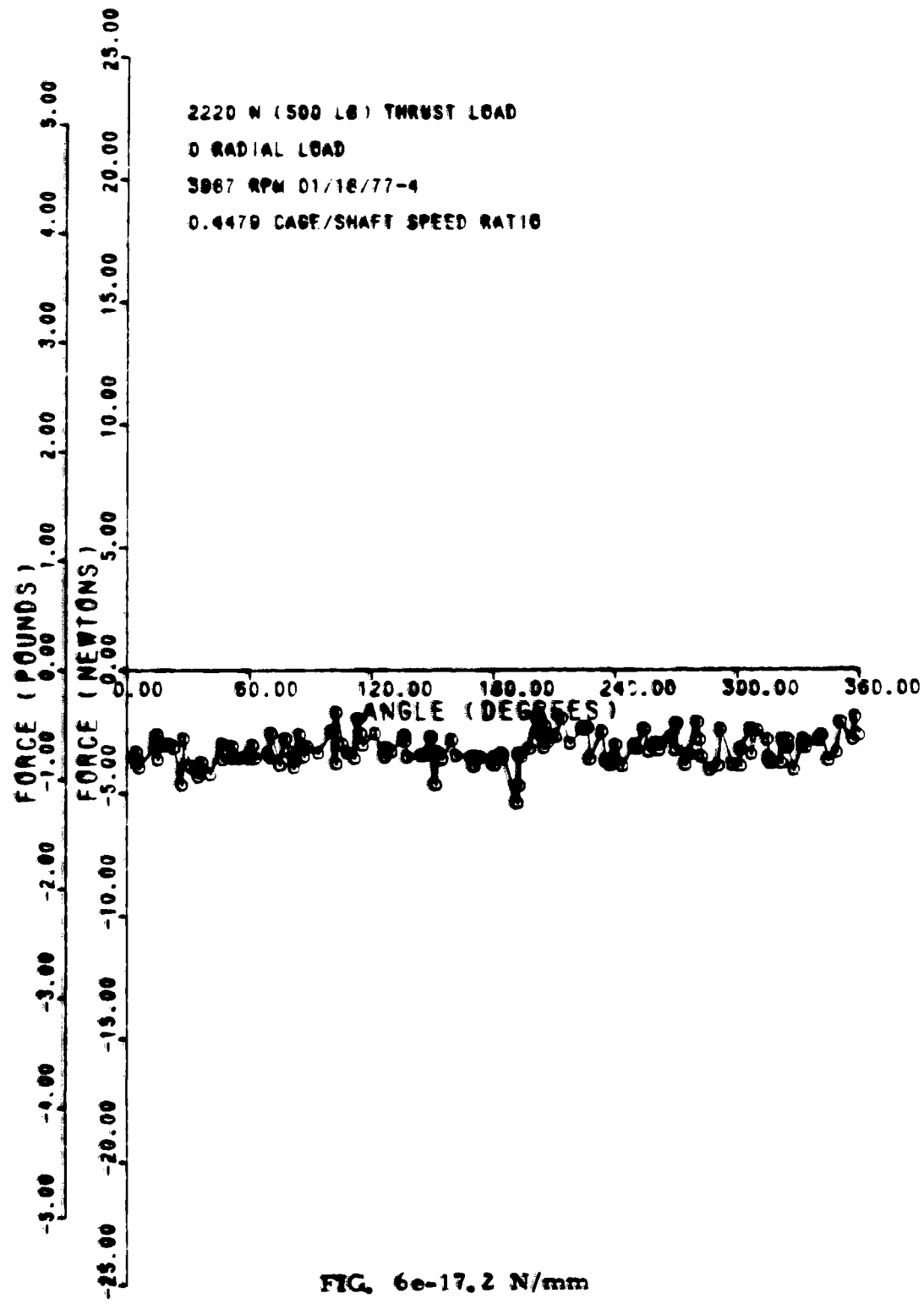


FIG. 6e-17.2 N/mm

06/17/77

70-0997-15 NY PA IN 8

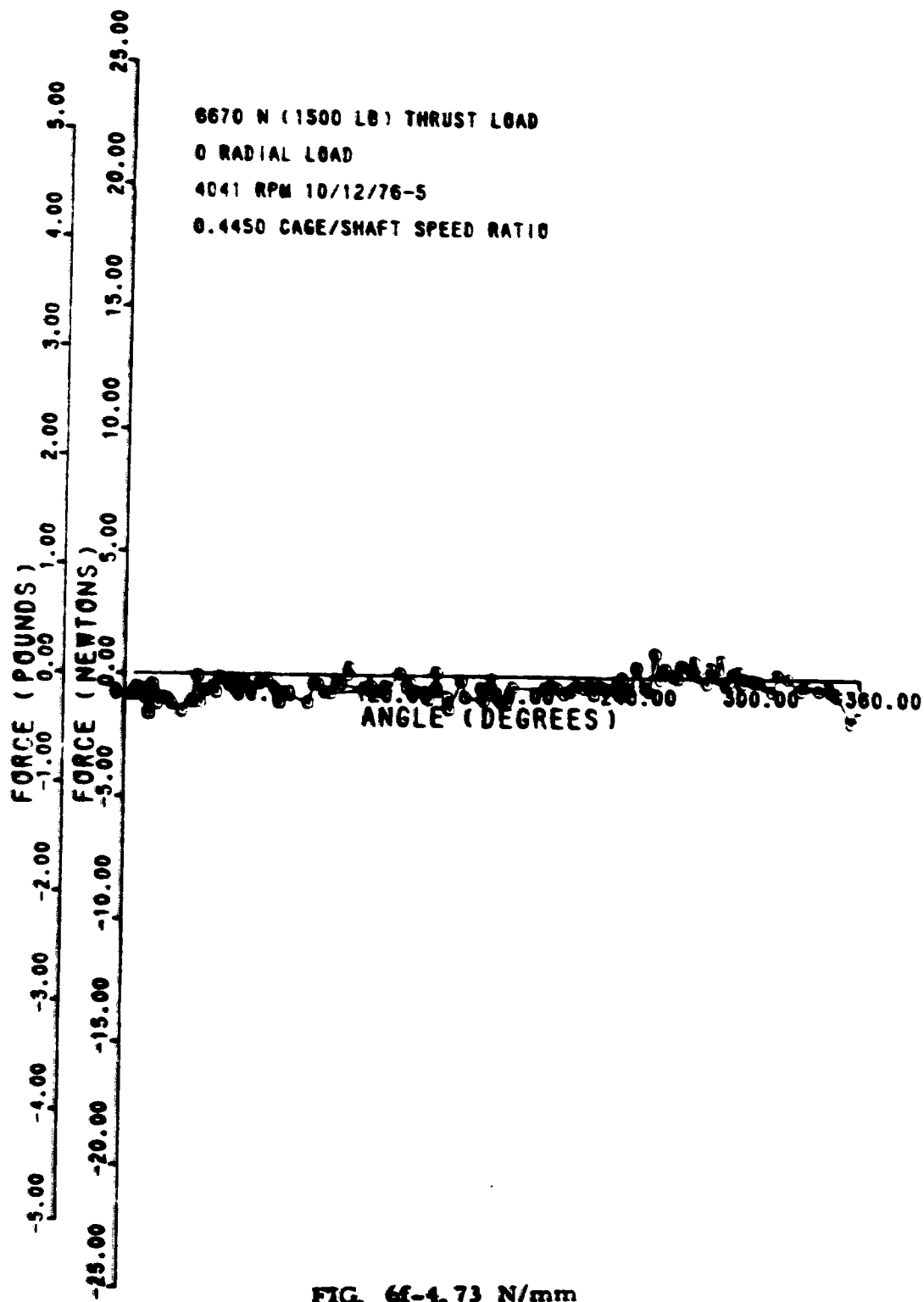


FIG. 6E-4.73 N/mm

TO 090115 NY FANTU

02/26/77

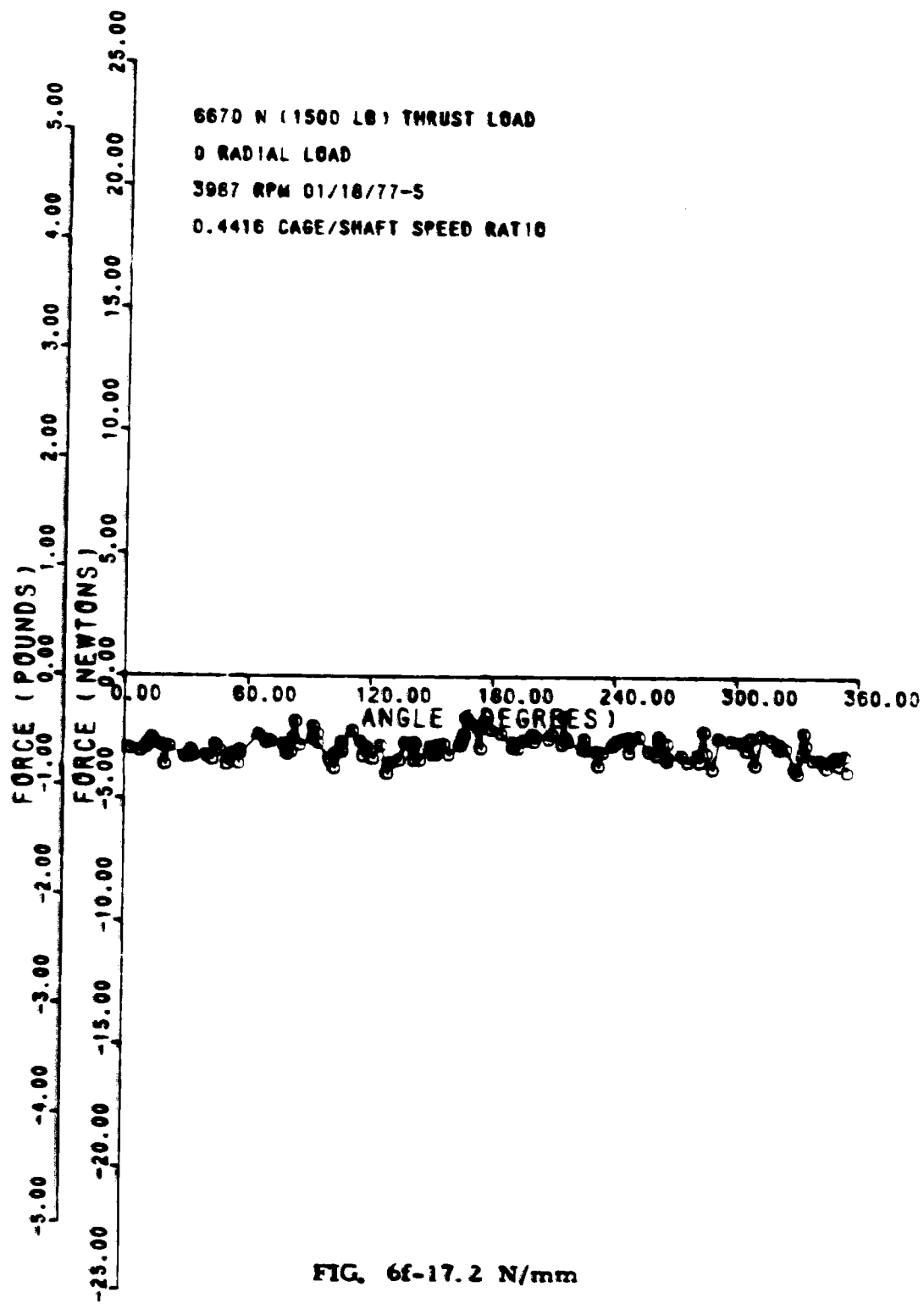


FIG. 6f-17.2 N/mm

F G O 9 0 H U S I N Y F A N 1 0 1 0

0 6 / 1 6 8 / 1 7 6 V 7

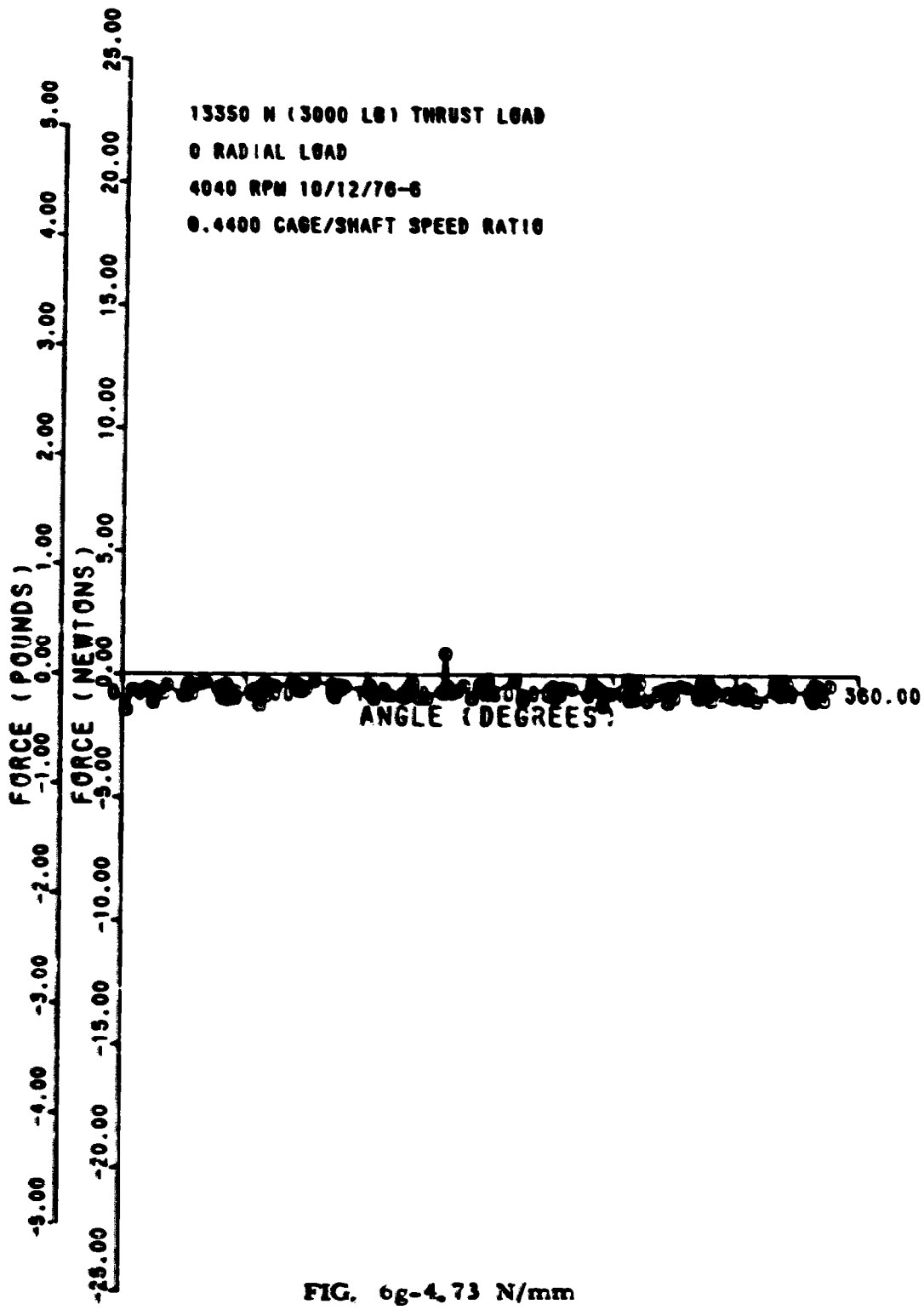
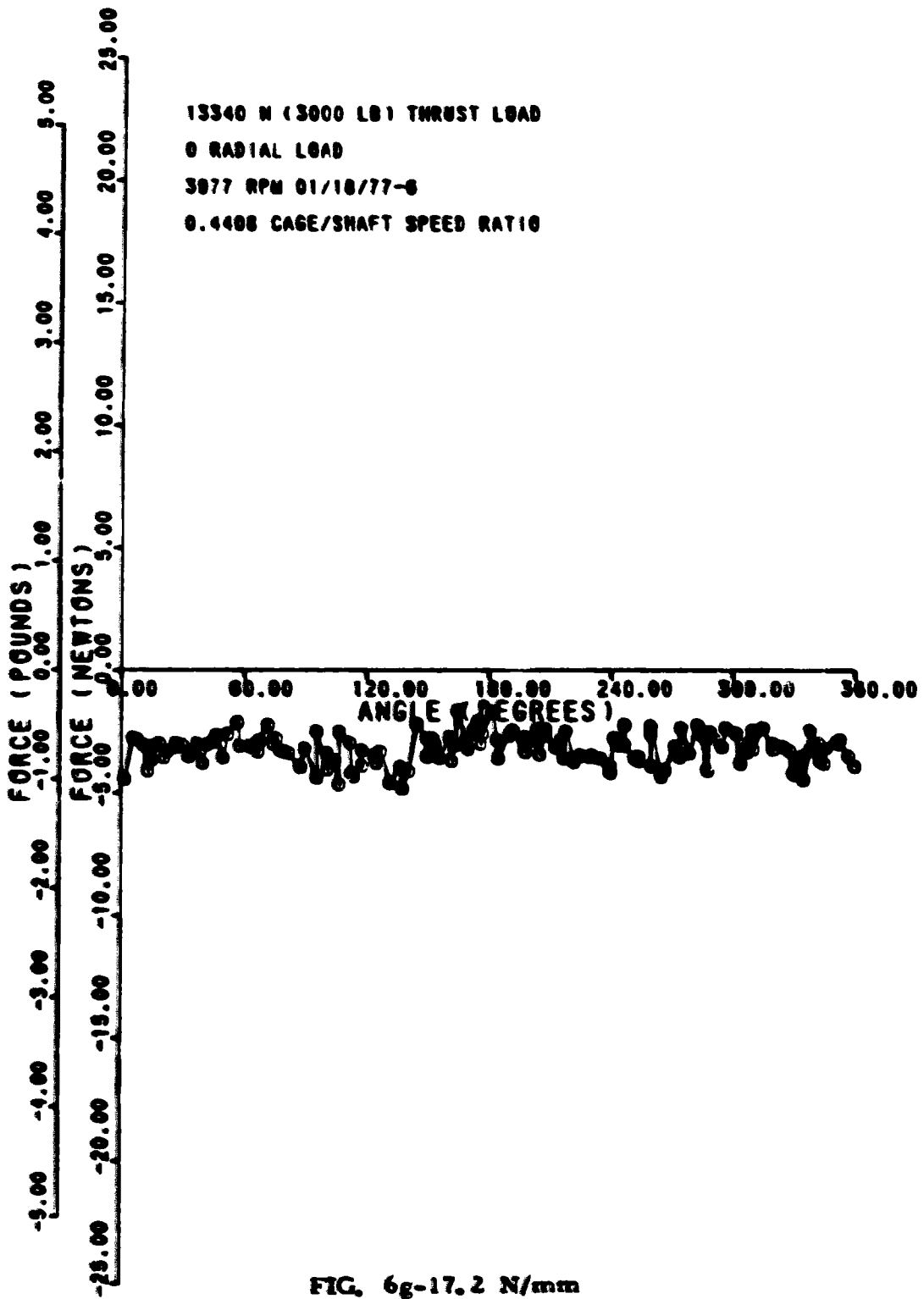


FIG. 6g-4. 73 N/mm

70030000000000000000000000000000

06/17/77



7009011:3 IN PIANI

06/15/77

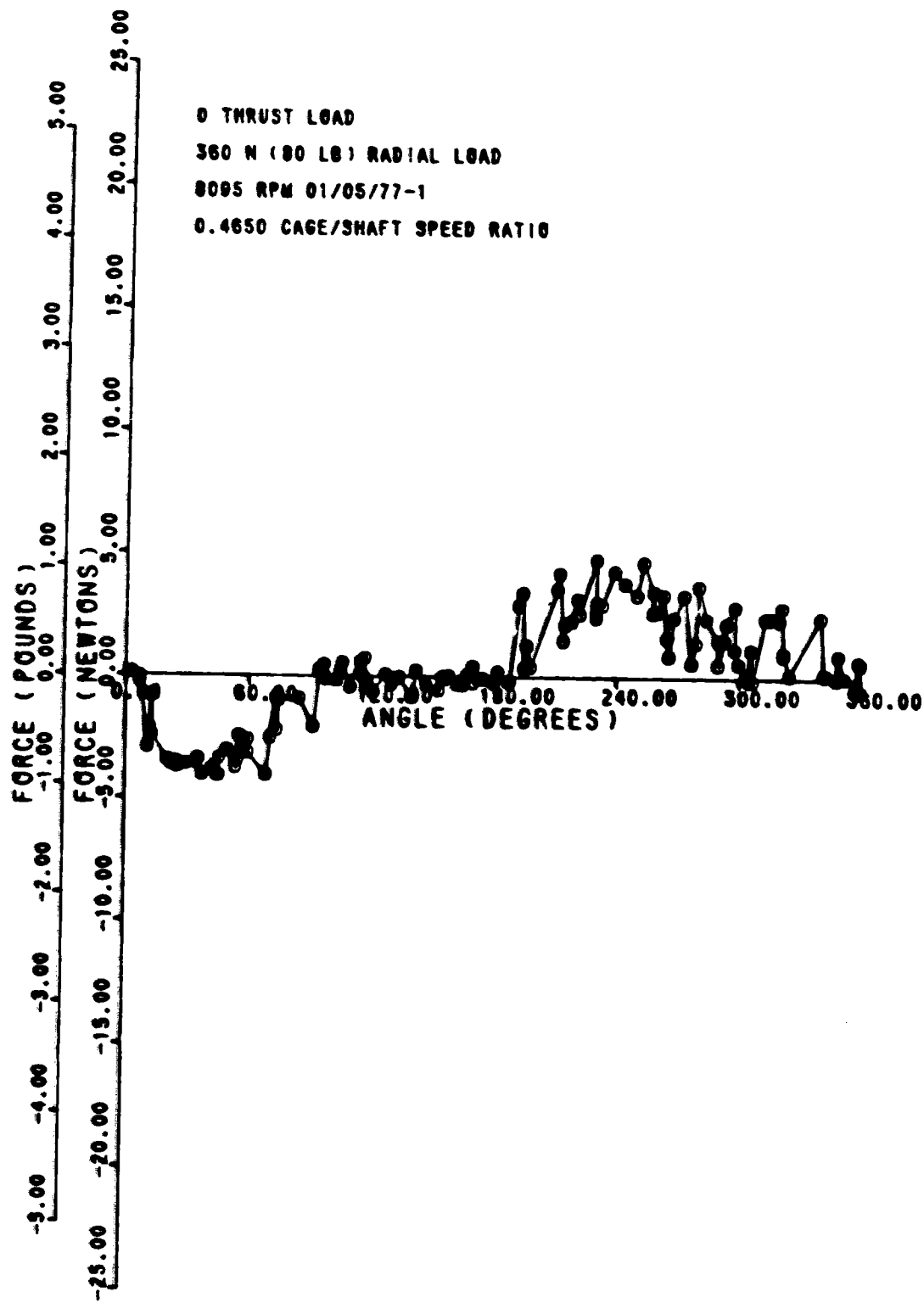


FIG. 7a-4.73 N/mm

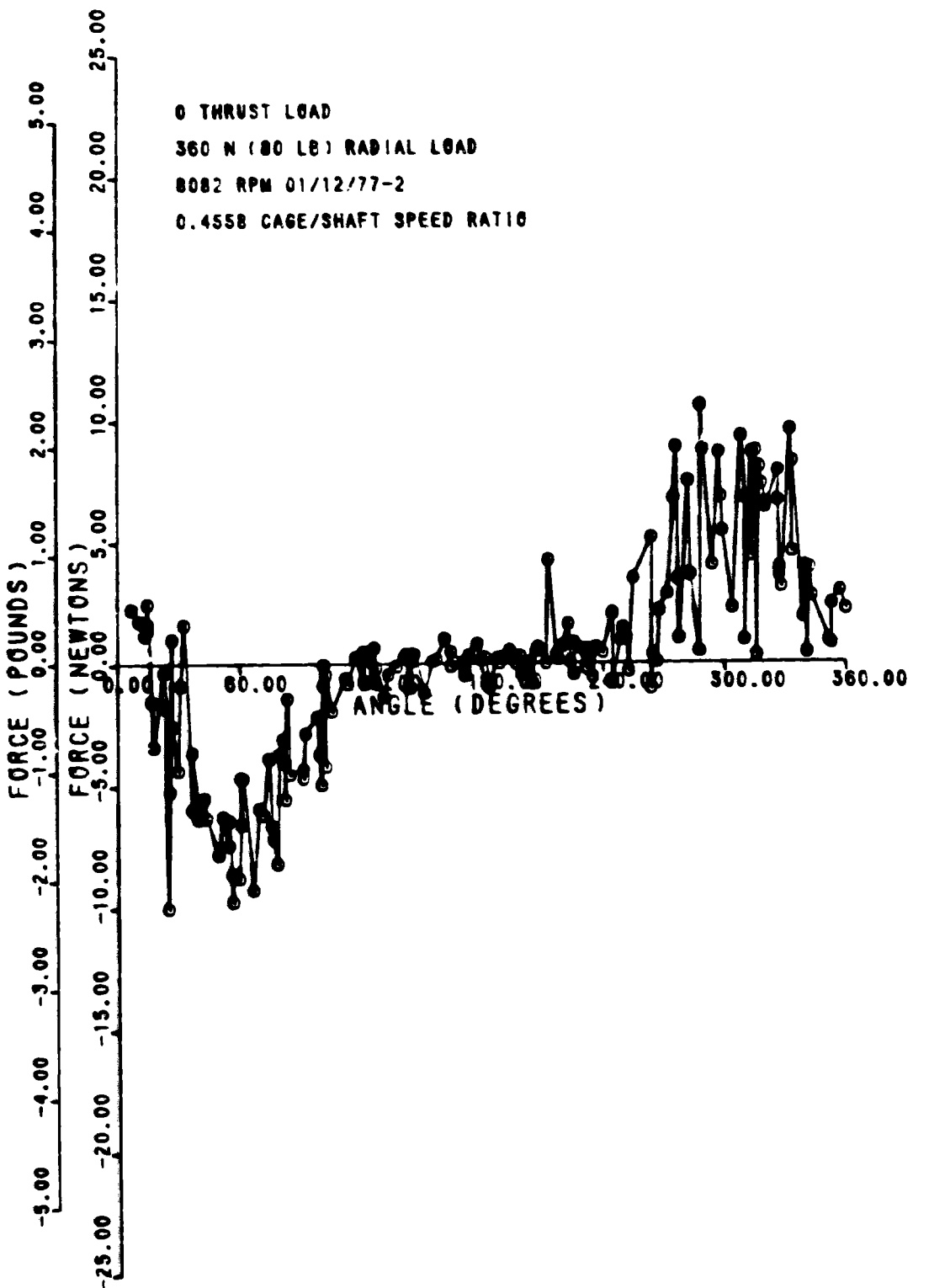


FIG. 7a-17.2 N/mm

700901103NYFANN

06/14/77

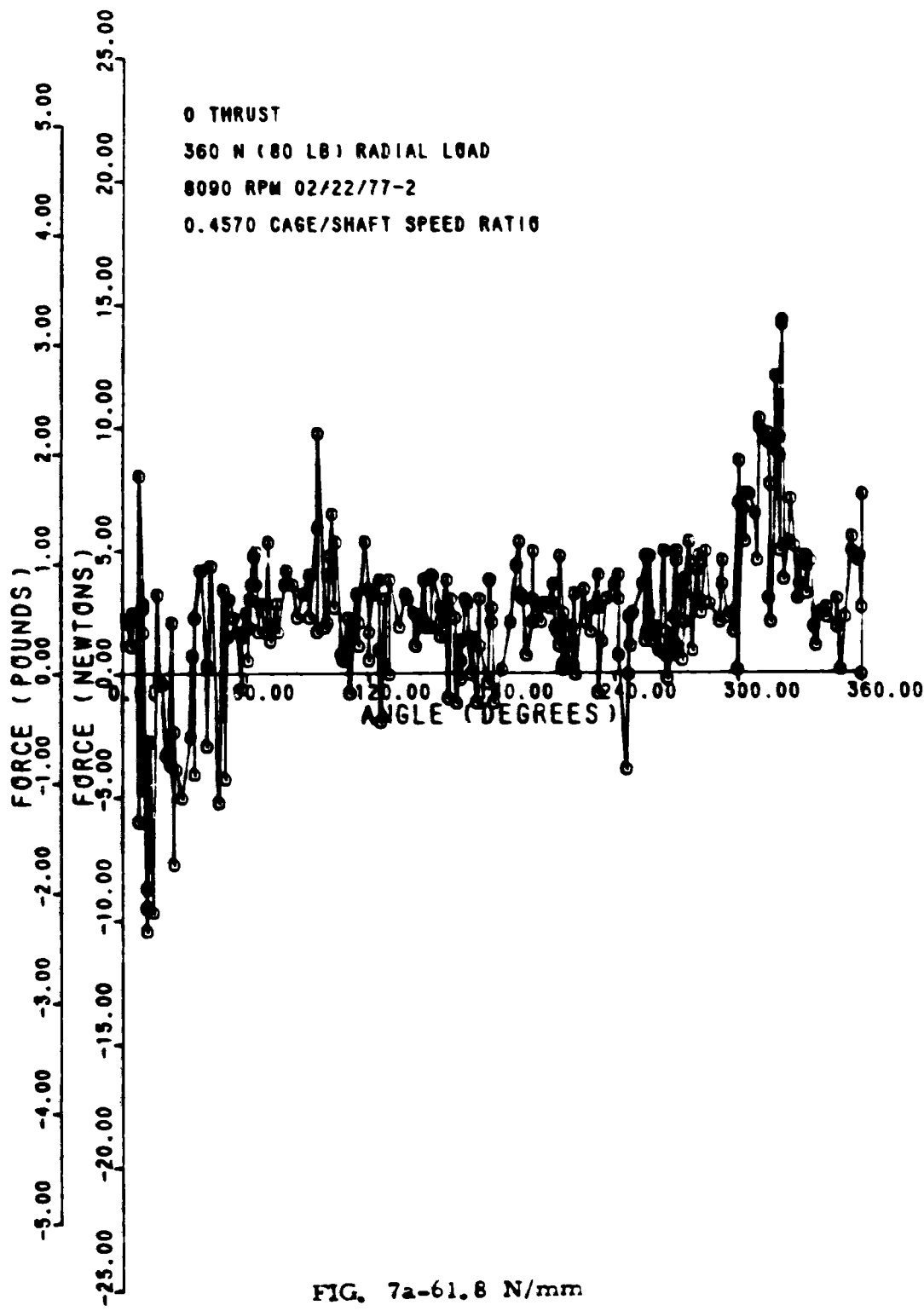


FIG. 7a-61.8 N/mm

06/15/77

700 GEARING ANALYSIS

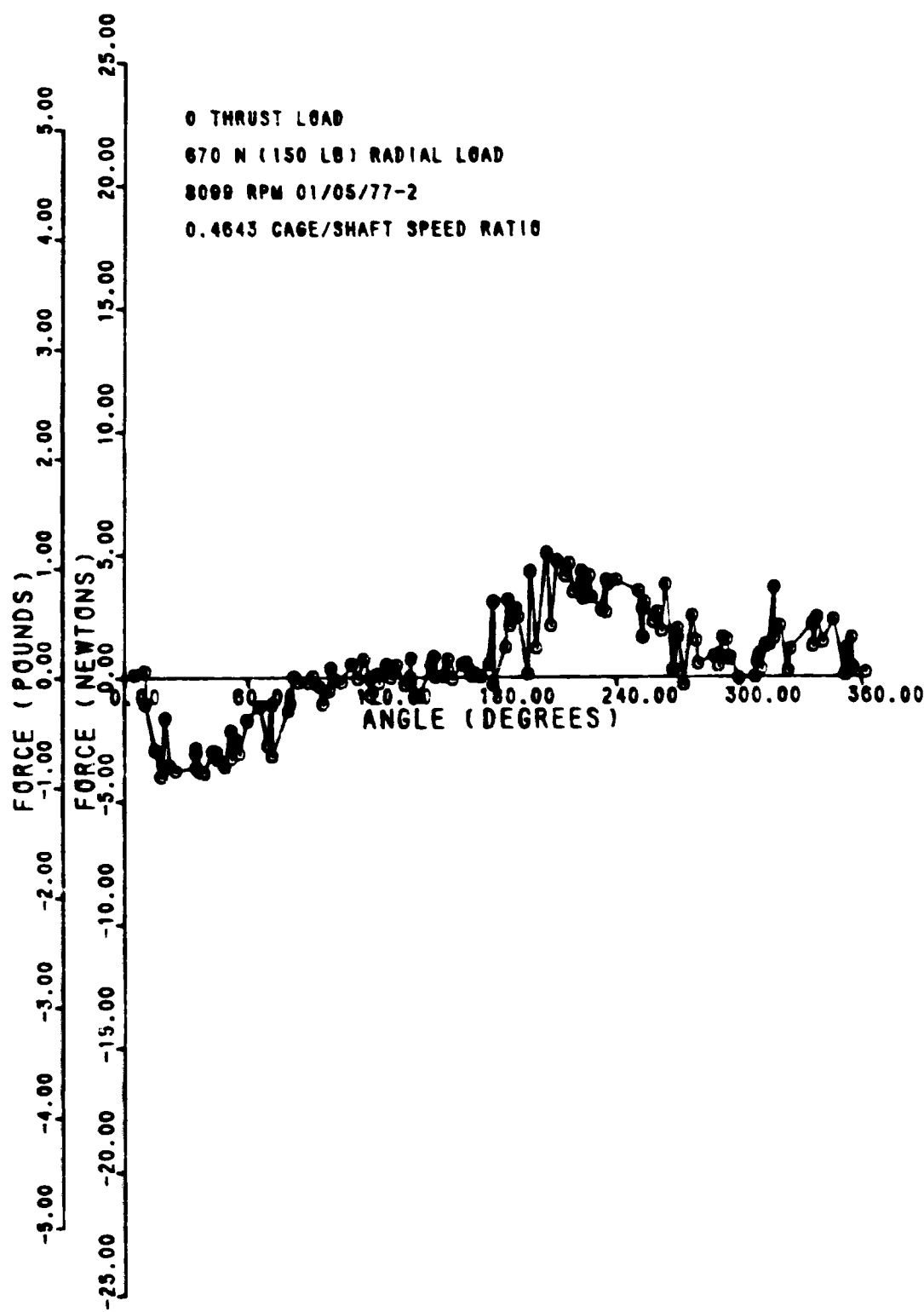
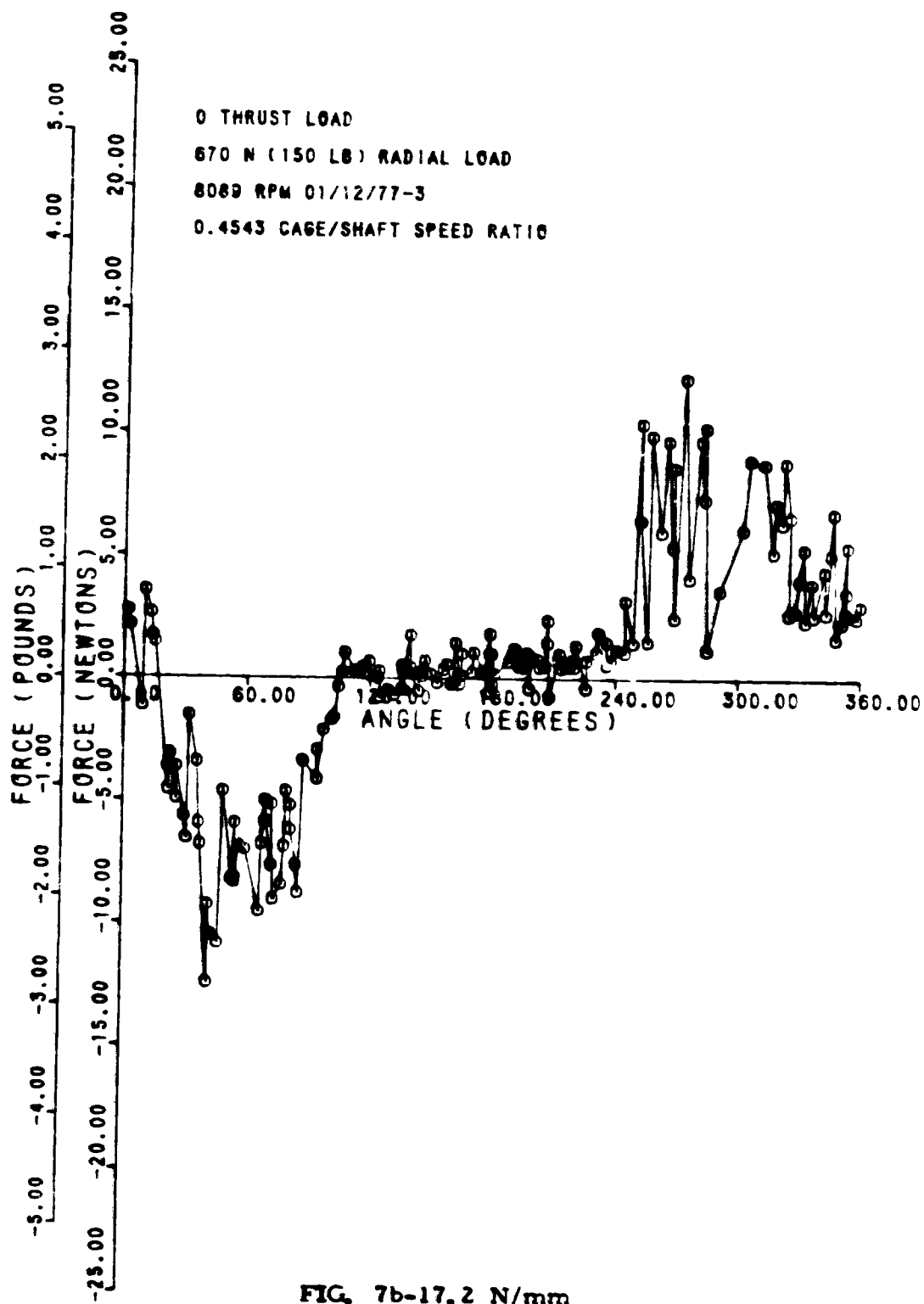


FIG. 7b-4. 73 N/mm

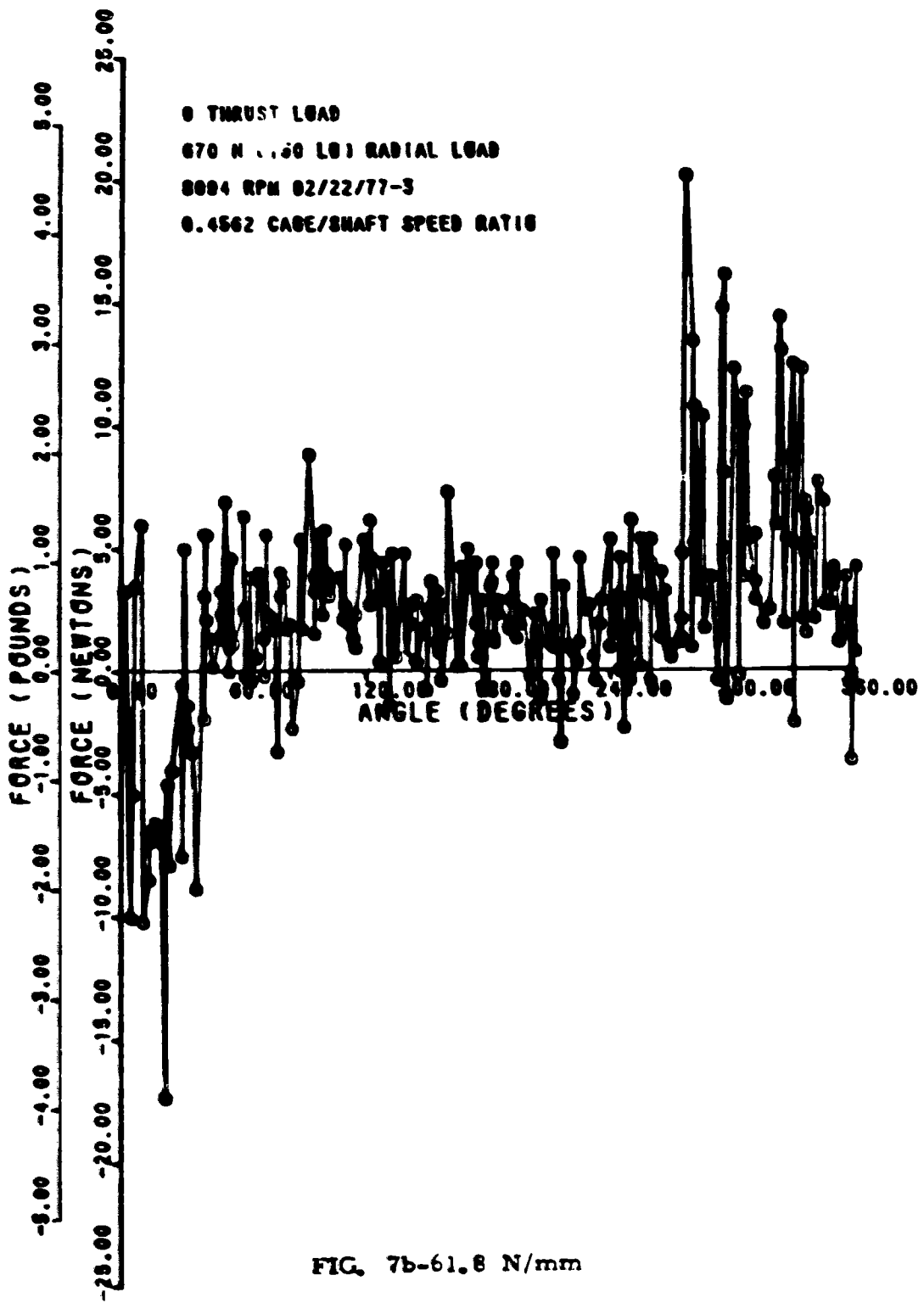
Y 0 0 9 0 || U N Y P A N ||

02/22/77



700900900900900900

06/11/77



70050119NYPANV

06/15/77

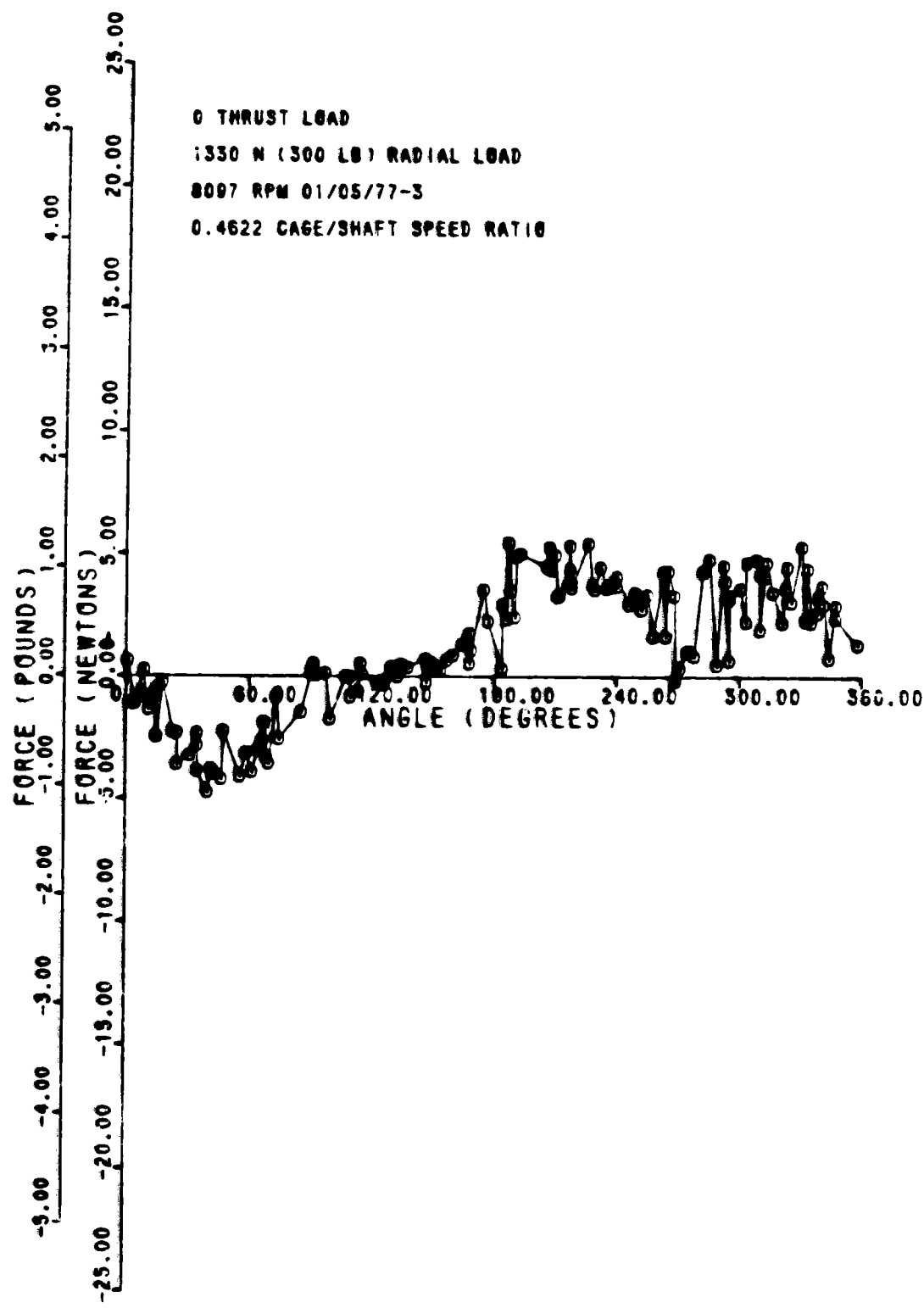
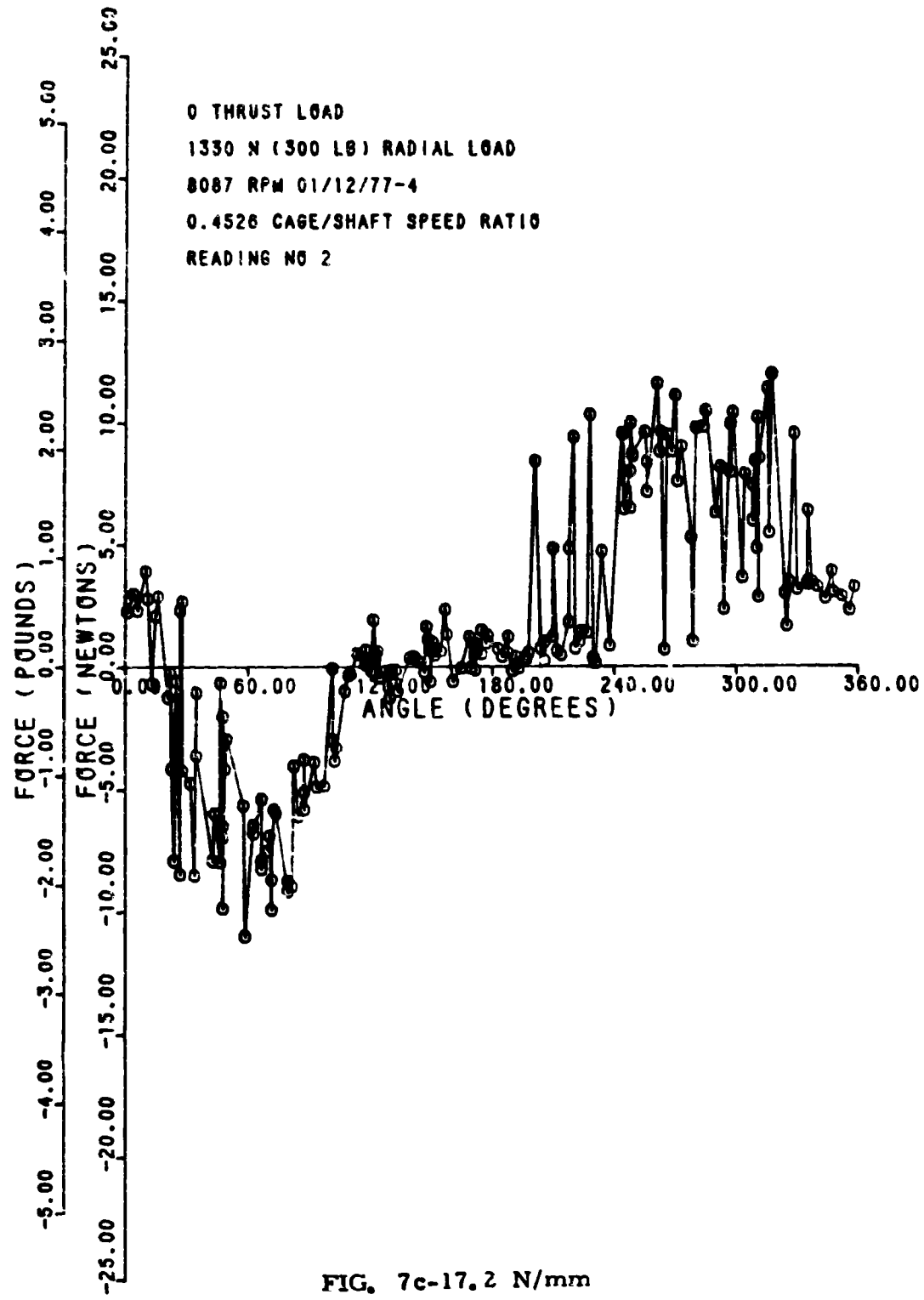


FIG. 7c-4.73 N/mm

WUGO 113 IN FANTIC

06/14/77



70609119 NY PAN 1-6 06/15/77

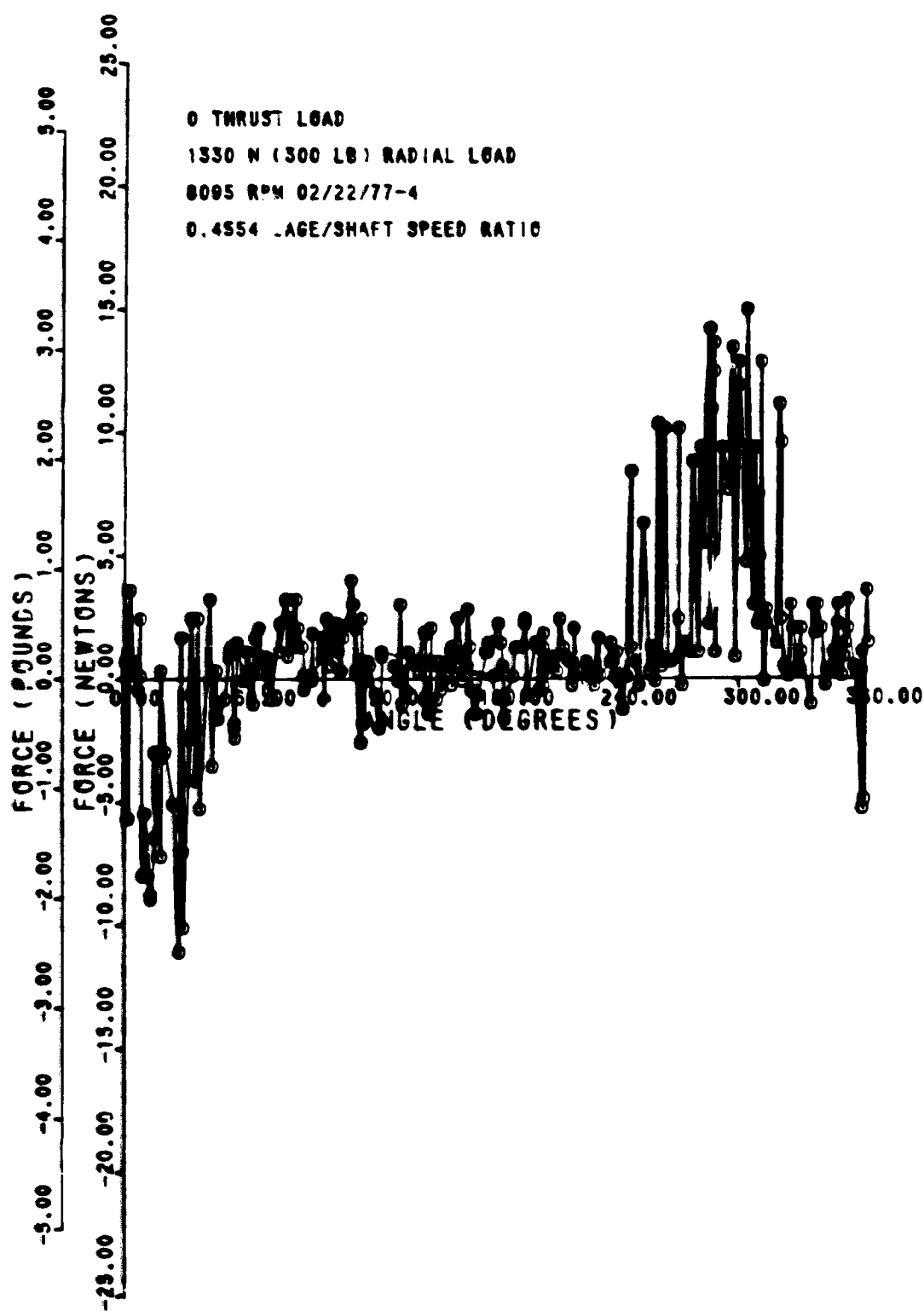
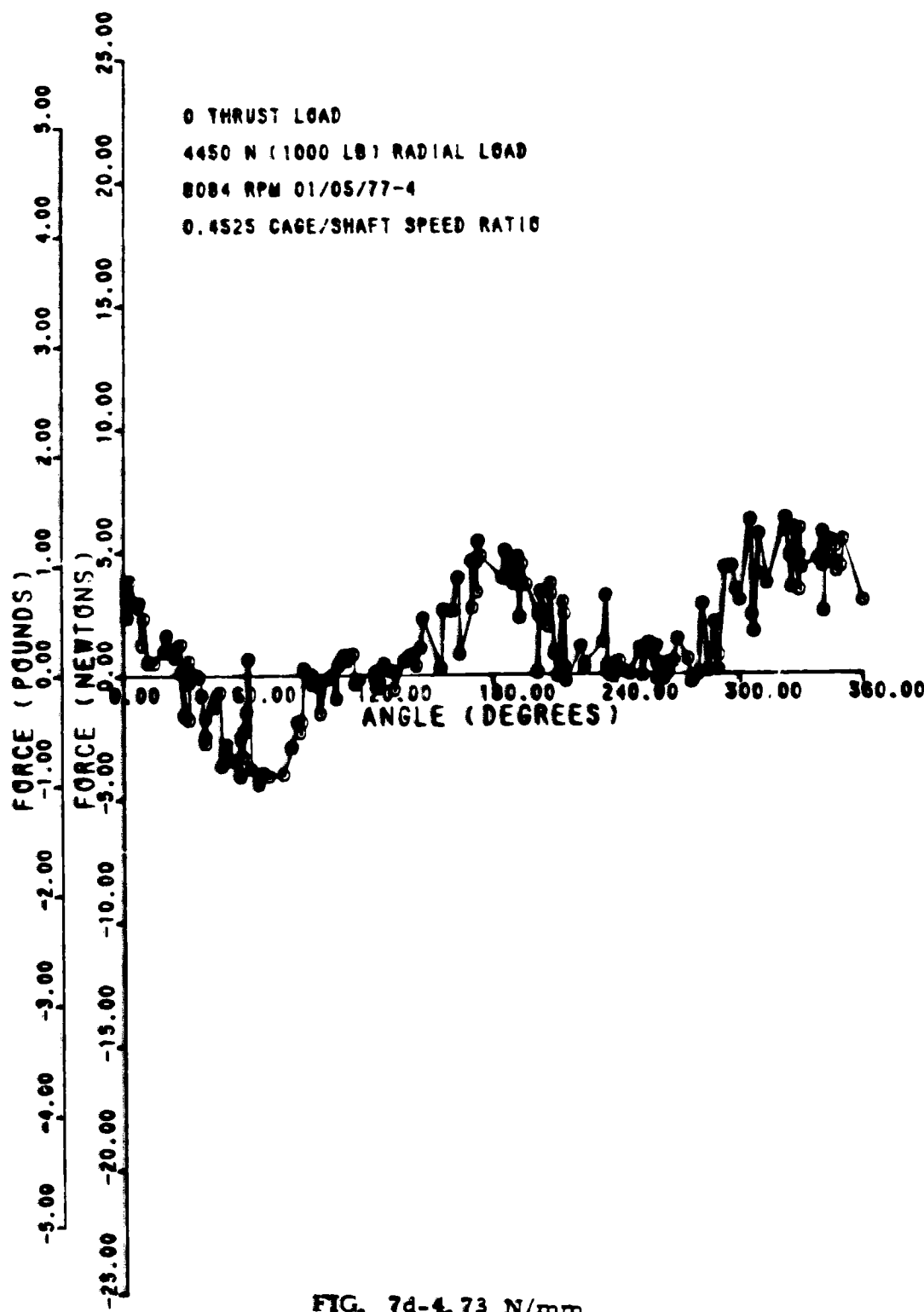


FIG. 7c-61.8 N/mm

70060113N1FAN10



UTG0901H3 IN PARING

05/06/77

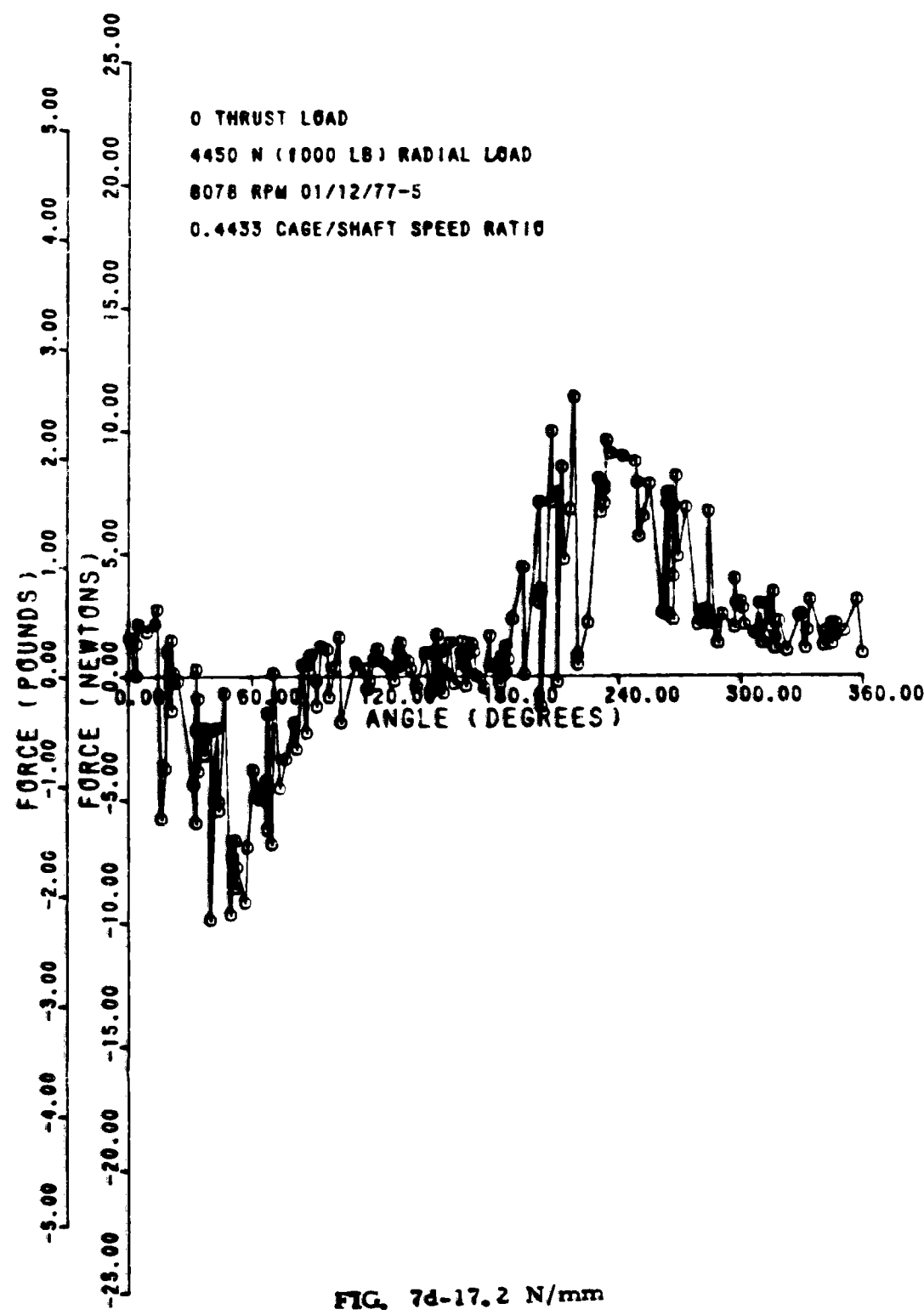
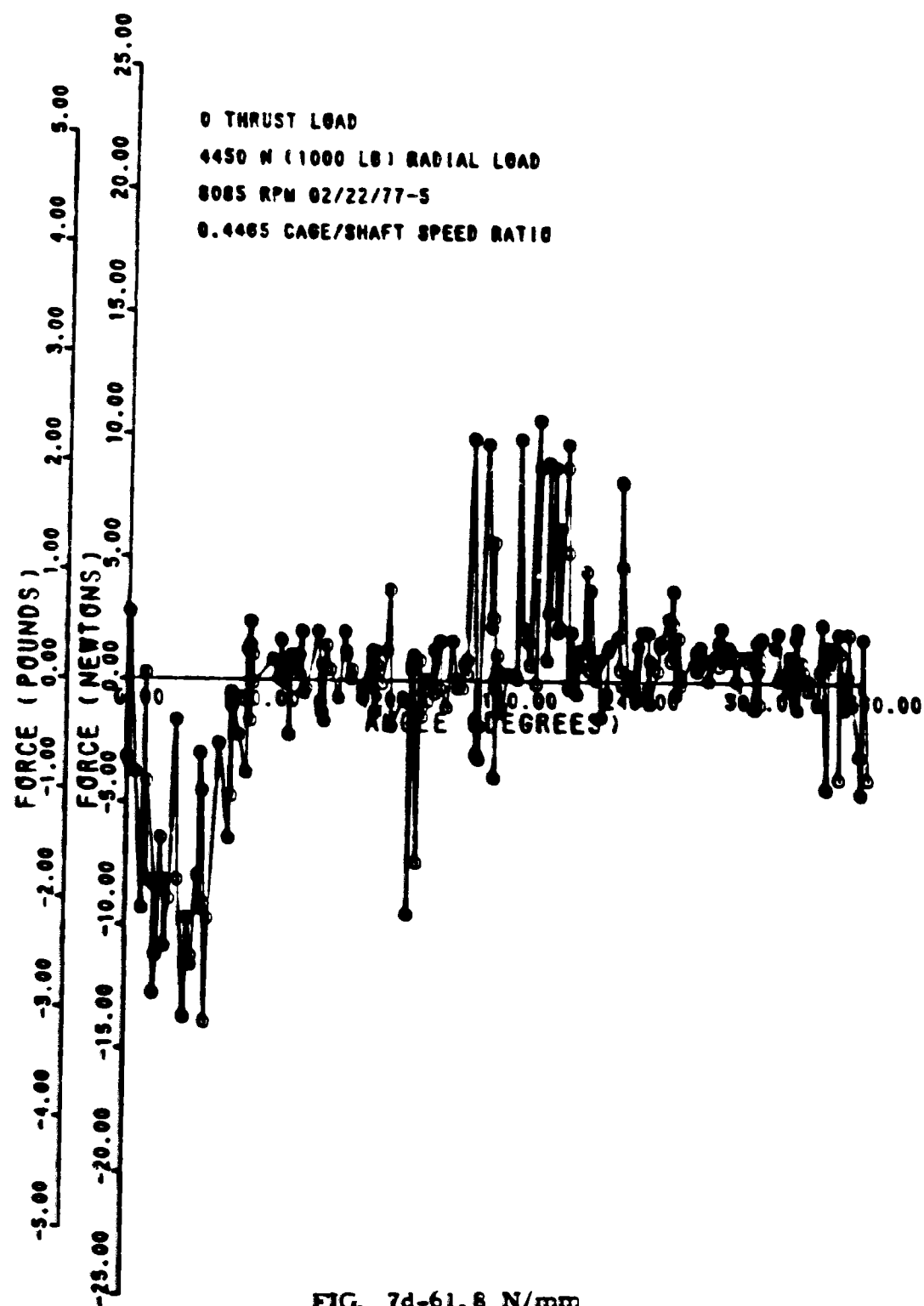


FIG. 7d-17.2 N/mm

7 0 0 3 0 0 0 6 0 5 0 0 0 6

06/01/77



700-0-11-93NFA-N-06/16/77

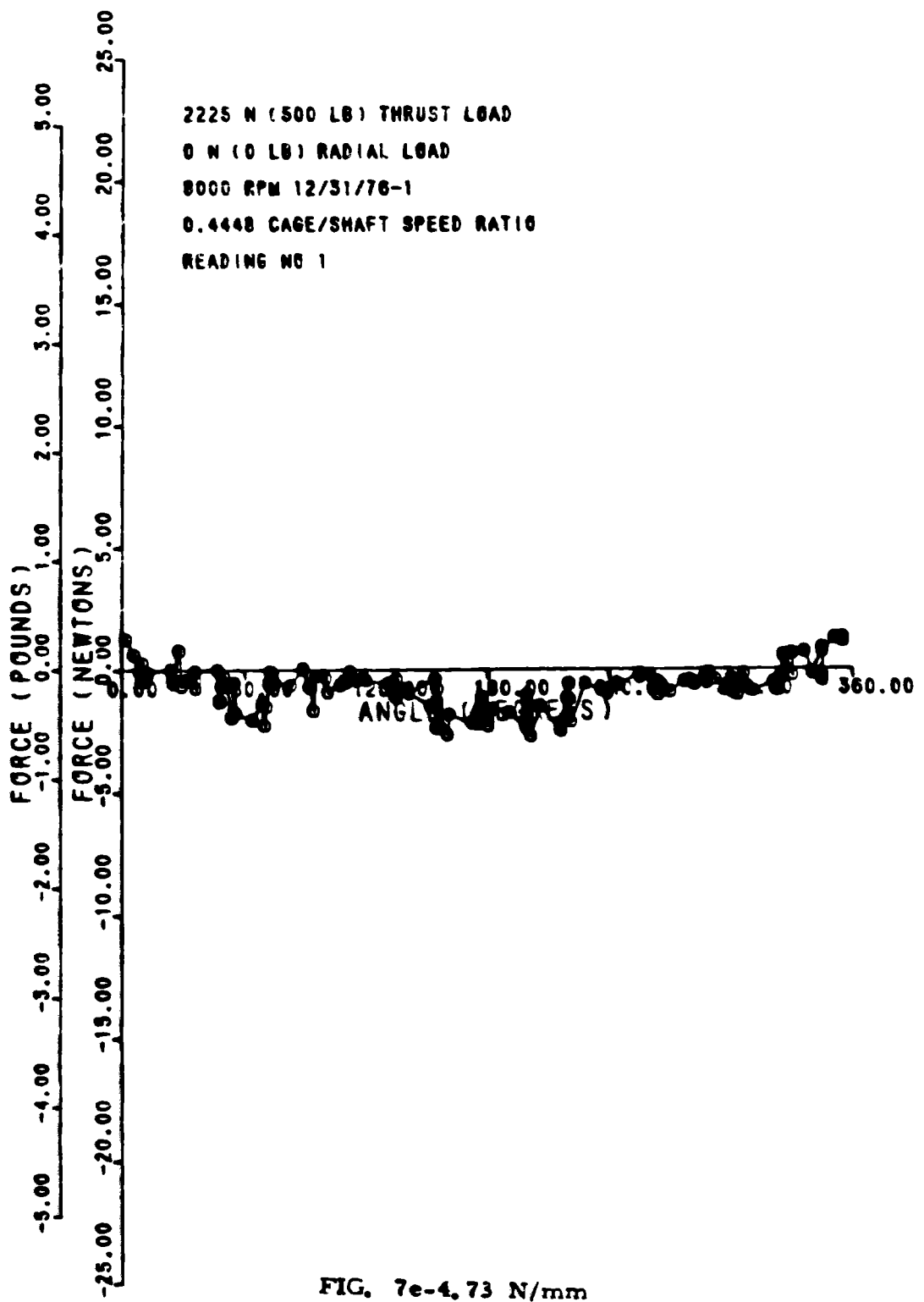


FIG. 7e-4. 73 N/mm

70090119 NY PAN 12 02/23/77

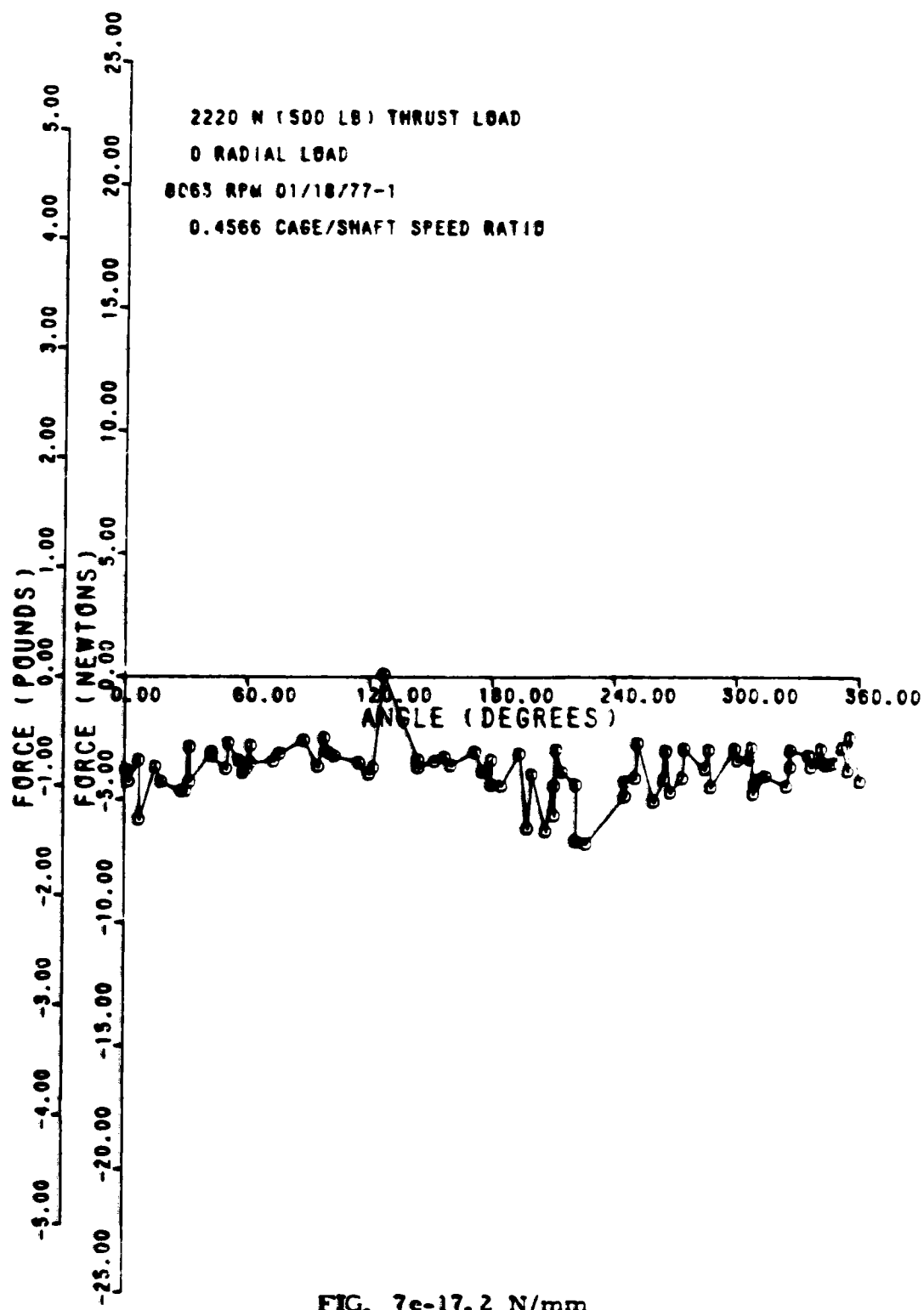
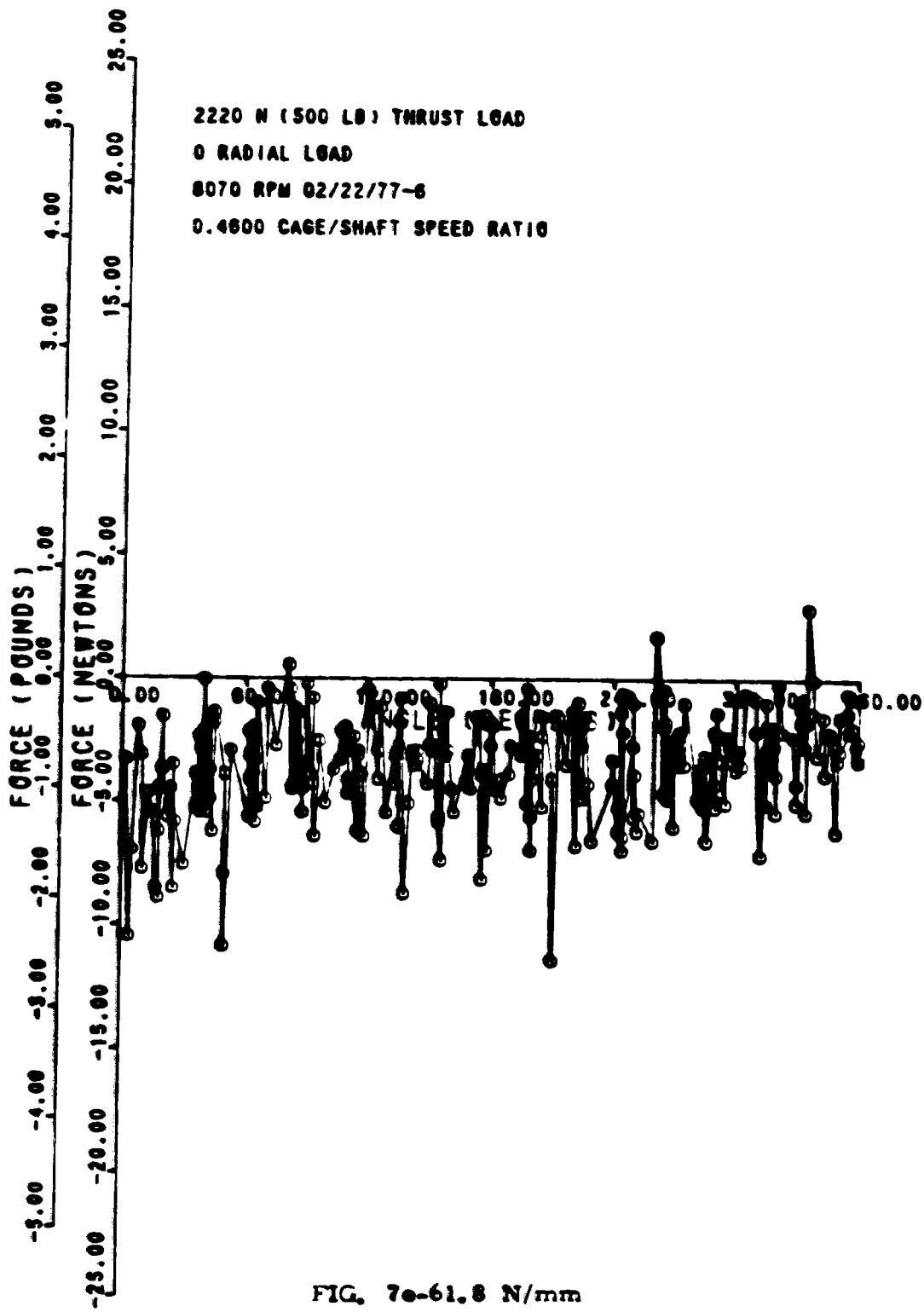


FIG. 7e-17.2 N/mm

WINDING UP IN YPA IN 7

03/17/77



TESTING 1 2 IN Y-A-N-8

06/15/77

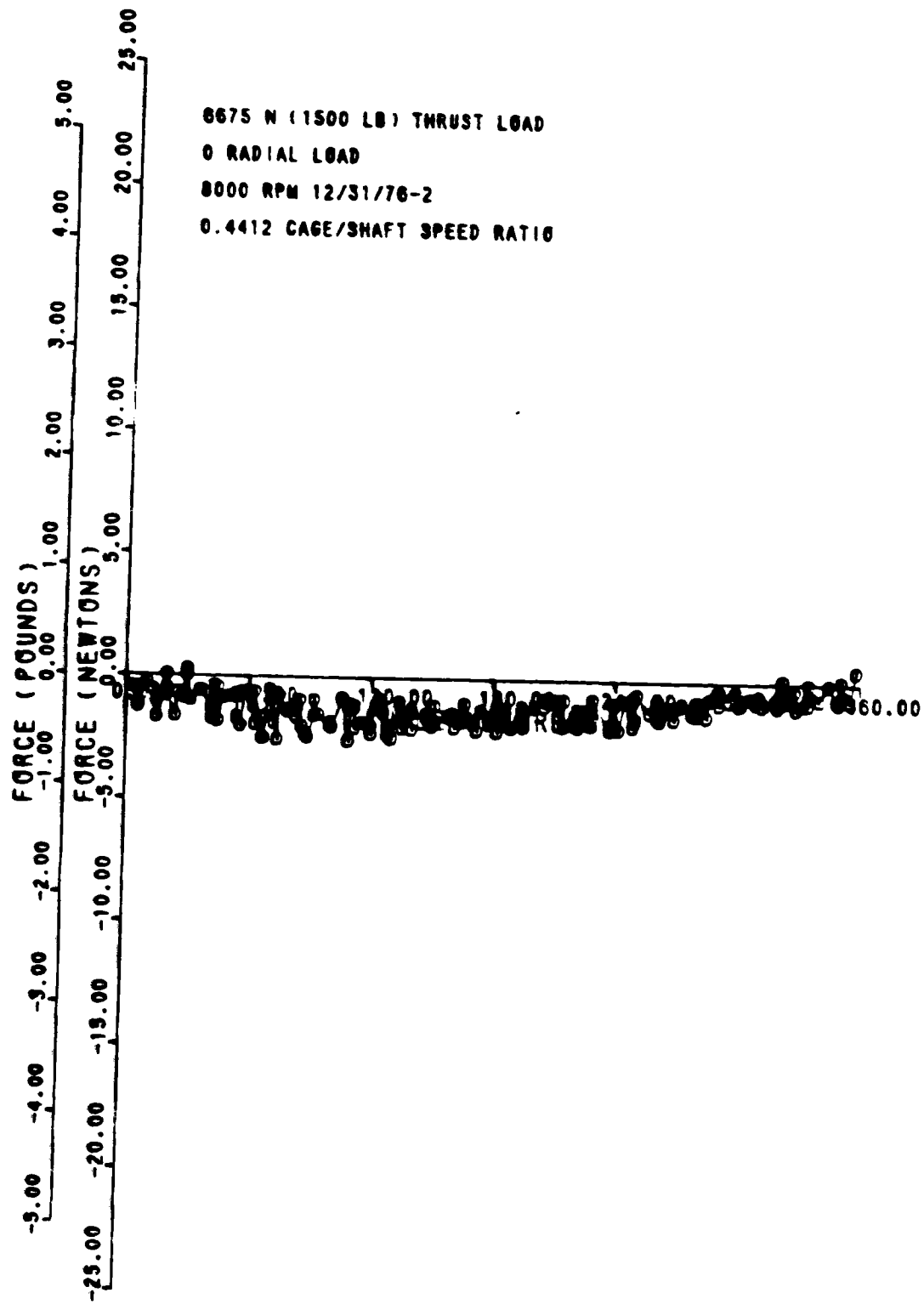
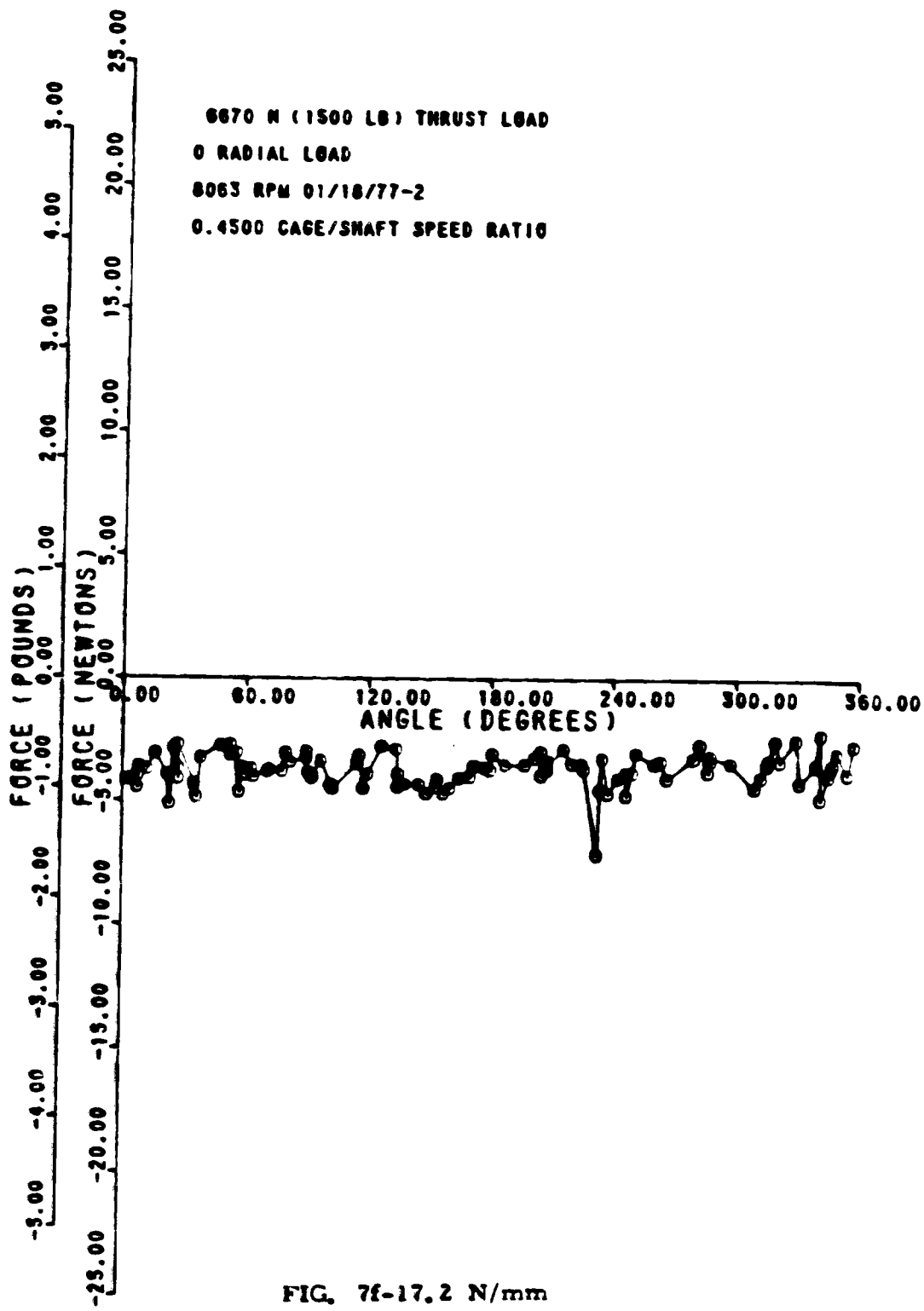


FIG. 7E-4.73 N/mm

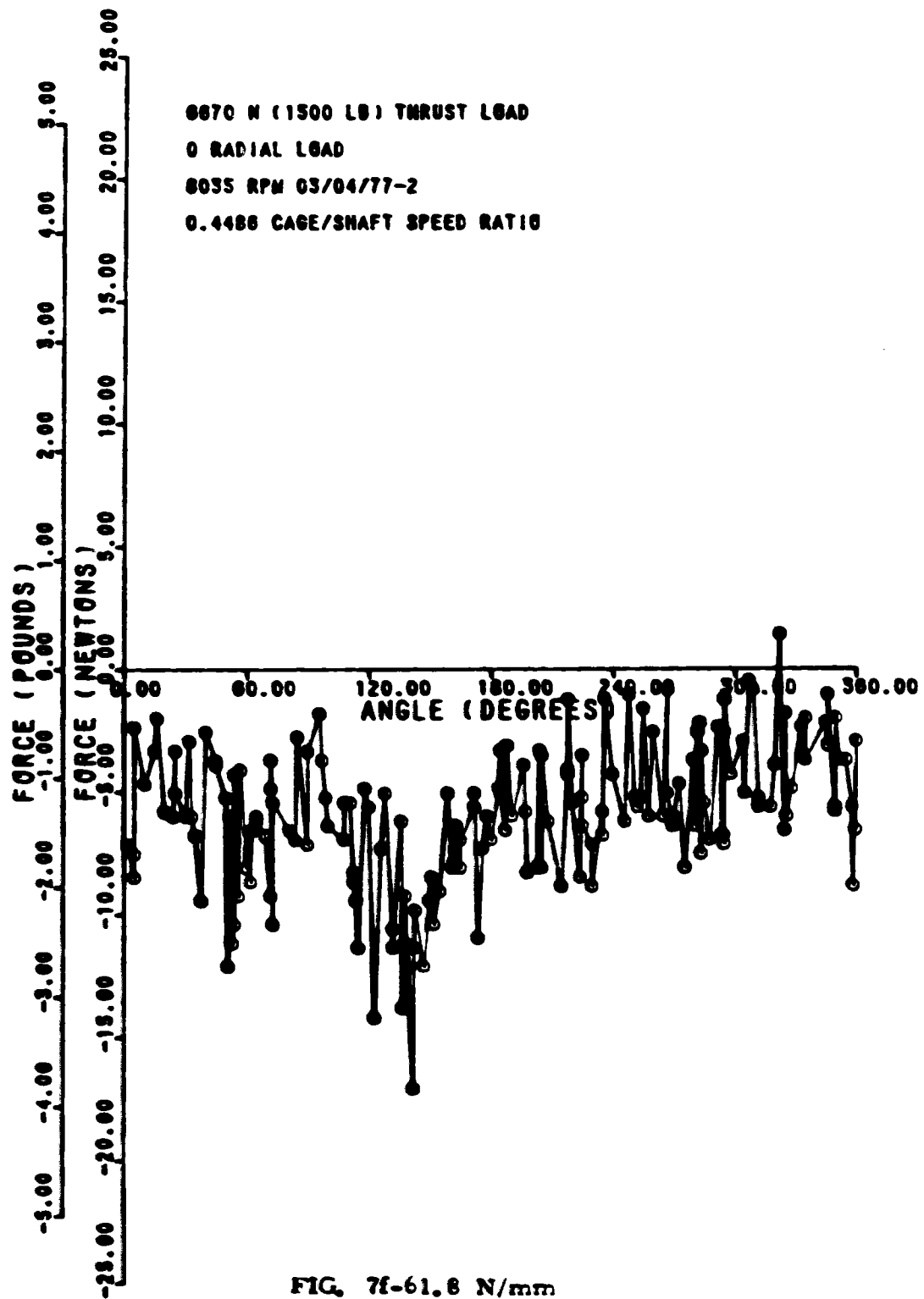
70-2507-1 TIGHTENING

02/23/77



03/19/77

70090119INYFANZ



7/0/93 01:44:47 AM PT
07/14/77

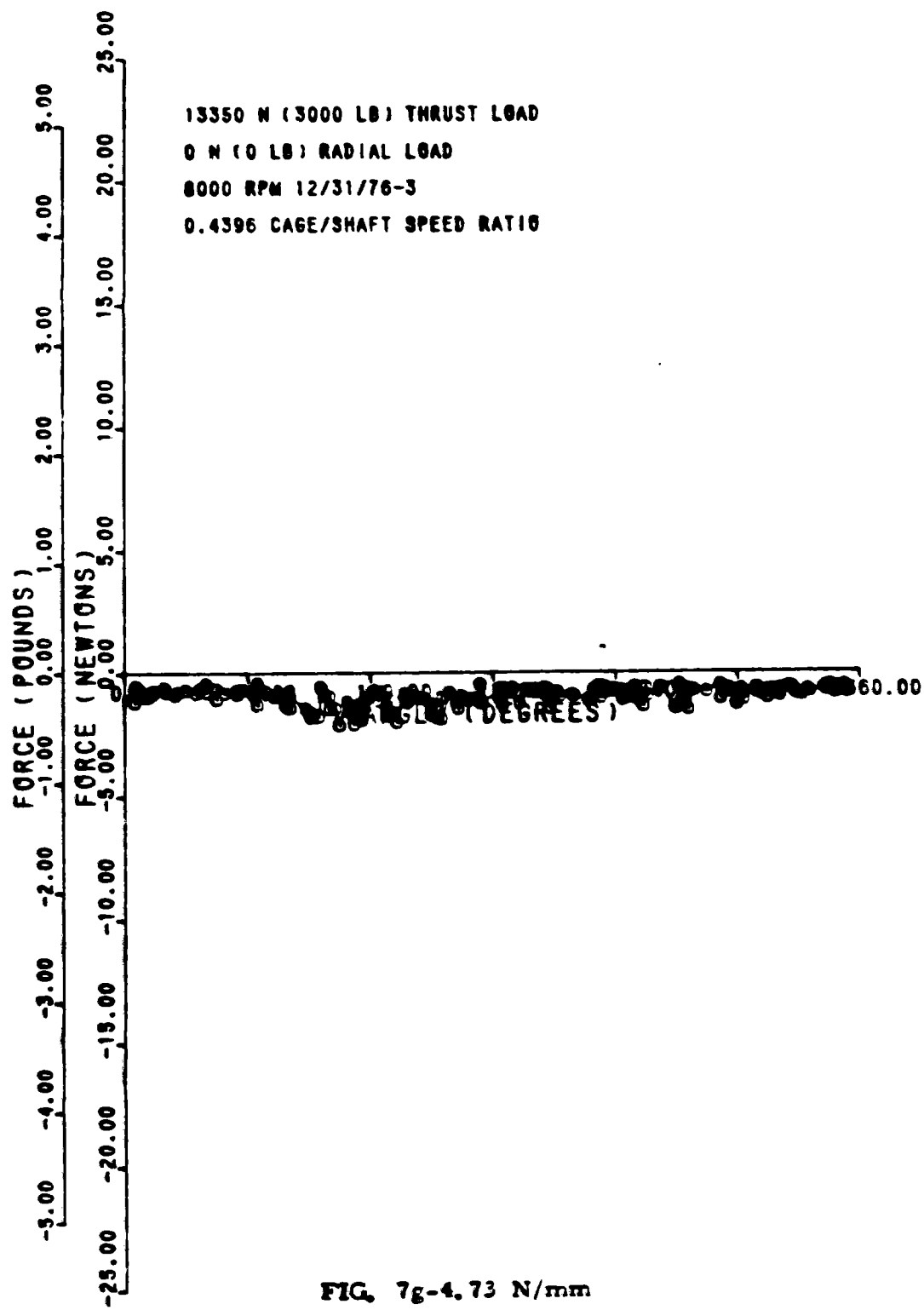


FIG. 7g-4.73 N/mm

7005019NYPANTT 02/23/77

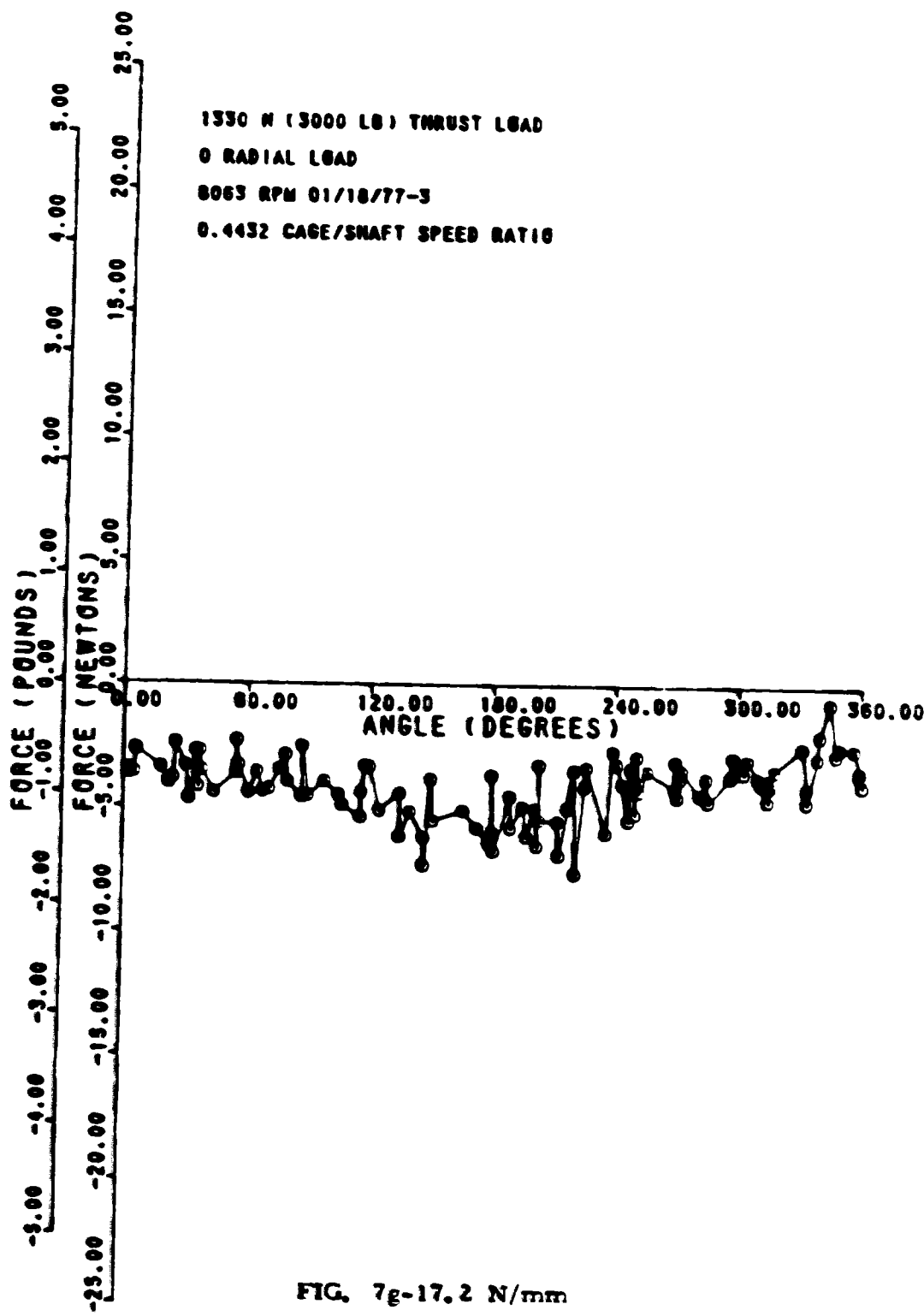
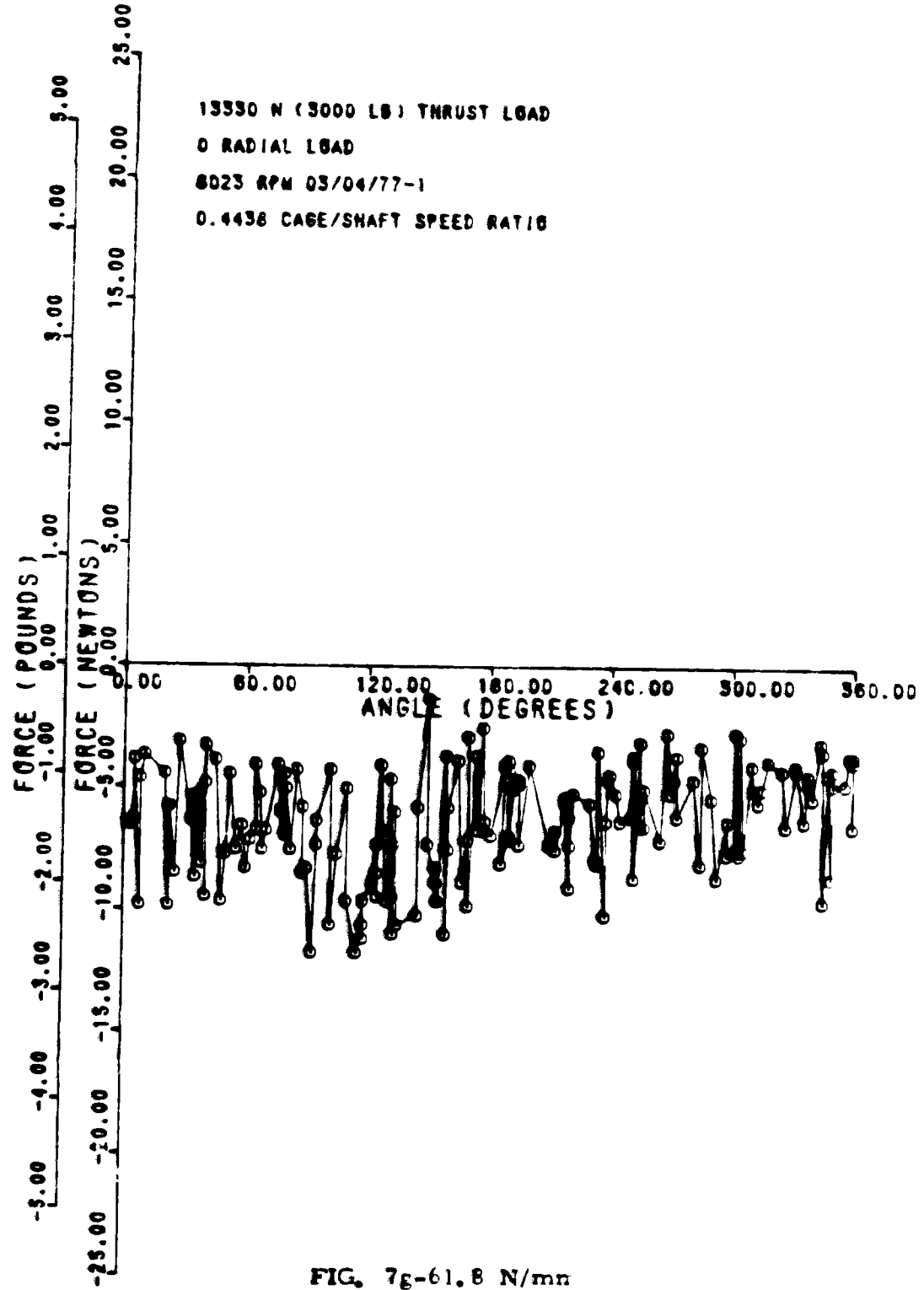


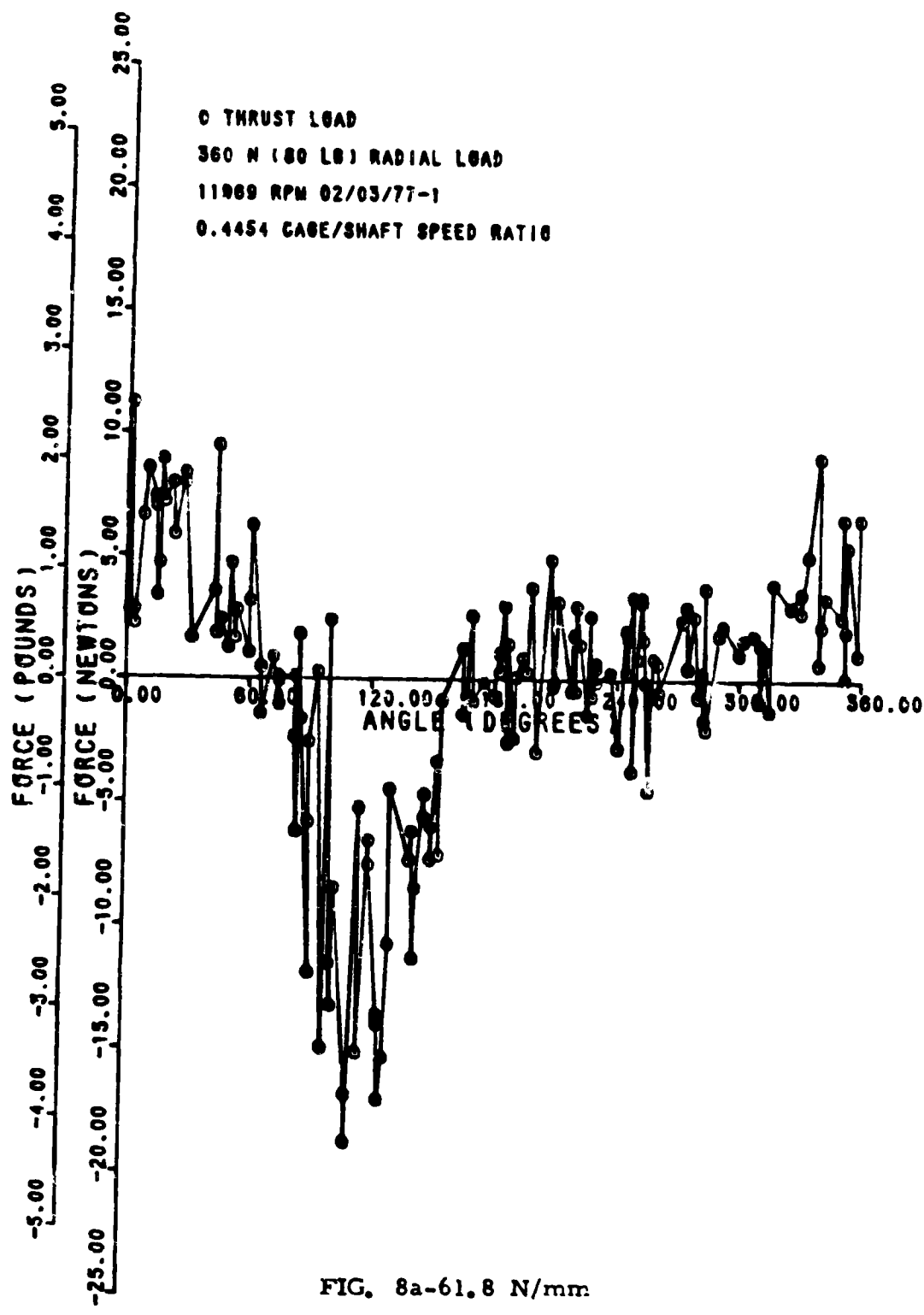
FIG. 7g-17.2 N/mm

170090119 NY PAN 5

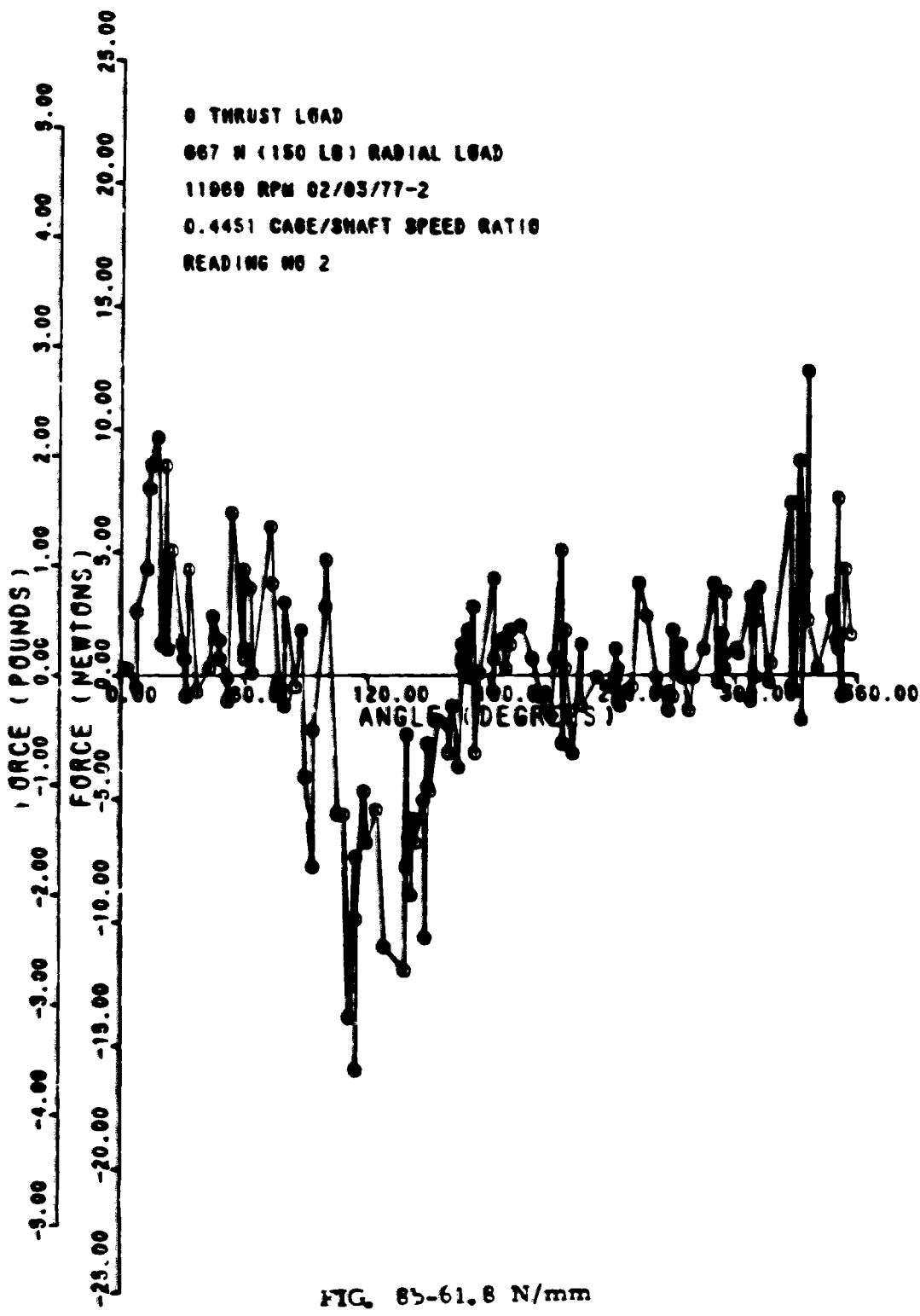
03/12/77



06/13/77

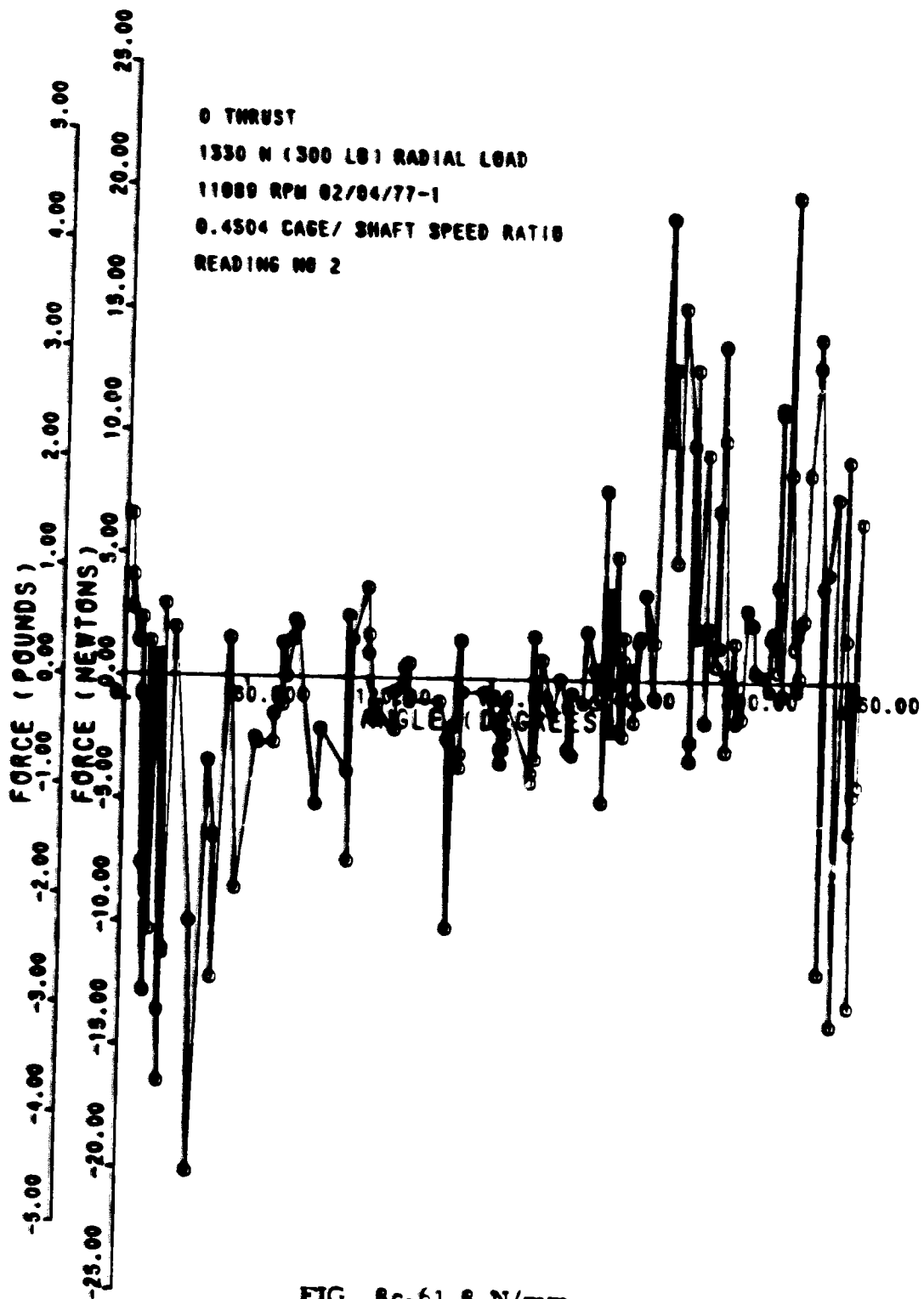


DATA SHEET FOR TEST NO. 06/14/77



T G G O 0 0 1 1 9 N Y F A N 5

06/17/77



700907 TUNNYPANN

06/14/77

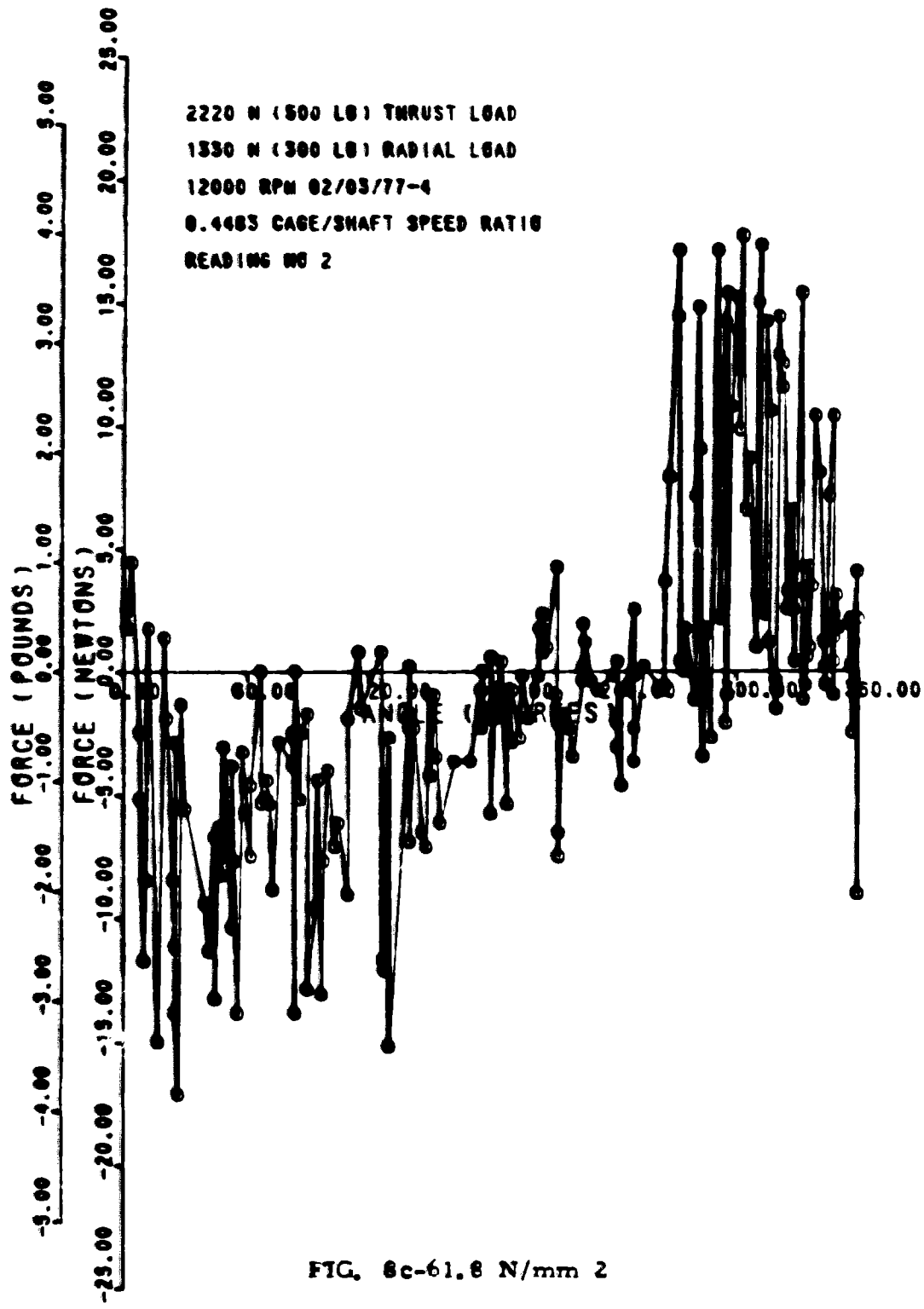


FIG. Sc-61.8 N/mm 2

70030119NYPAIN4

03/11/77

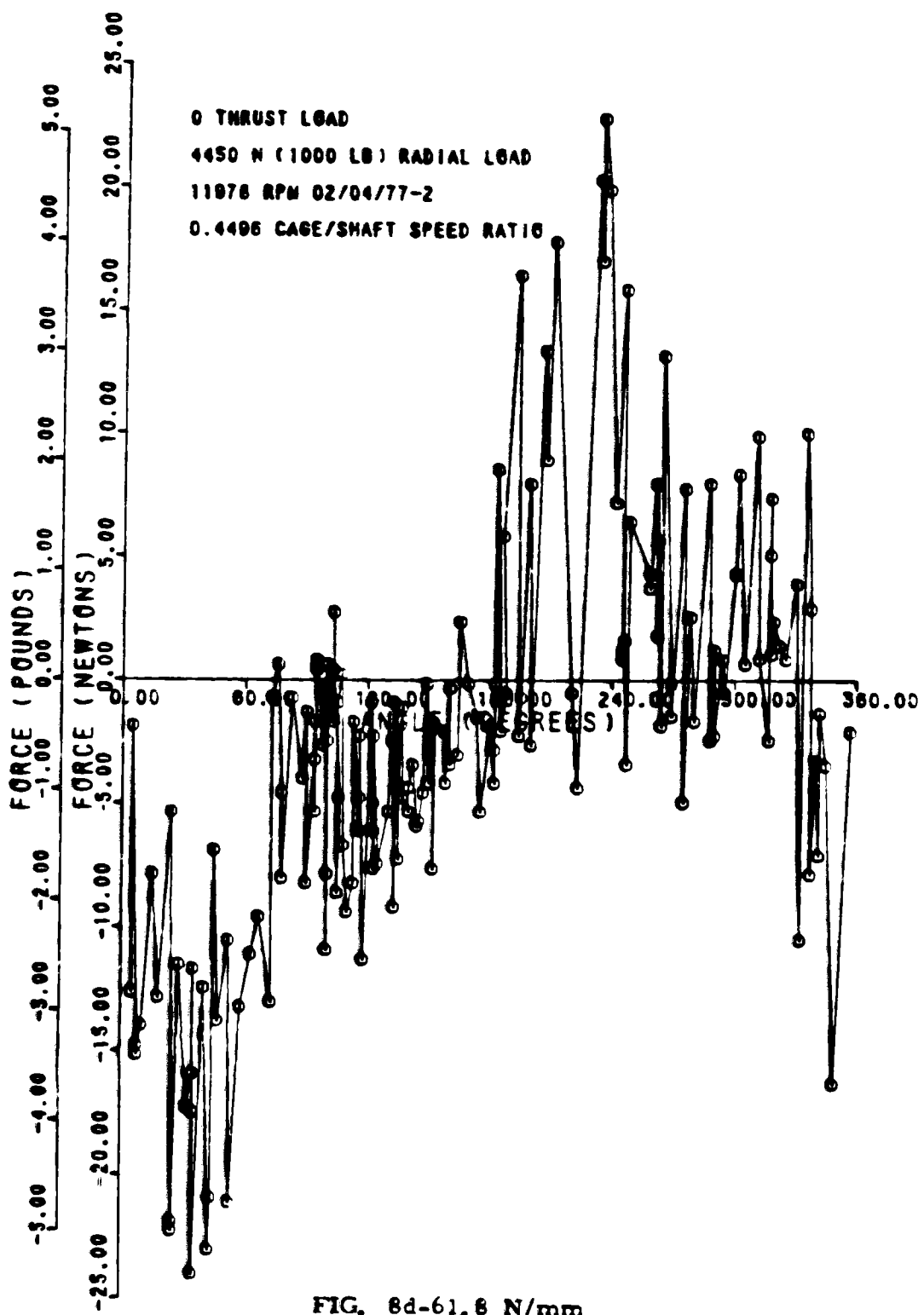
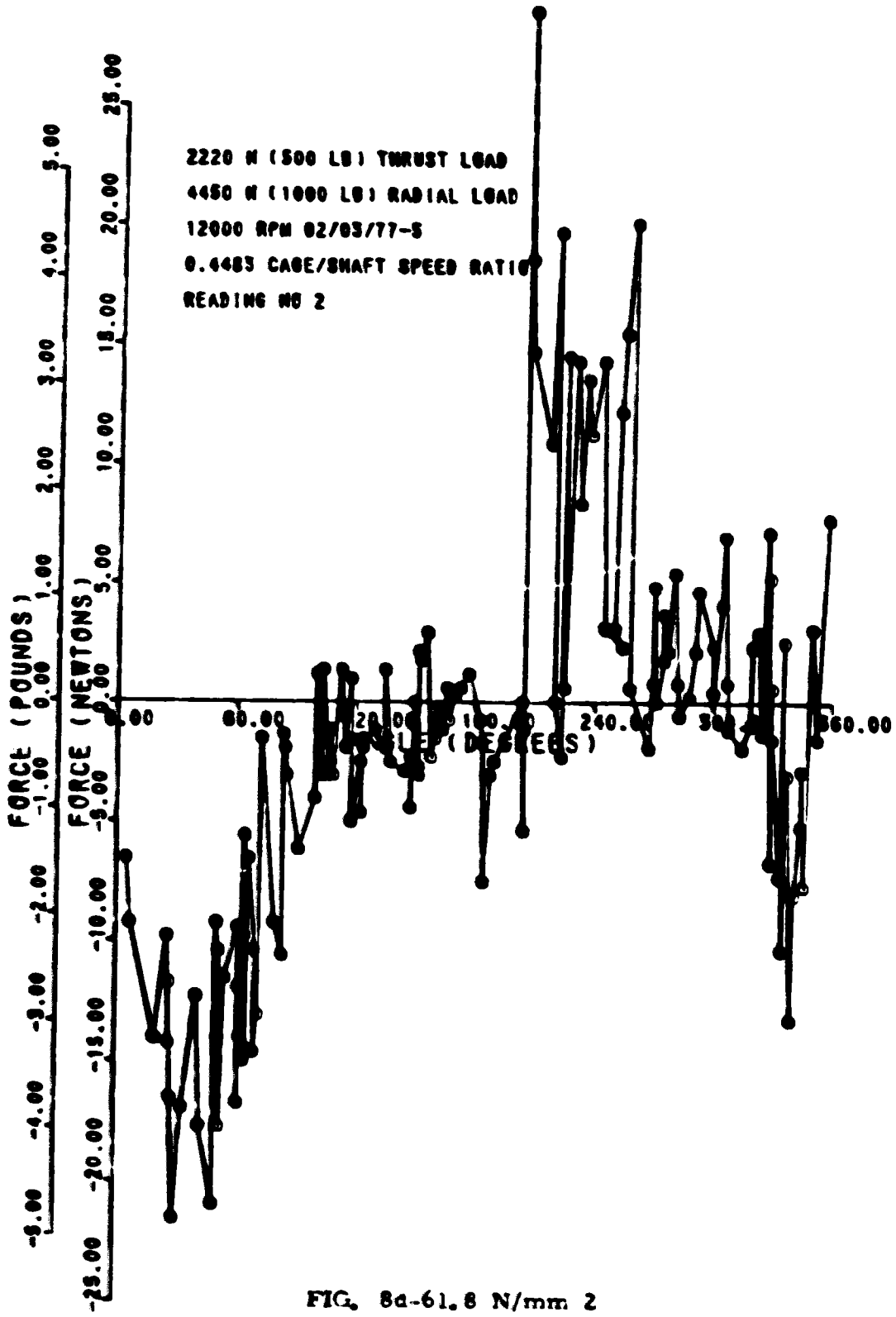


FIG. 8d-61.8 N/mm

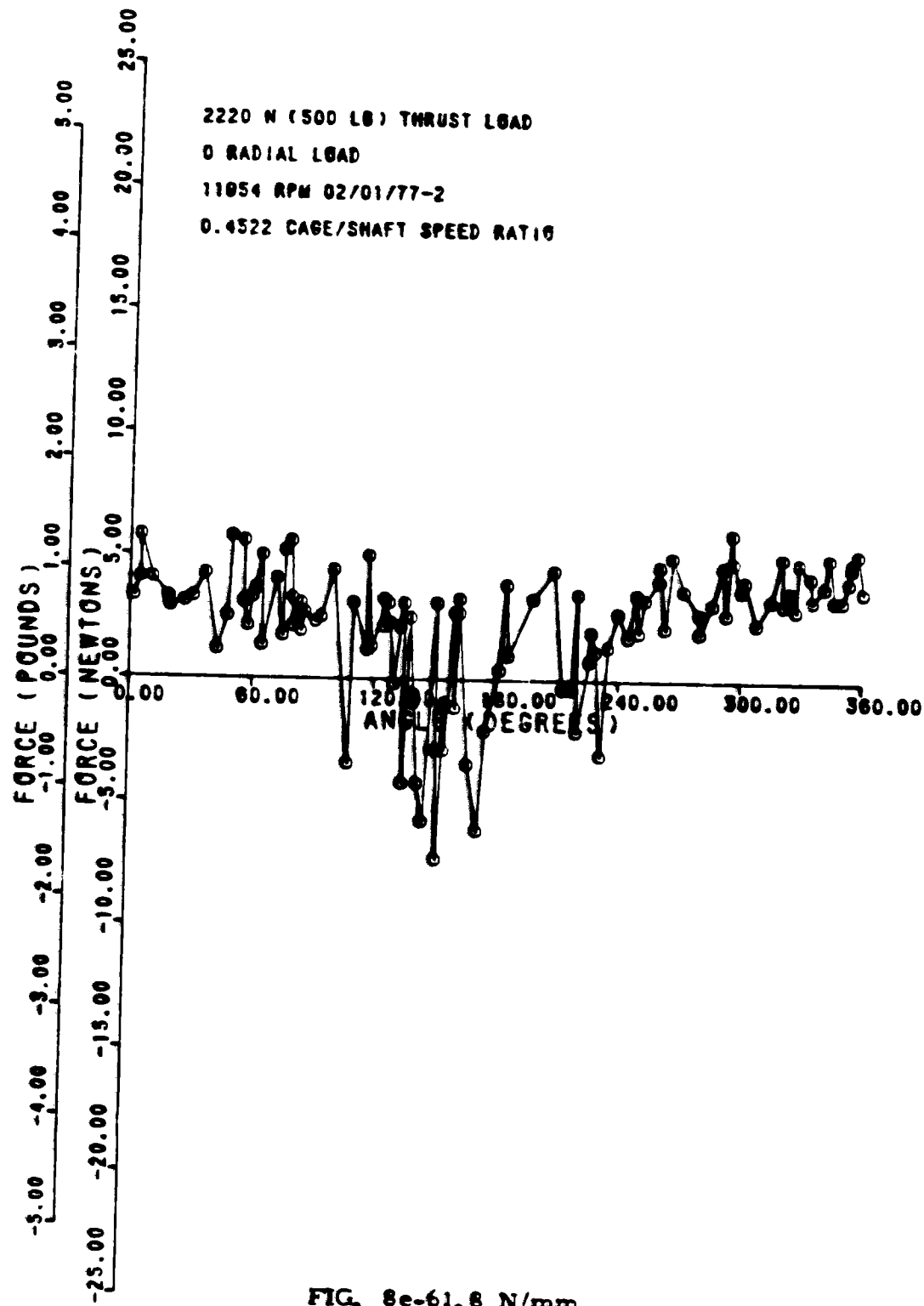
7000 6000 5000 4000 3000 2000 1000 0 -1000 -2000 -3000 -4000 -5000 -6000 -7000

06/13/77



700 ENGINEERING DRAWINGS

02/25/77



70000TITANTP

- - - 03/15/77

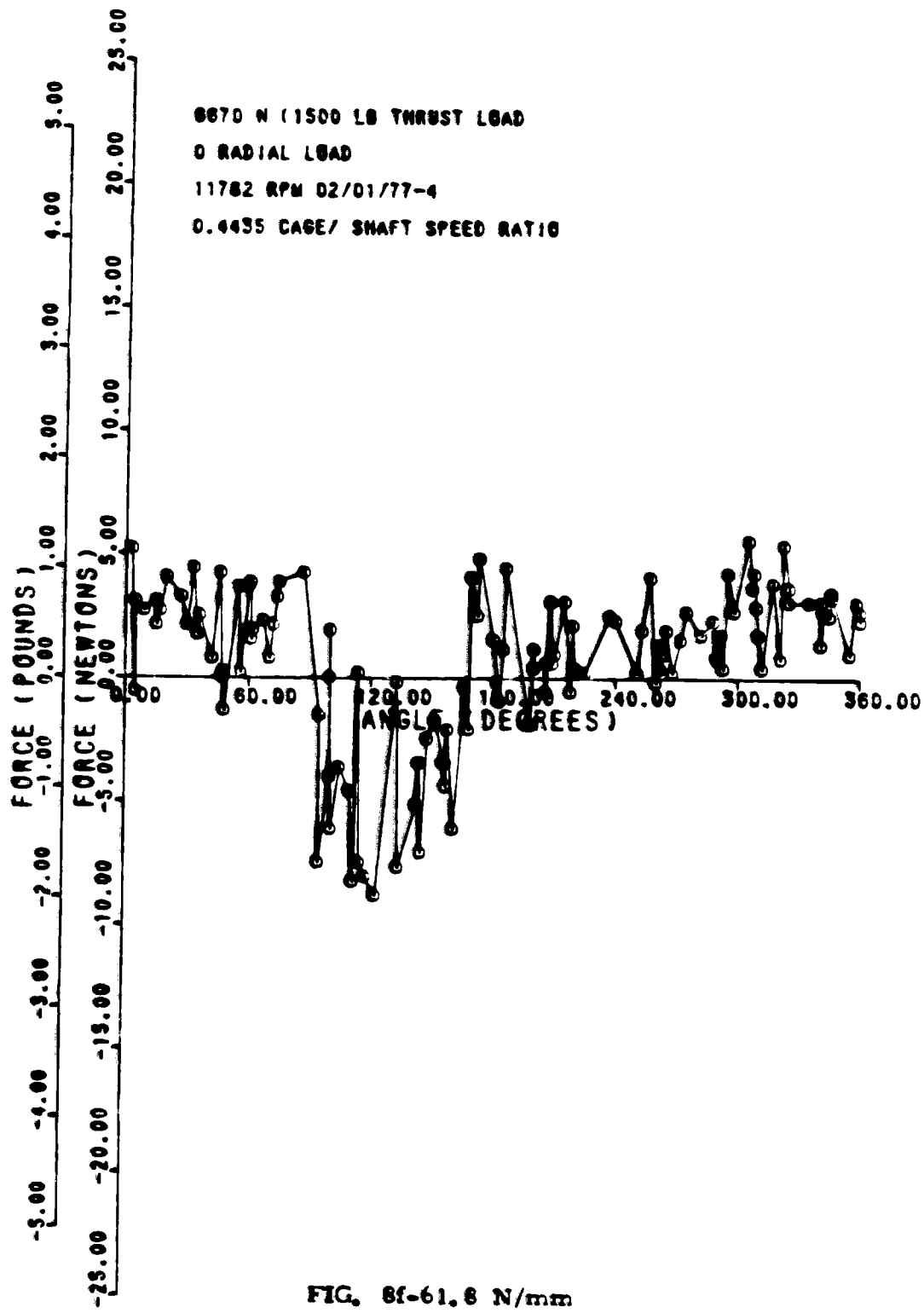
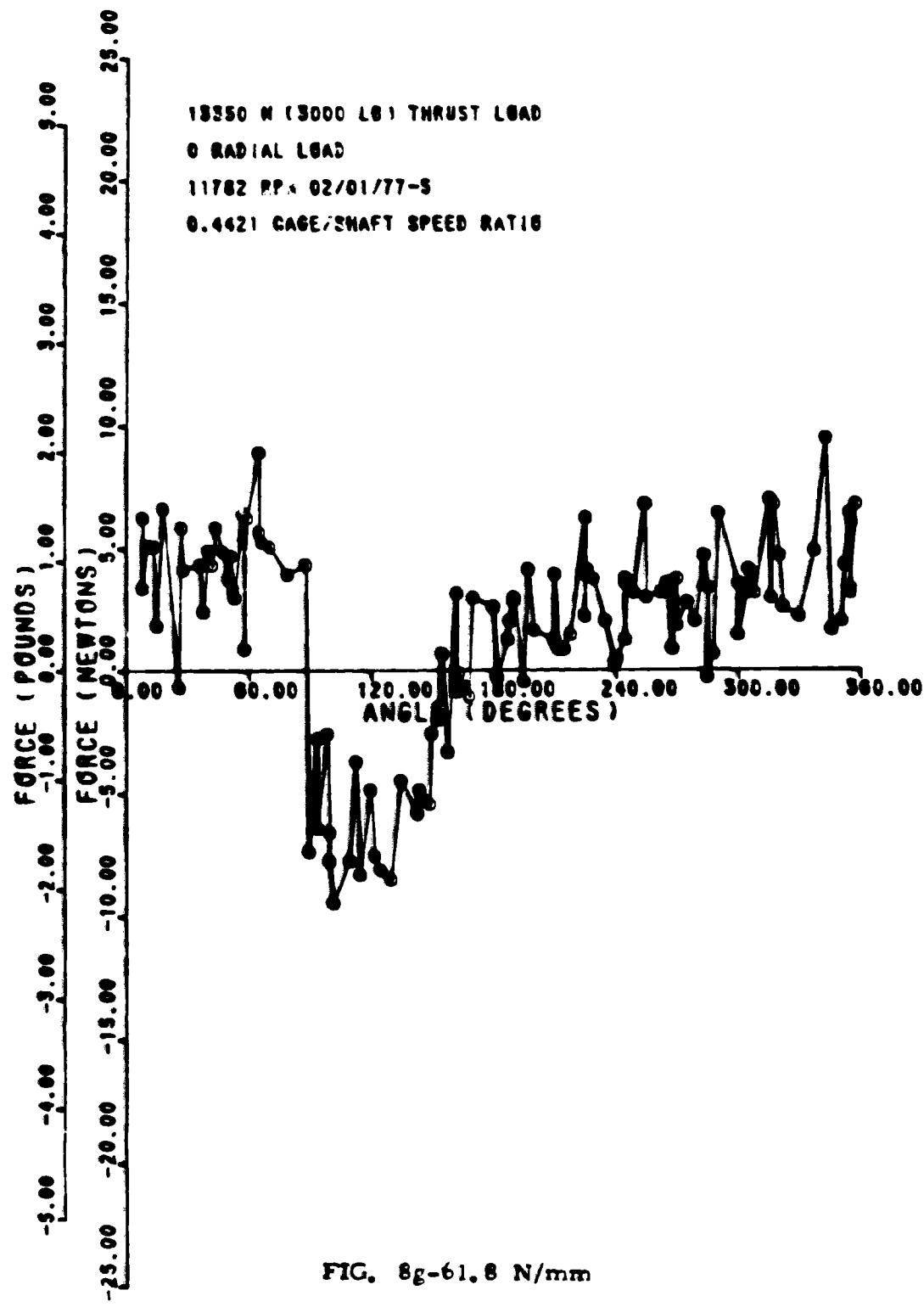


FIG. 8f-61.8 N/mm

06/11/77

THREE-DIMENSIONAL
UNBALANCE PATTERN



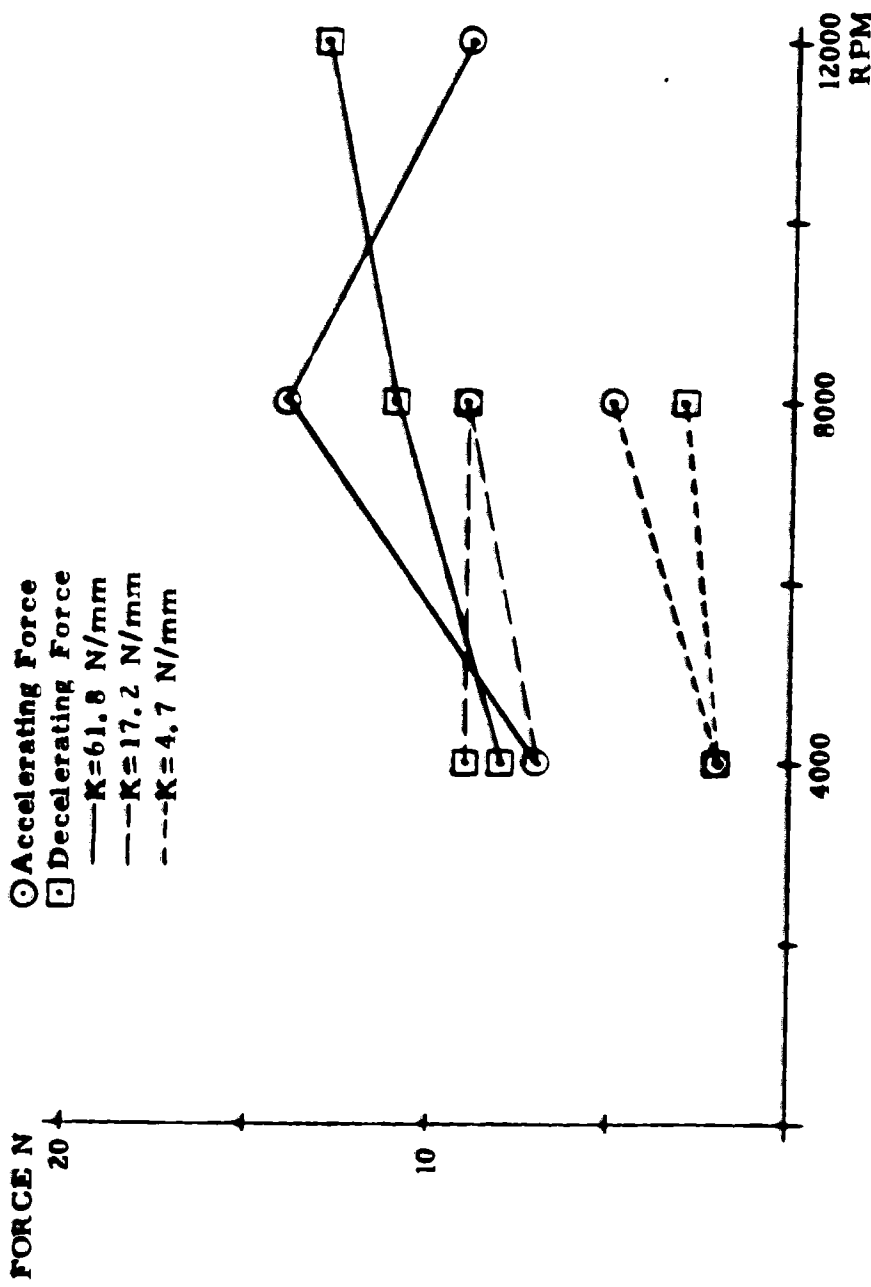


FIGURE 9a Cage Force Magnitude Versus Shaft Speed, 360 N Radial Load

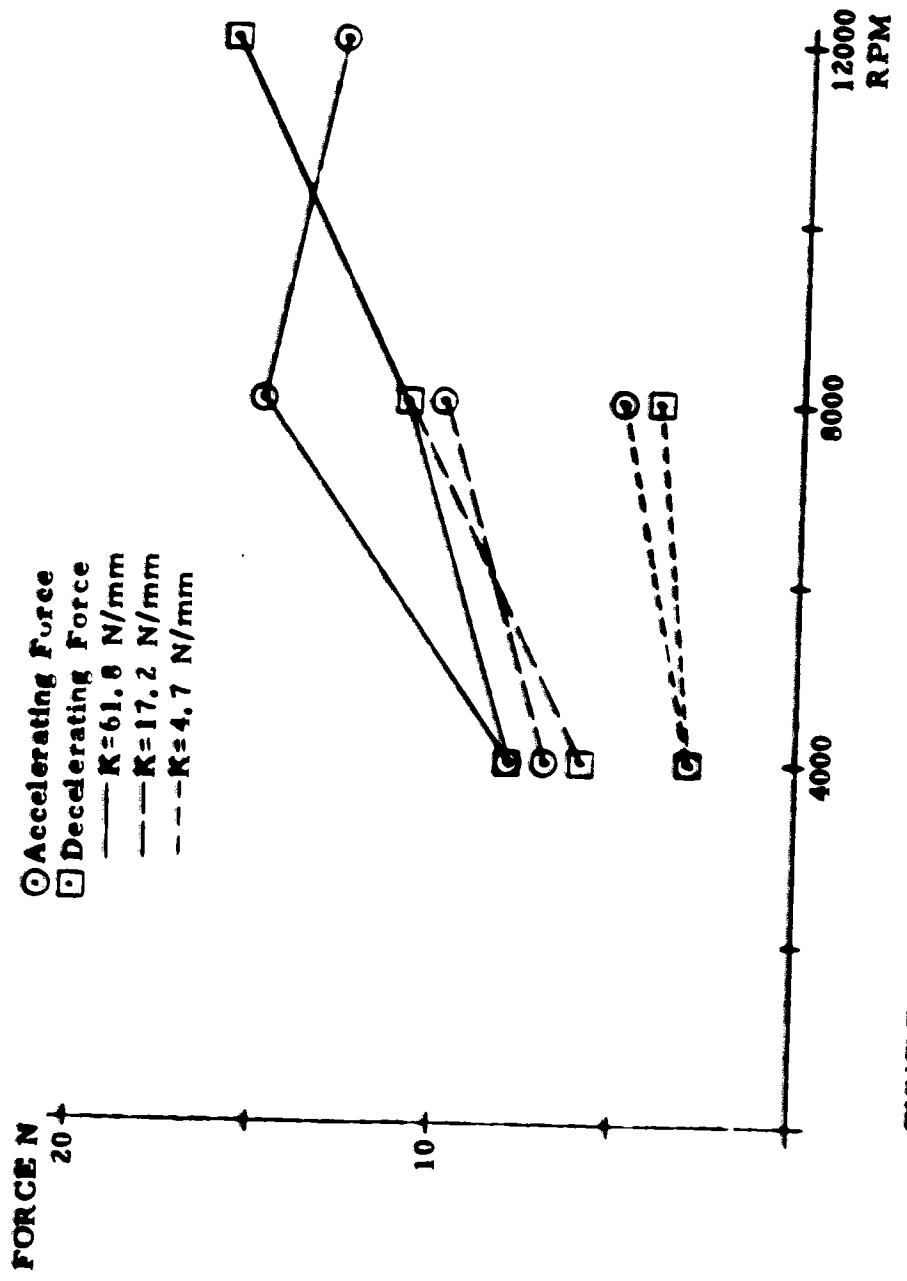


FIGURE 9b Cage Force Magnitude Versus Shaft Speed, 670 N Radial Load

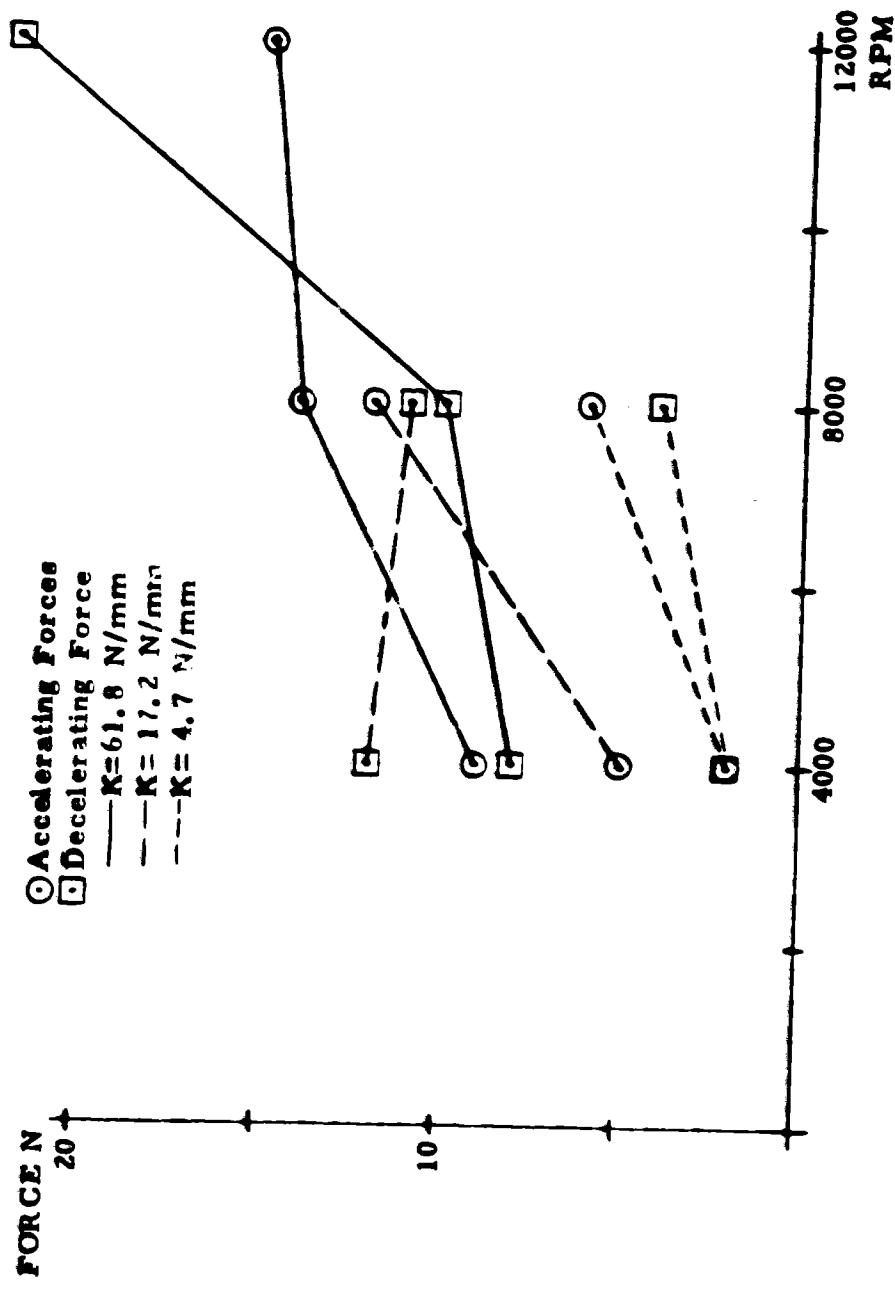


FIGURE 9c Cage Force Magnitude Versus Shaft Speed, 1330 N Radial Load

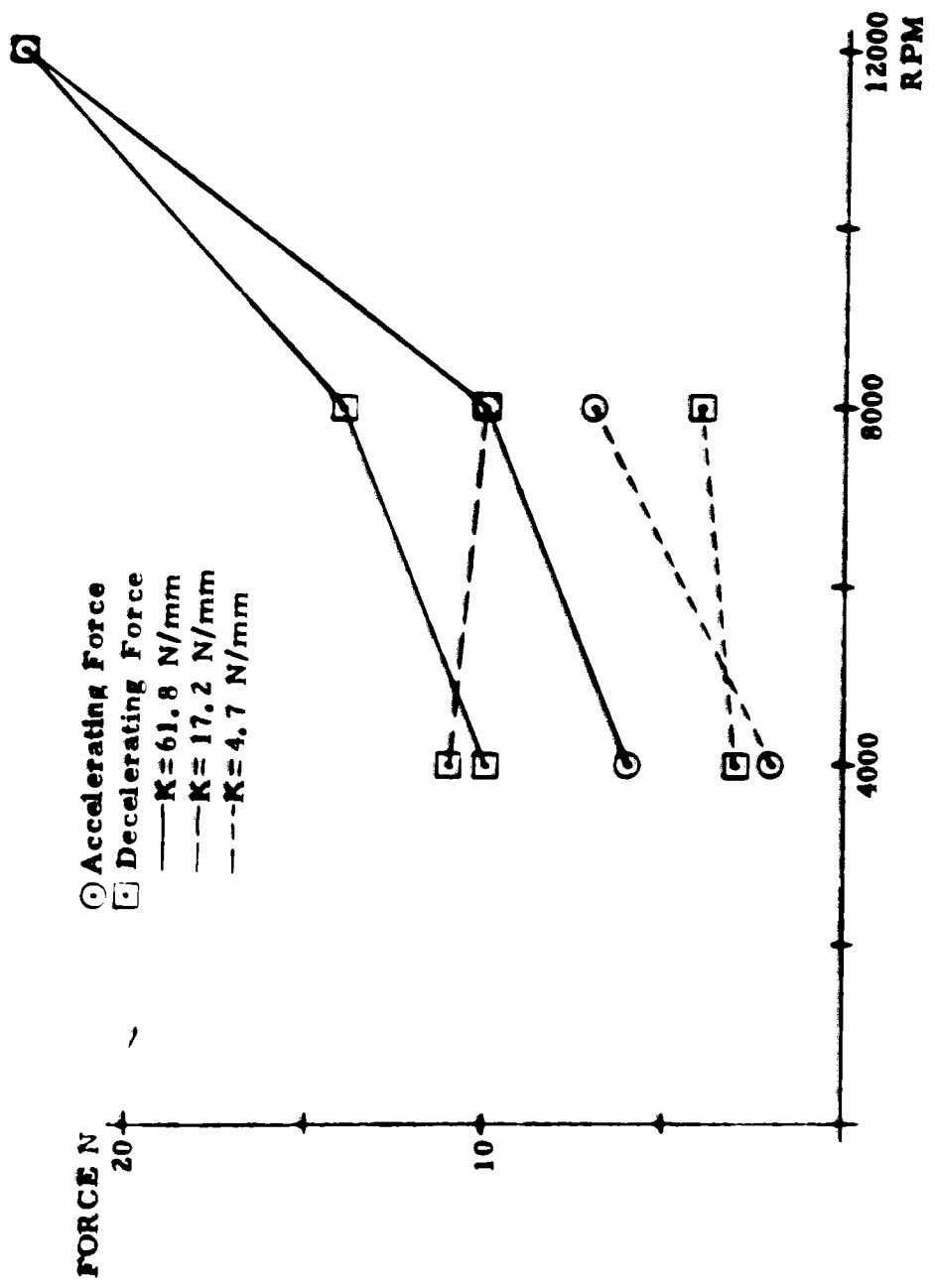


FIGURE 9d Cage Force Magnitude Versus Shaft Speed, 4450 N Radial Load

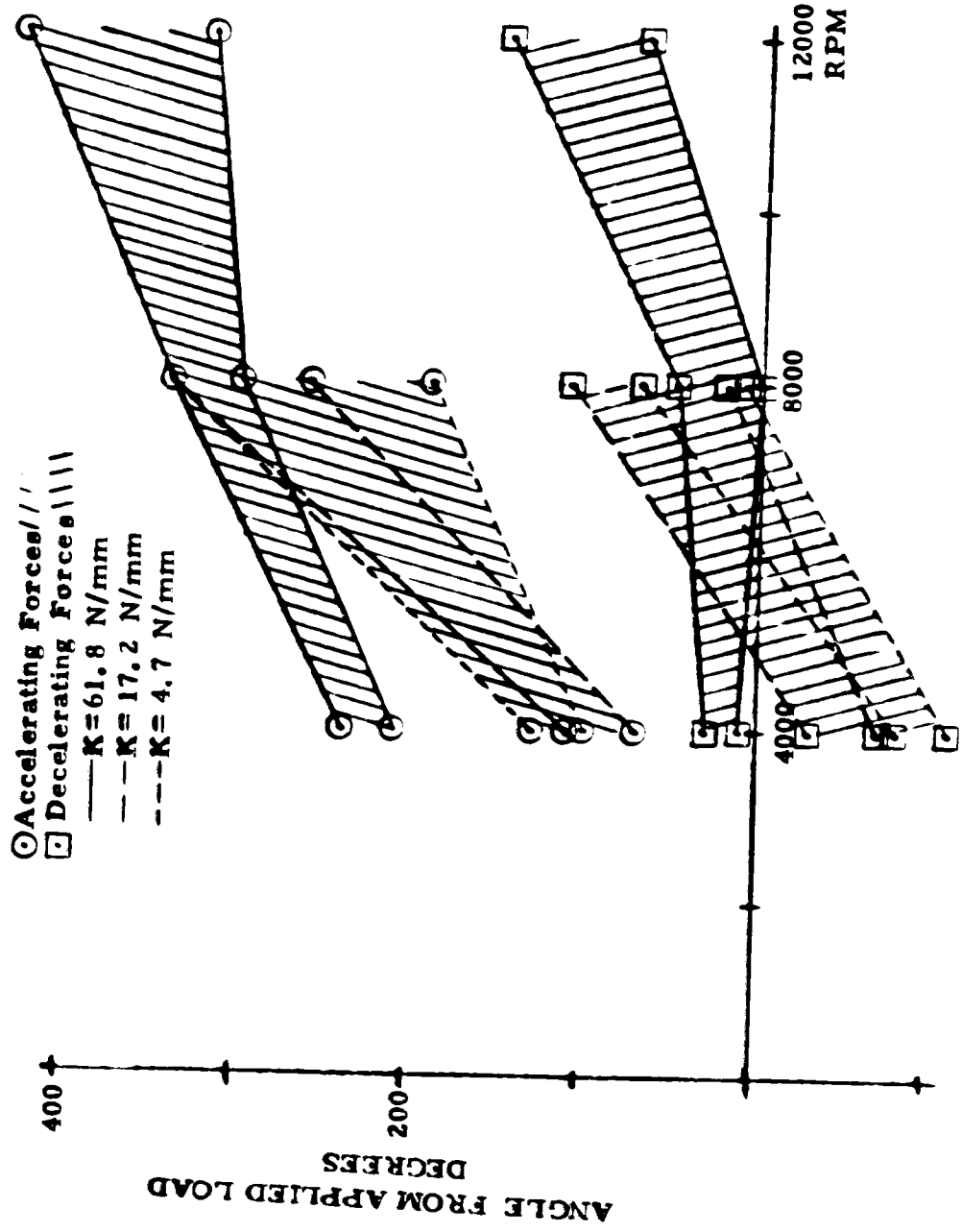


FIGURE 10a Locations of Accelerating and Decelerating Cage Forces as a Function of Shaft Speed, 360 N Radial Load

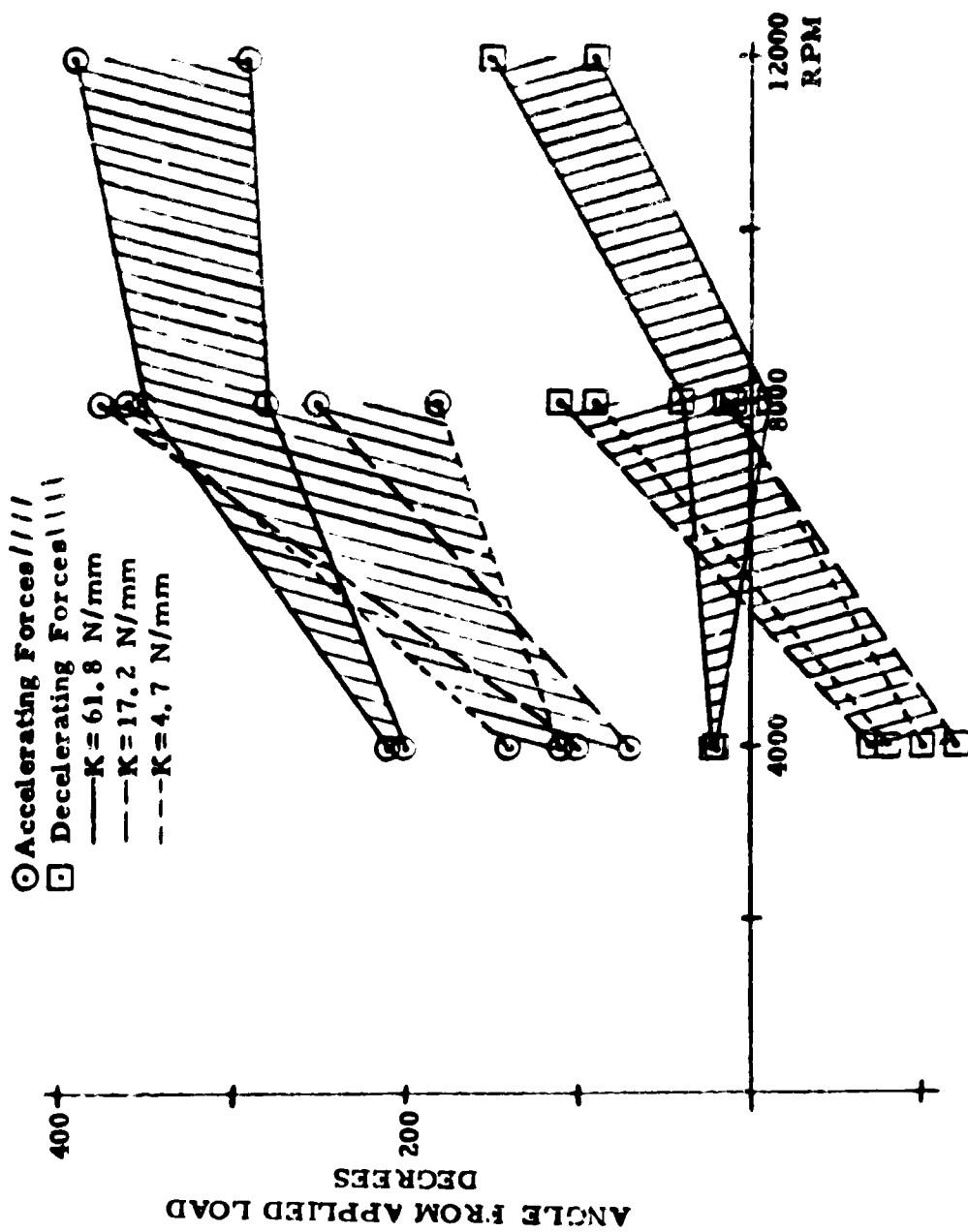
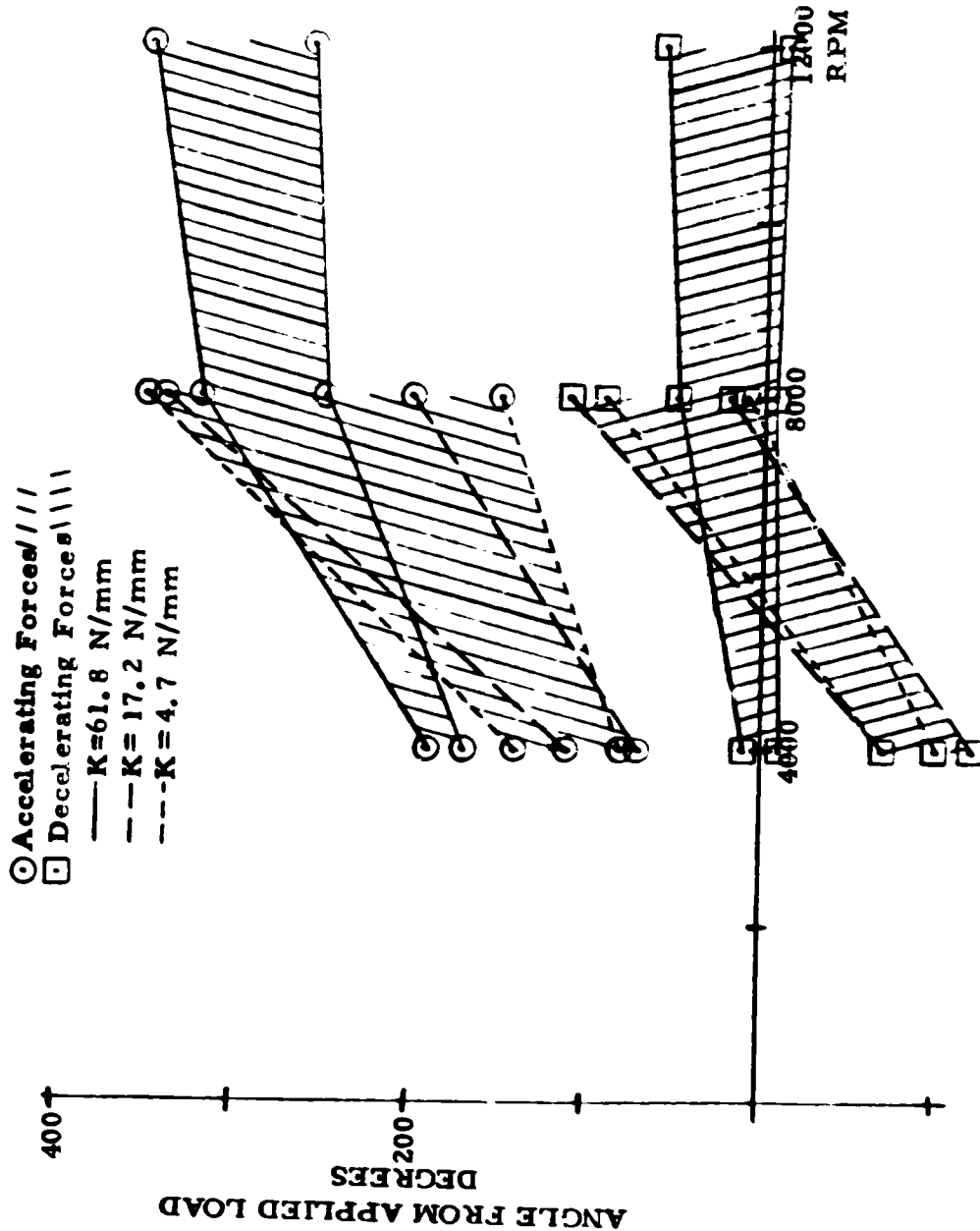


FIGURE 10b Locations of Accelerating and Decelerating Cage Forces as a Function of
Shaft Speed, 670 N Radial Load



PRECEDING PAGE BLANK NOT FILMED.

FIGURE 10c Locations of Accelerating and Decelerating Forces as a Function of Shaft Speed, 1330 N Radial Load

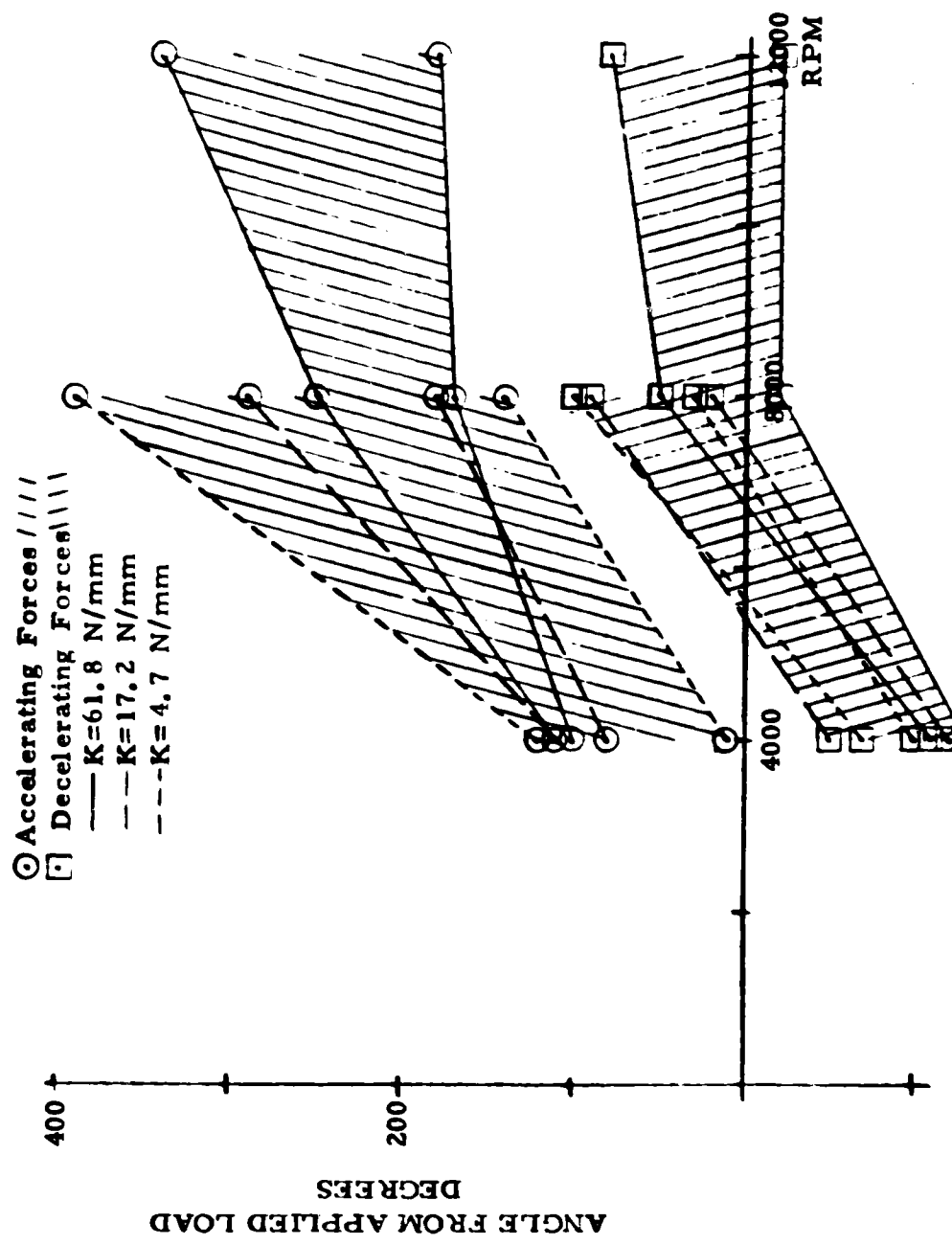
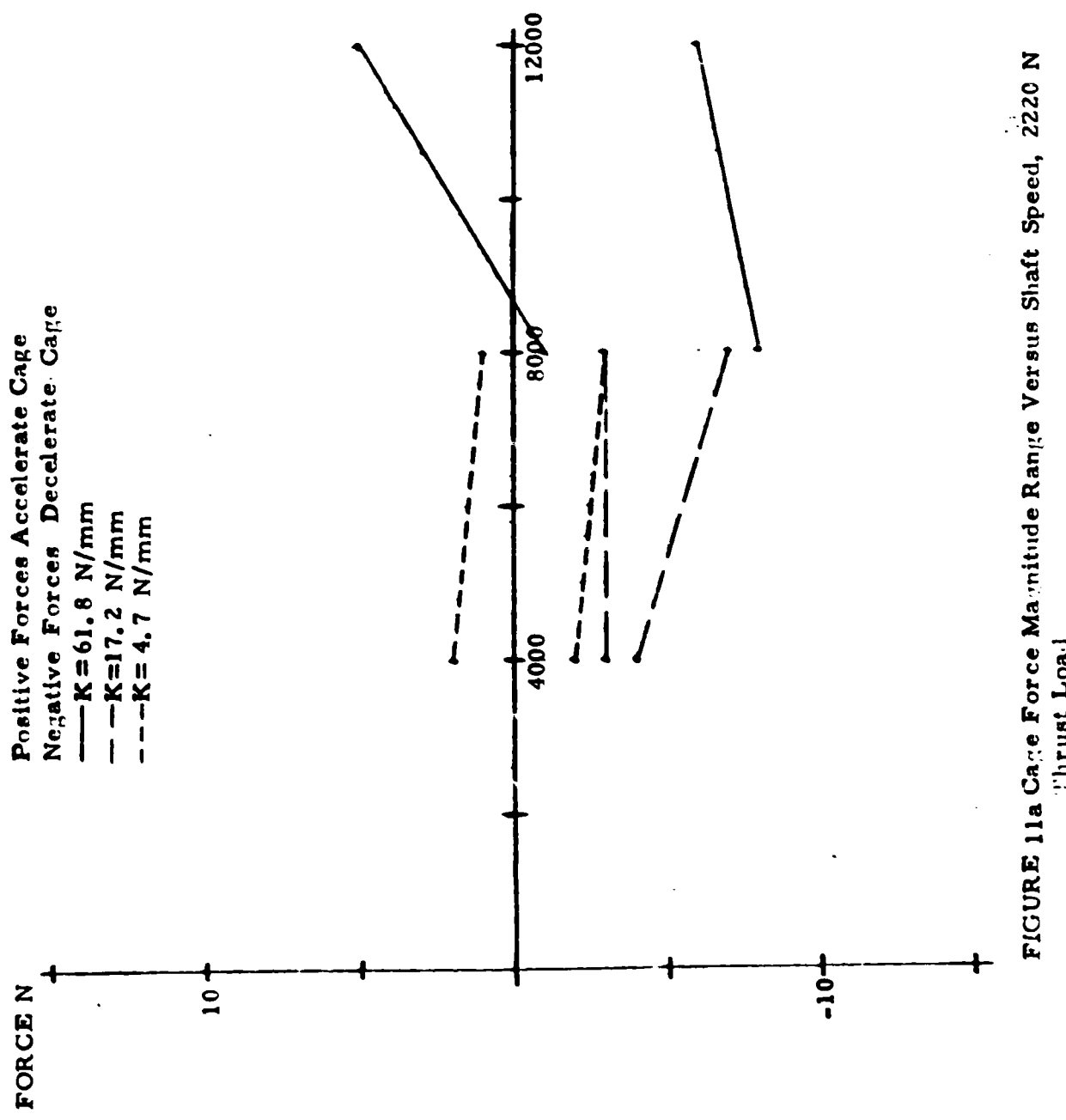


FIGURE 10d Locations of Accelerating and Decelerating Cage Forces as a Function of Shaft Speed, 4450 N Radial Load



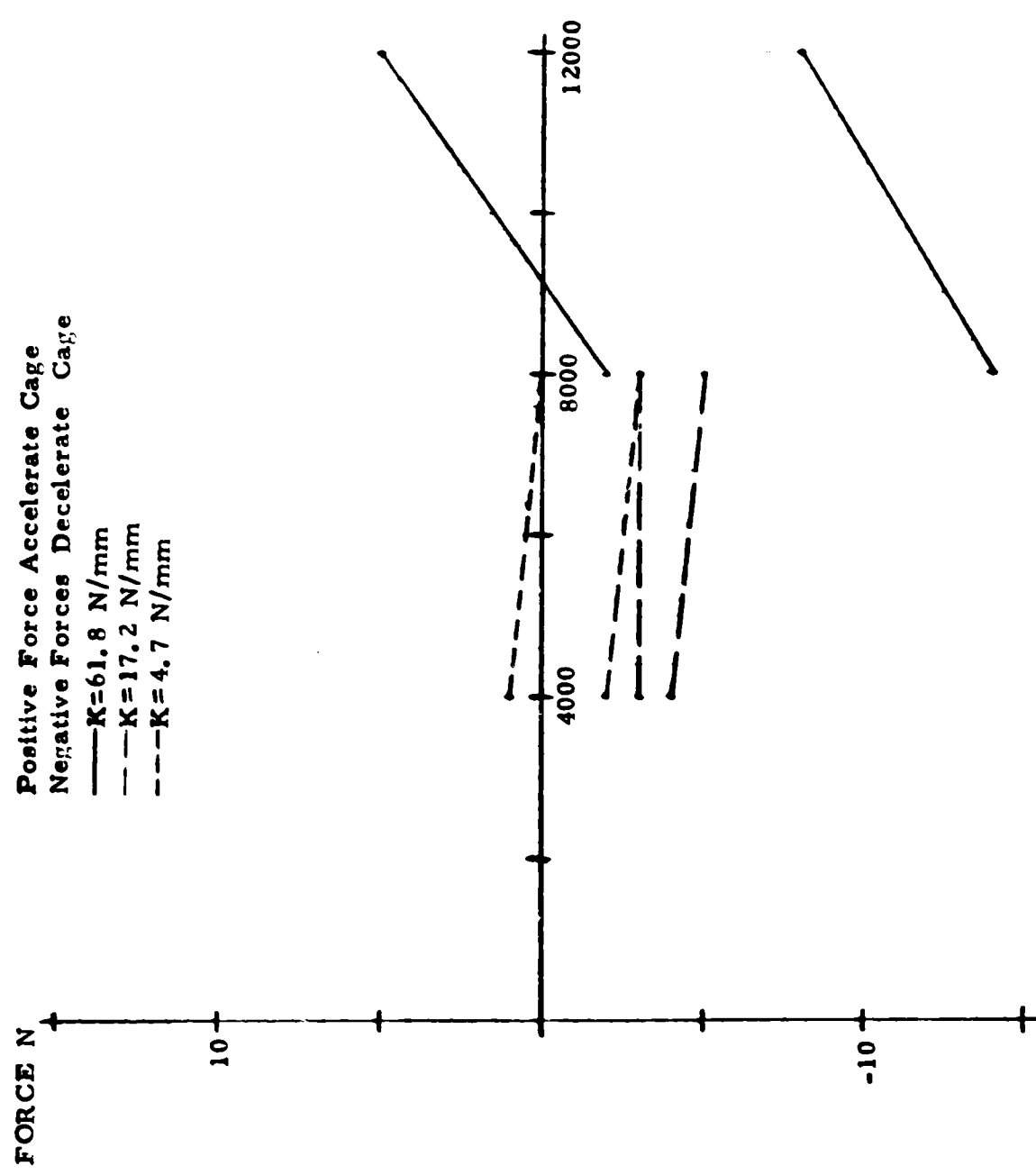


FIGURE 11b Cage Force Magnitude Range Versus Shaft Speed, 6670 N Thrust Load

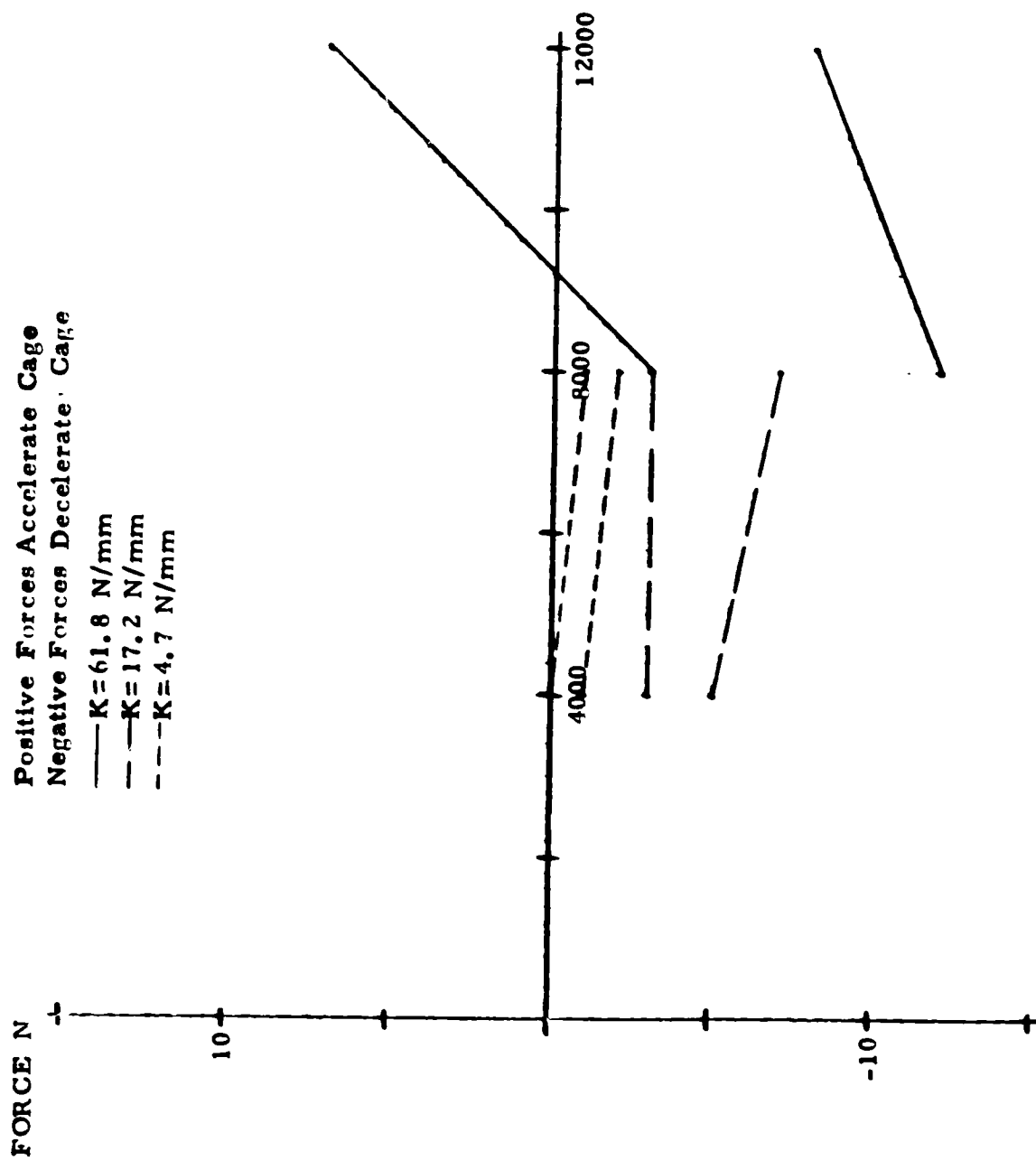


FIGURE 11c Cage Force Magnitude Range Versus Shaft Speed, 13330 N Thrust Load

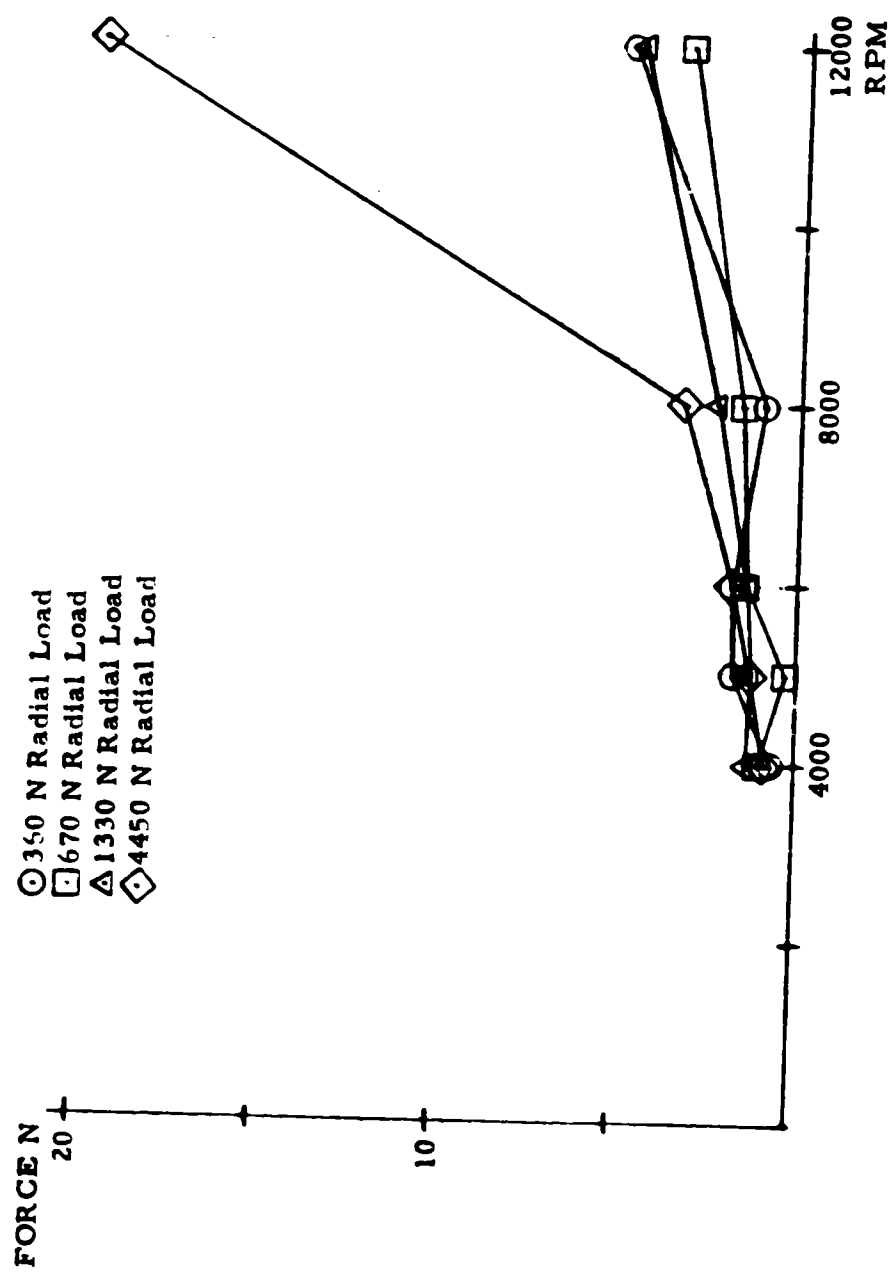


FIGURE 12a Resultant Cage Force Versus Shaft Speed

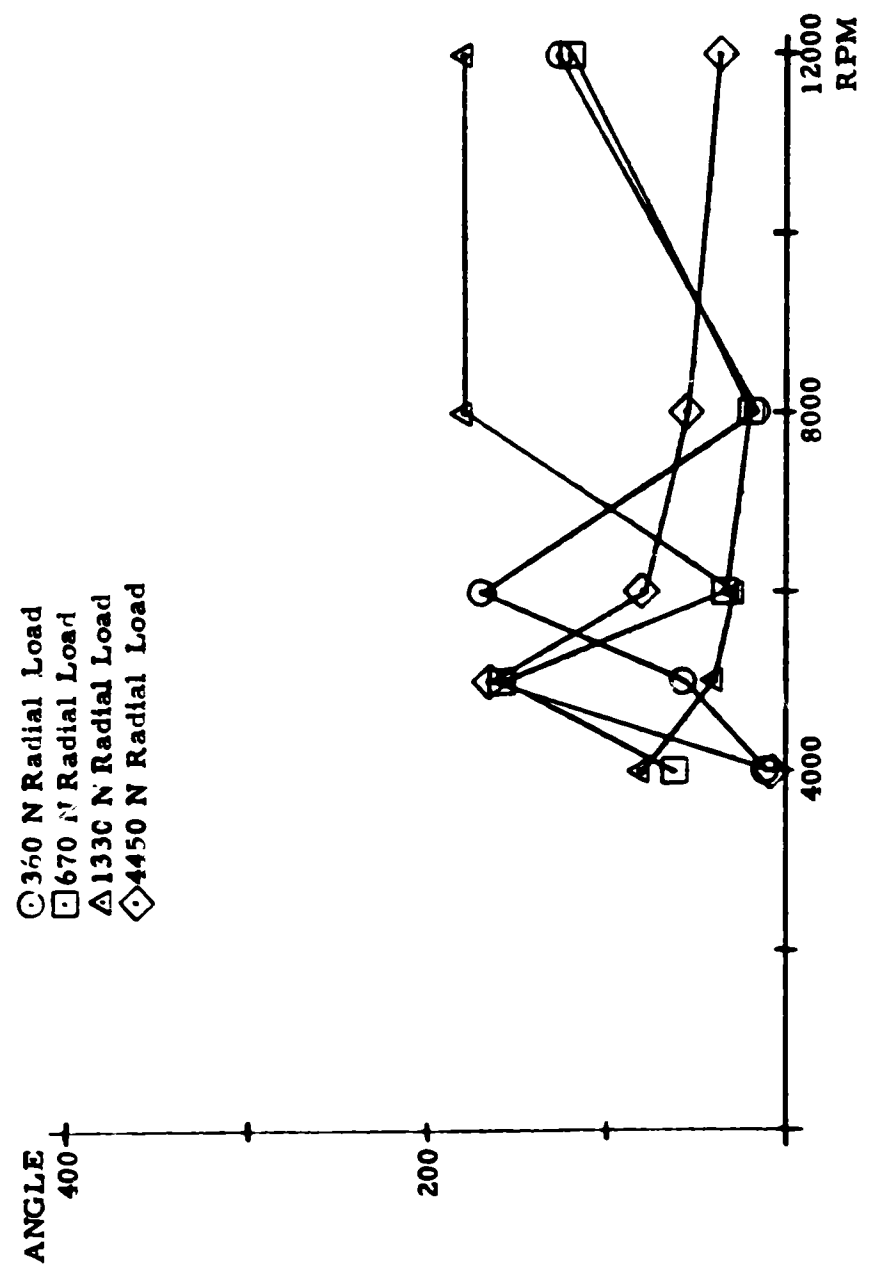


FIGURE 12b Resultant Cage Force Location Versus Shaft Speed

70000116 IN NY 06/17/77

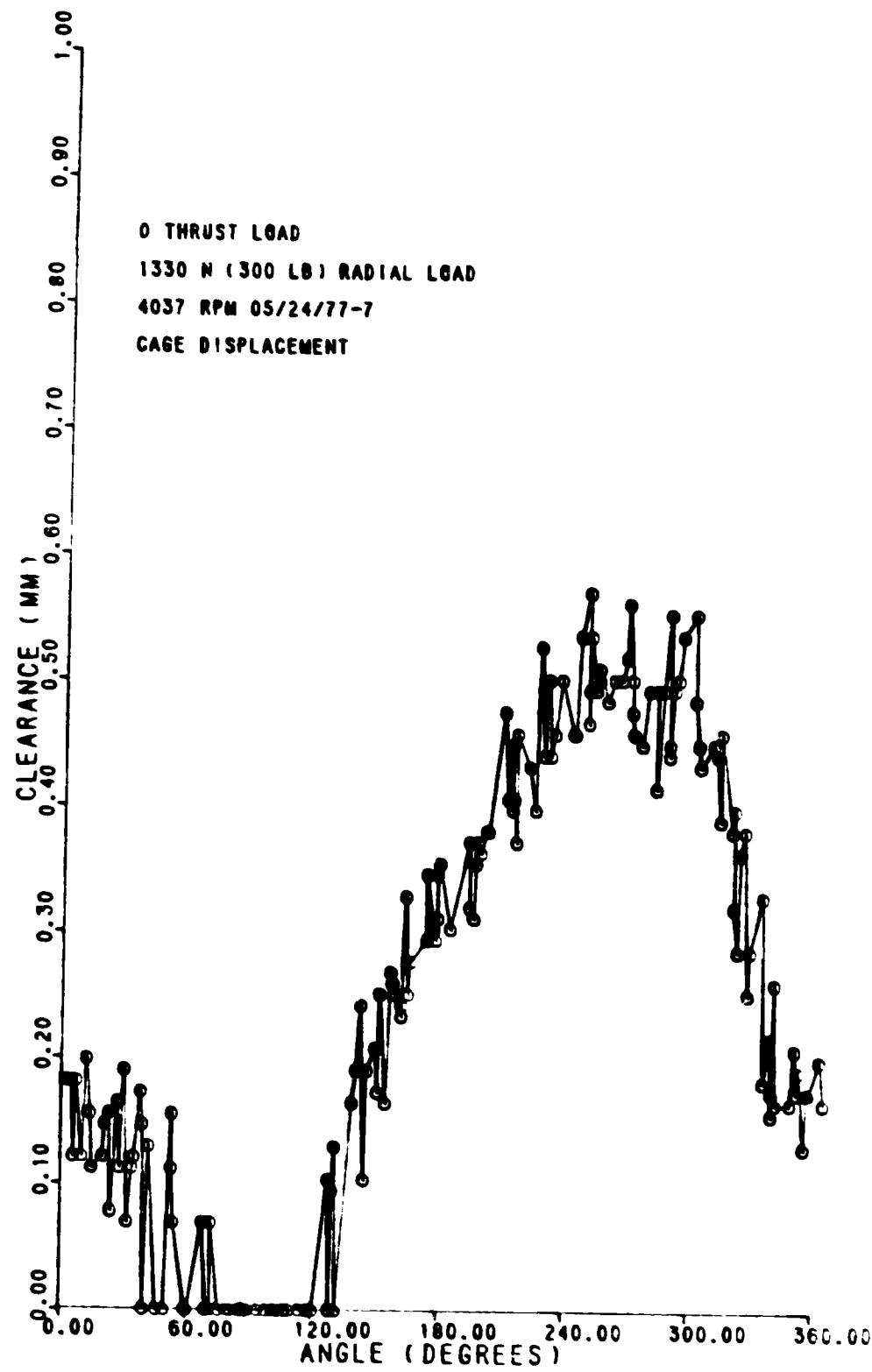


FIG. 13a

7000 TITANIC PLANT 06/09/77

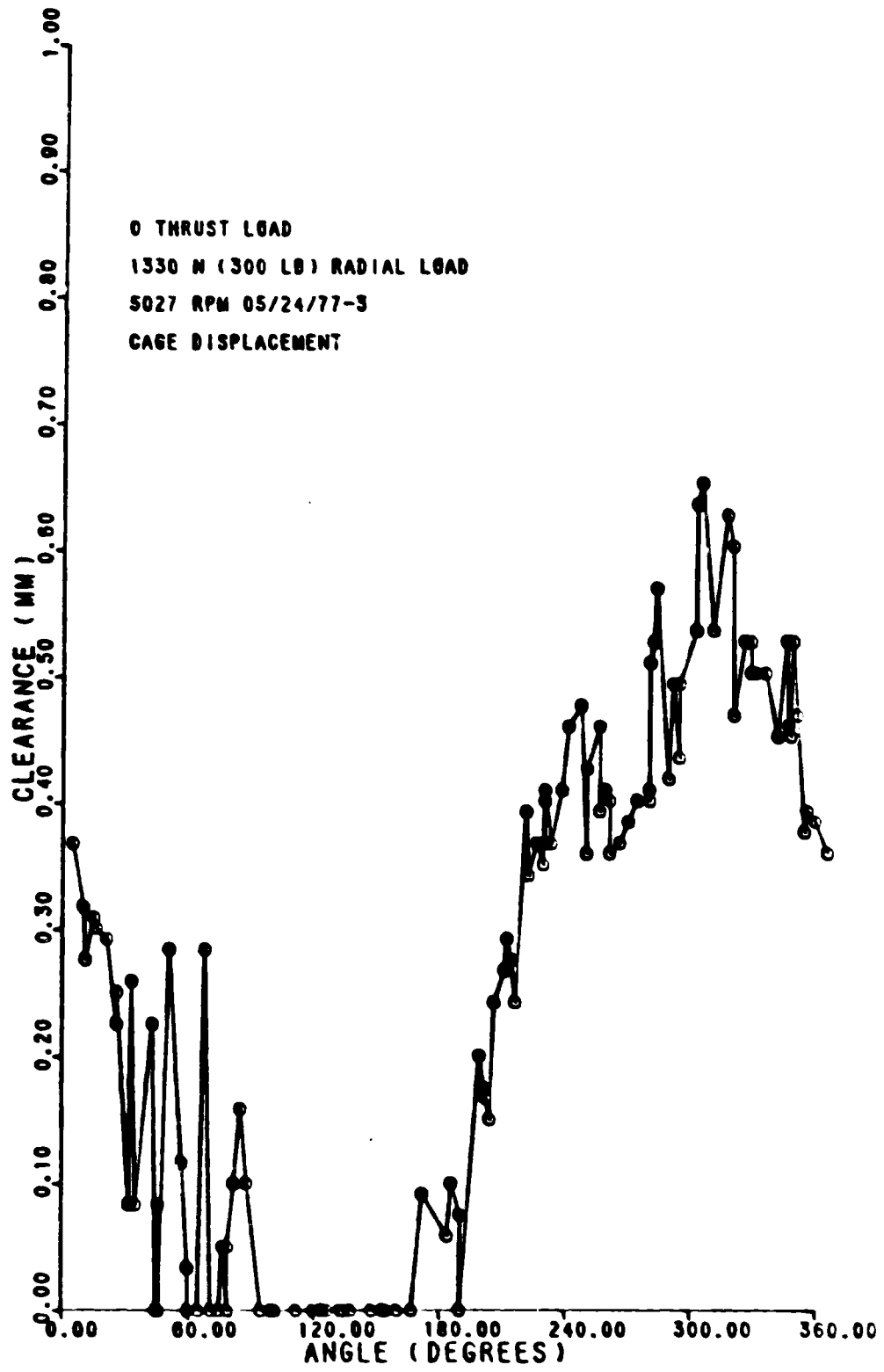
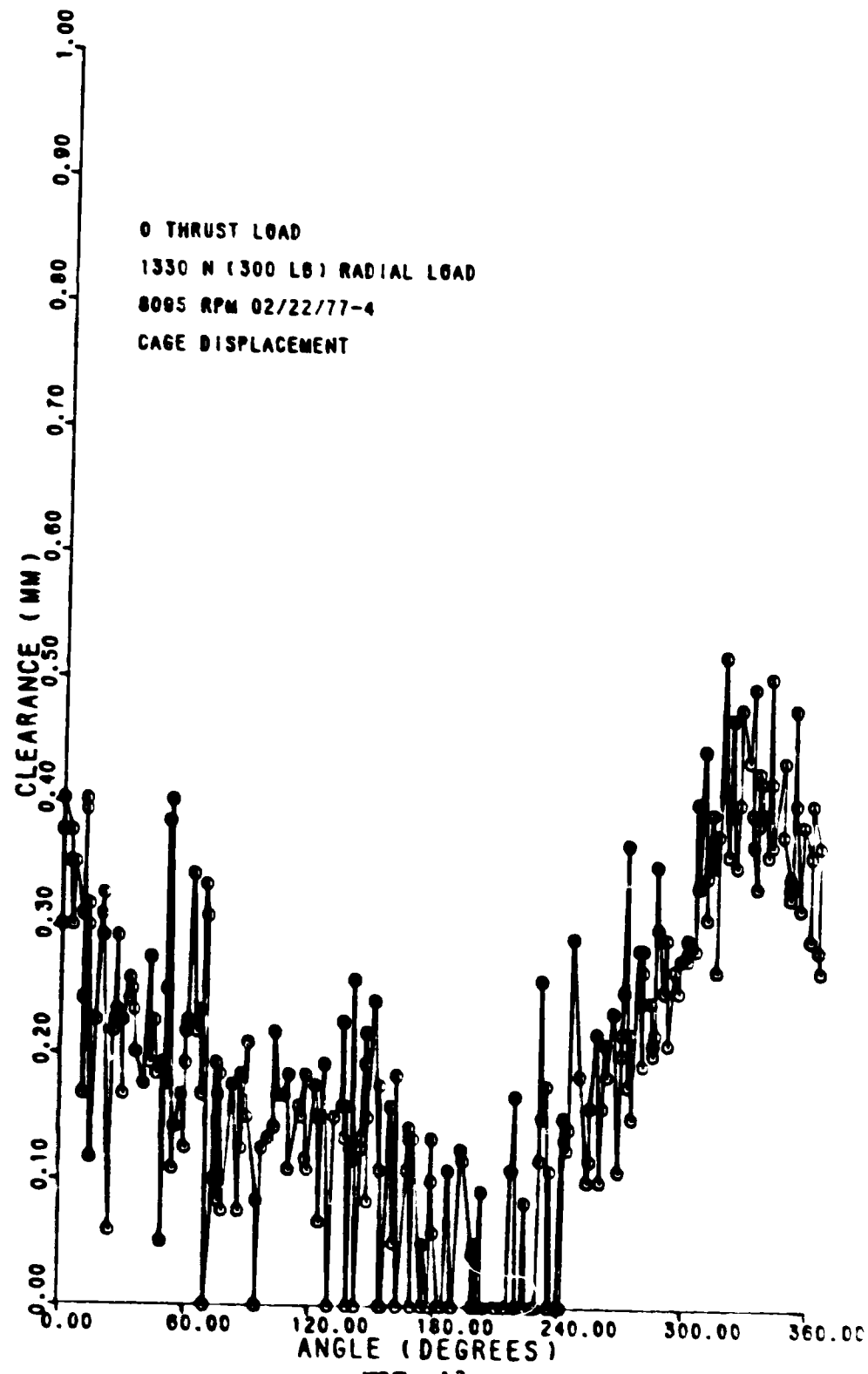


FIG. 13b

700 TEST CYCLES

06/09/77



70000 UFGNTYPTANJ - - 06/09/77

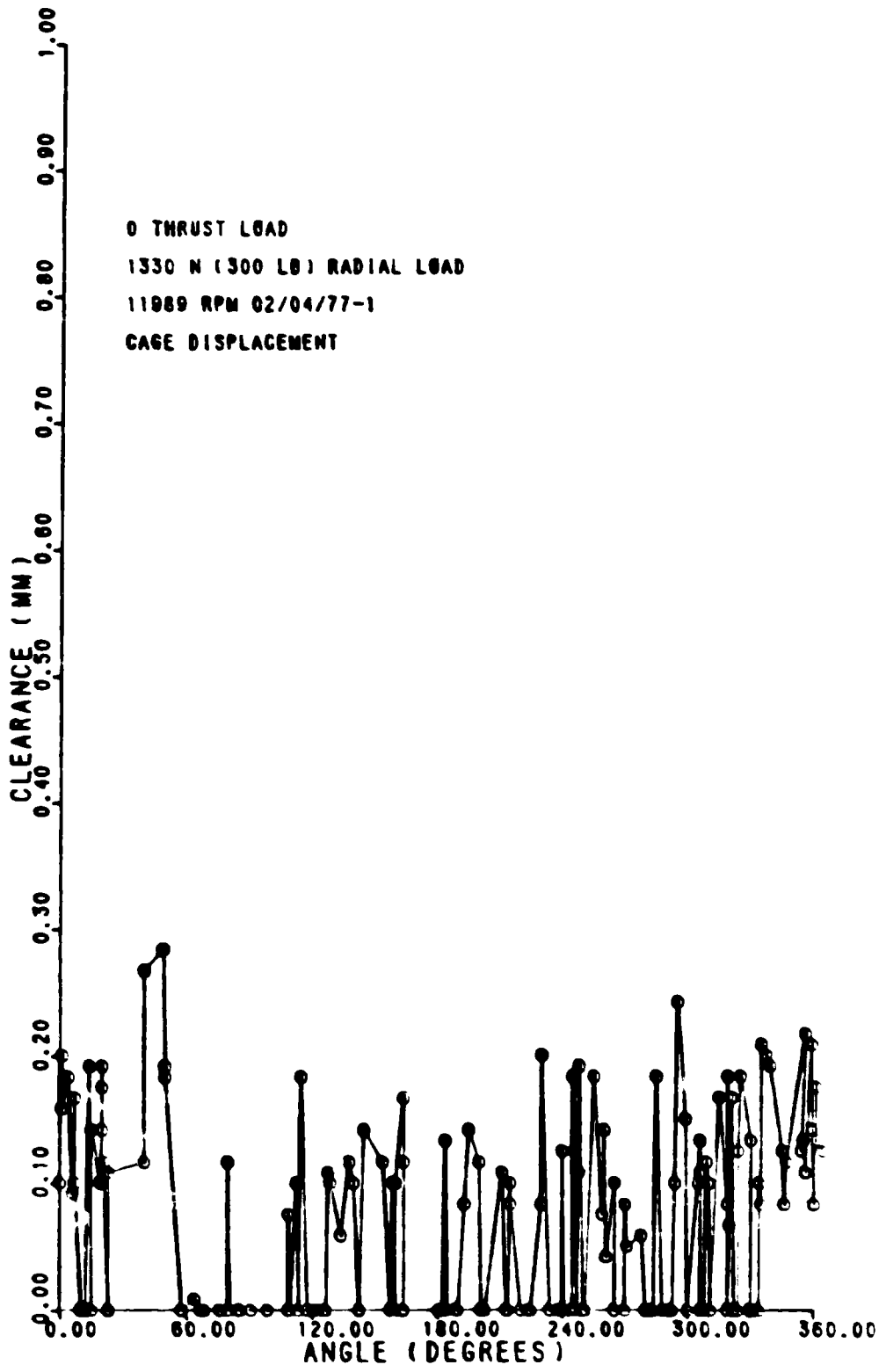


FIG. 13d

7000119NYPAN106/09/77

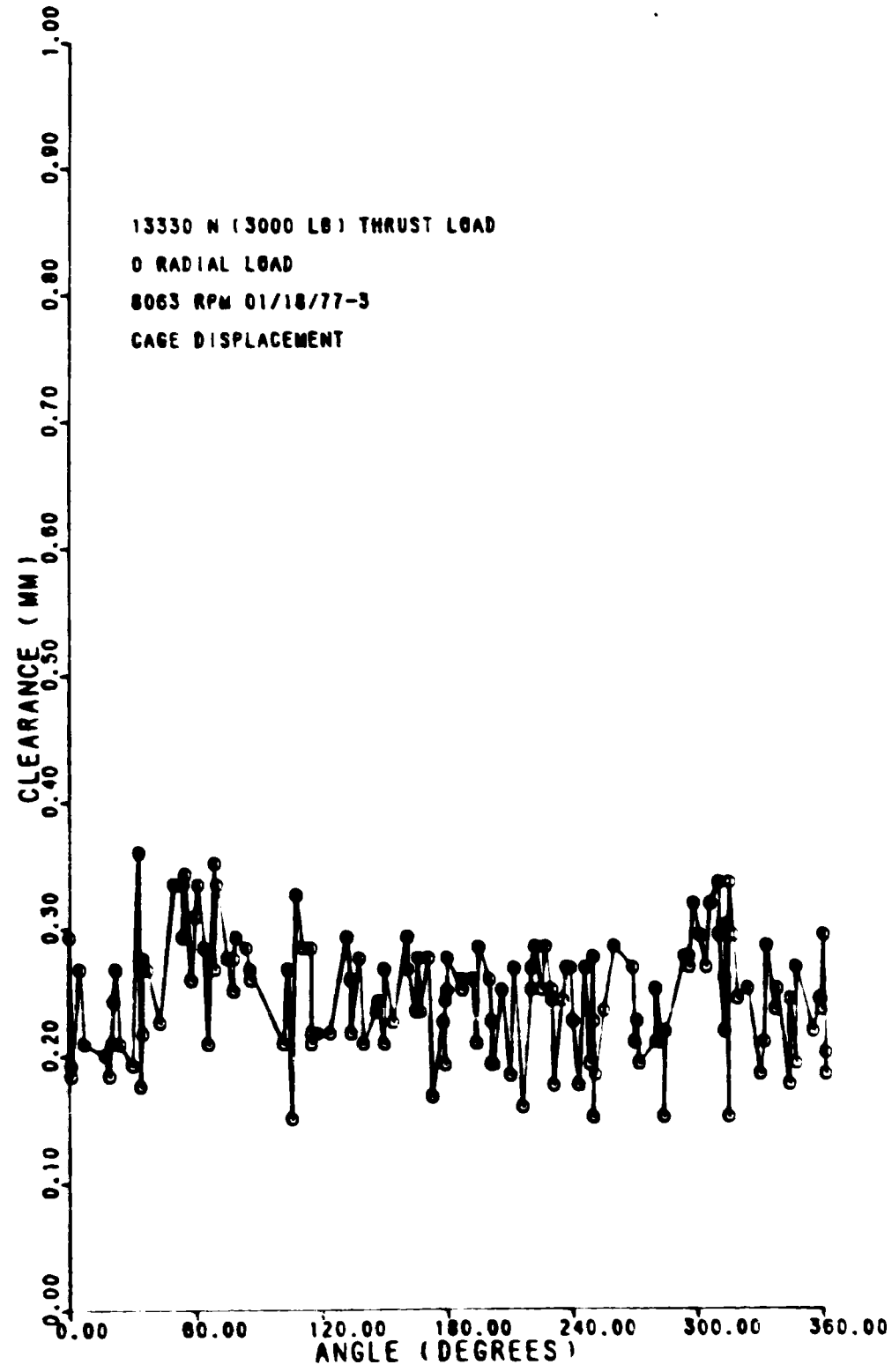


FIG. 13e

Y0030TUGNYPANT

06/30/77

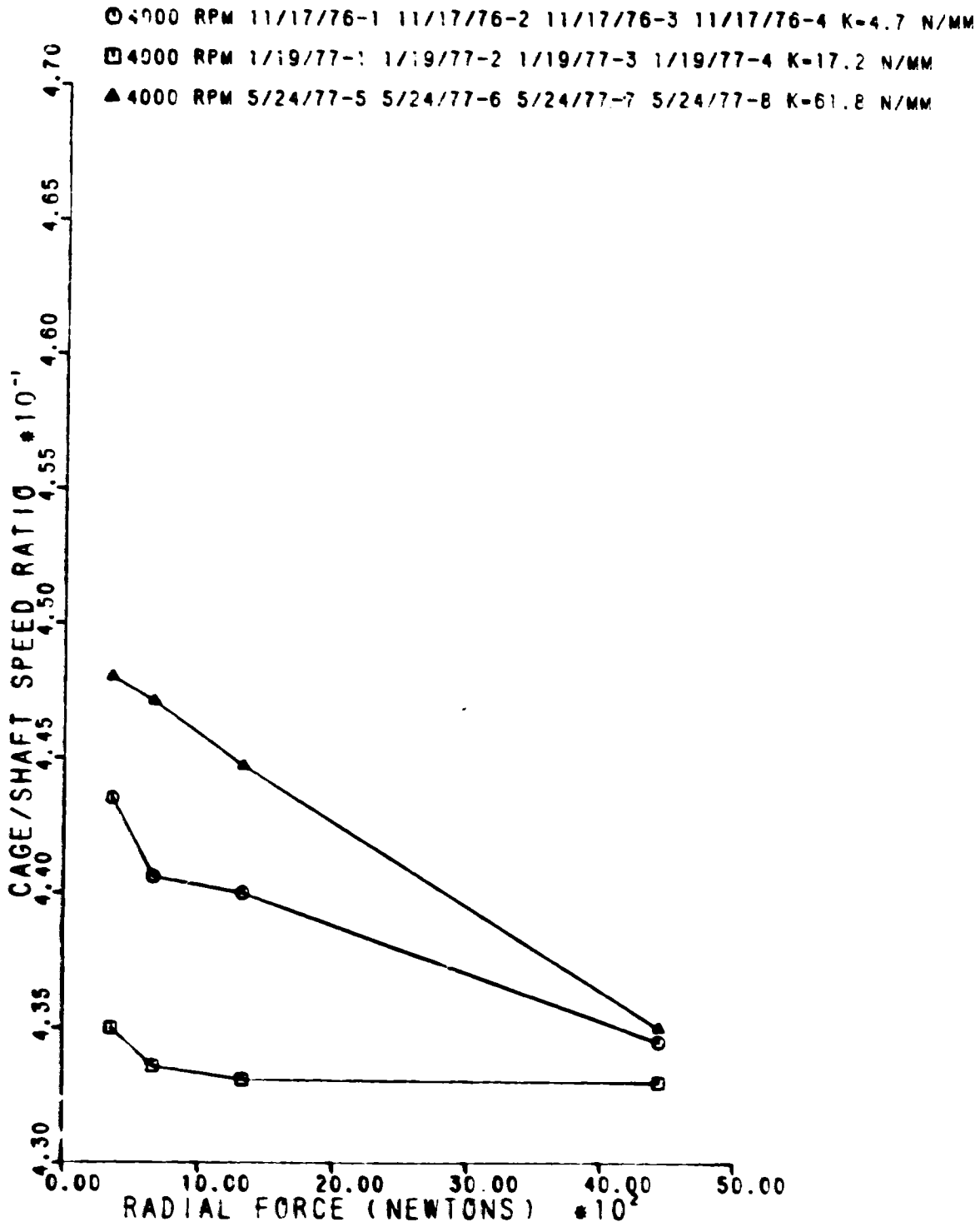


FIG. 14a

7/00/77 06/30/77

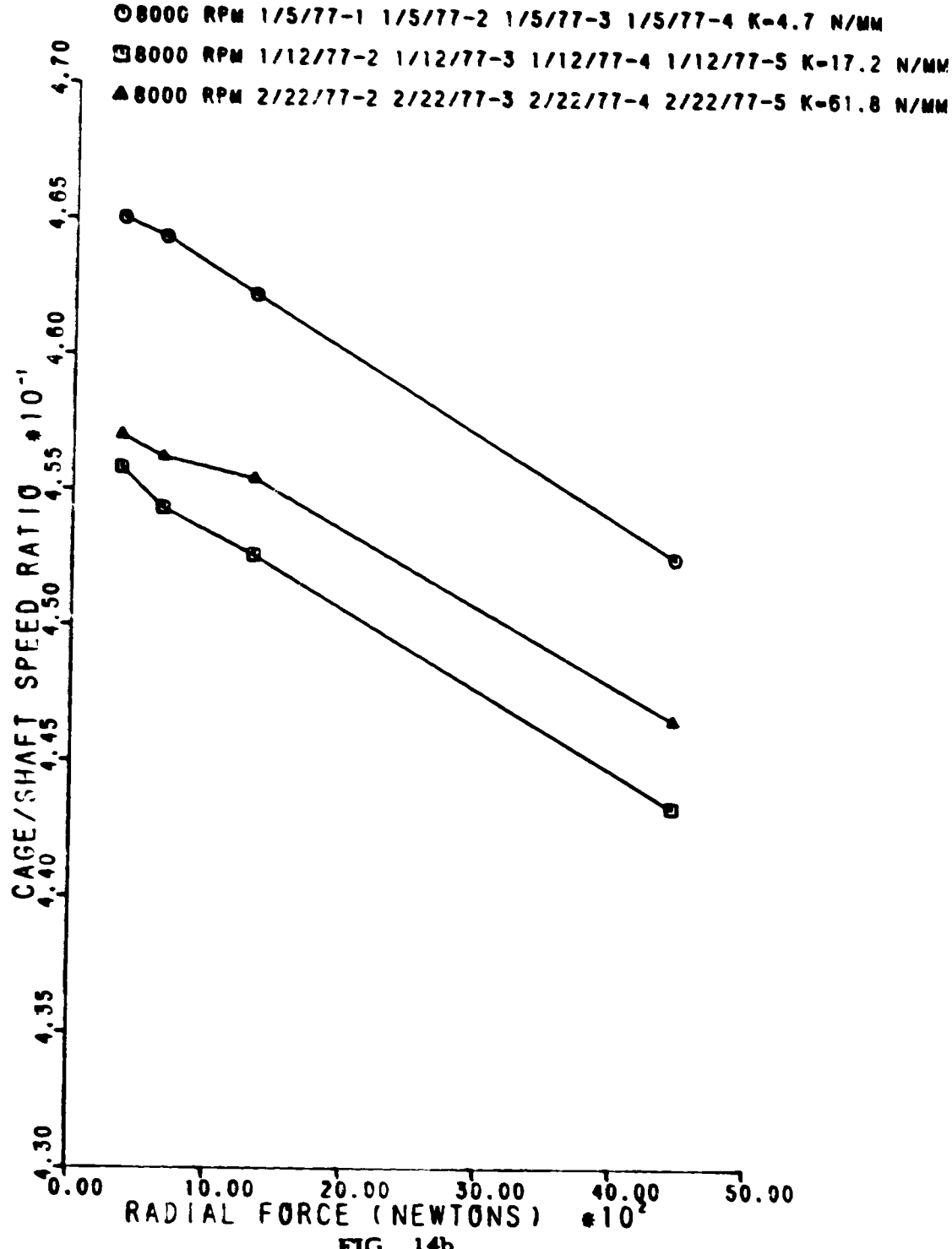


FIG. 14b

7-C-0-9-0-T-F-N-Y-F-A-N-H-3--07/06/77

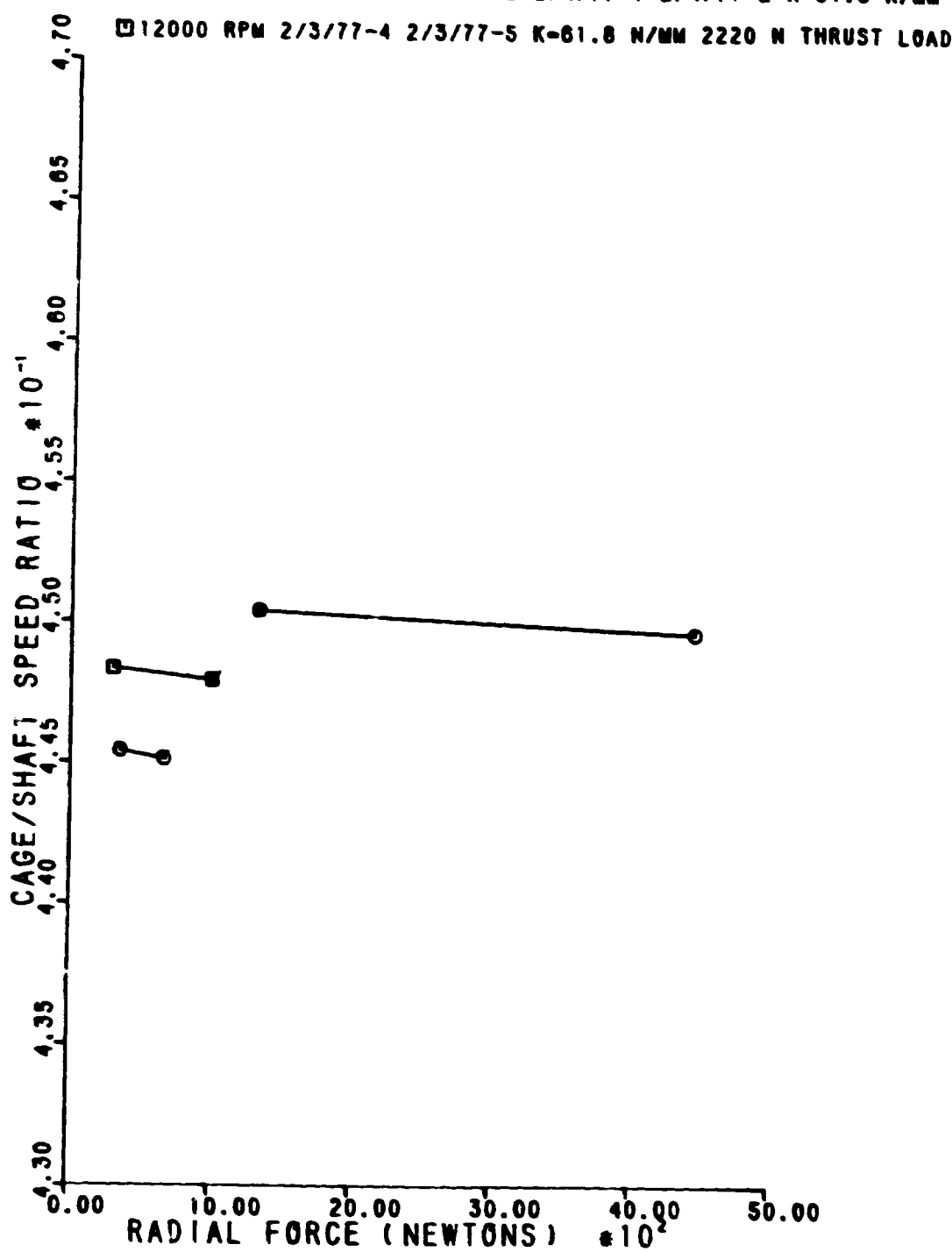
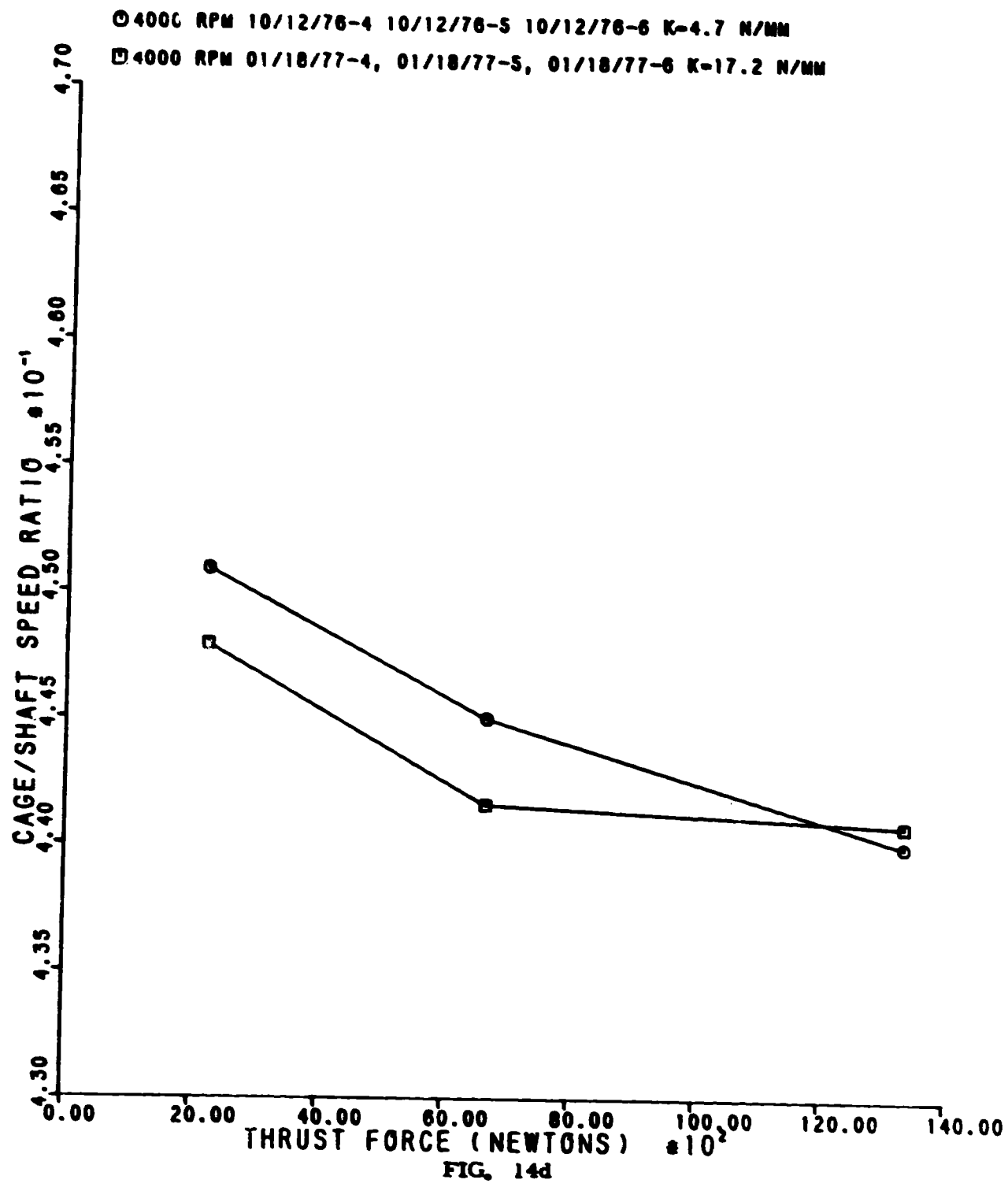


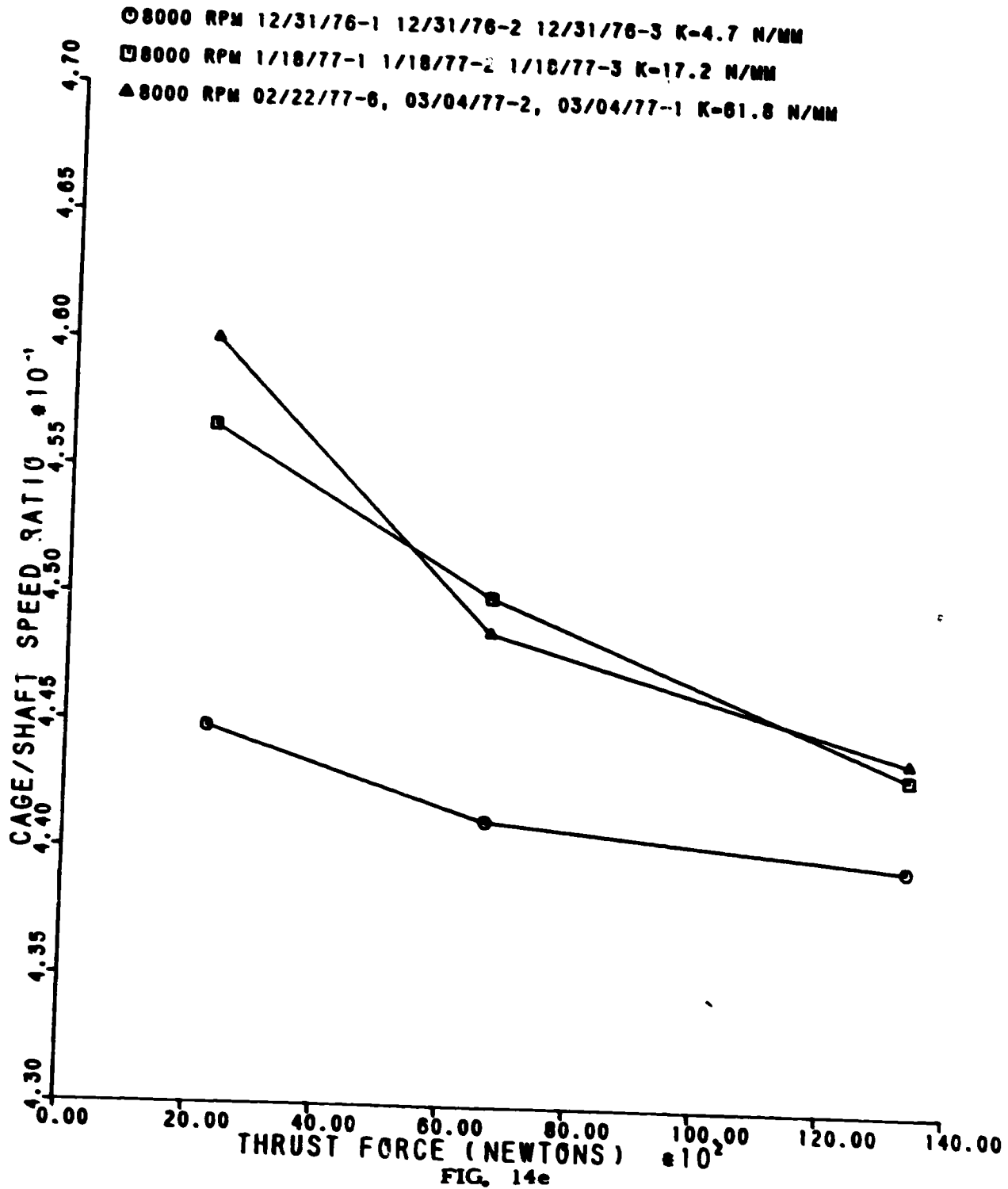
FIG. 14c

07/06/77



7-07-07 1977 PAN

07/06/77



THURST POINT TESTS
07/06/77

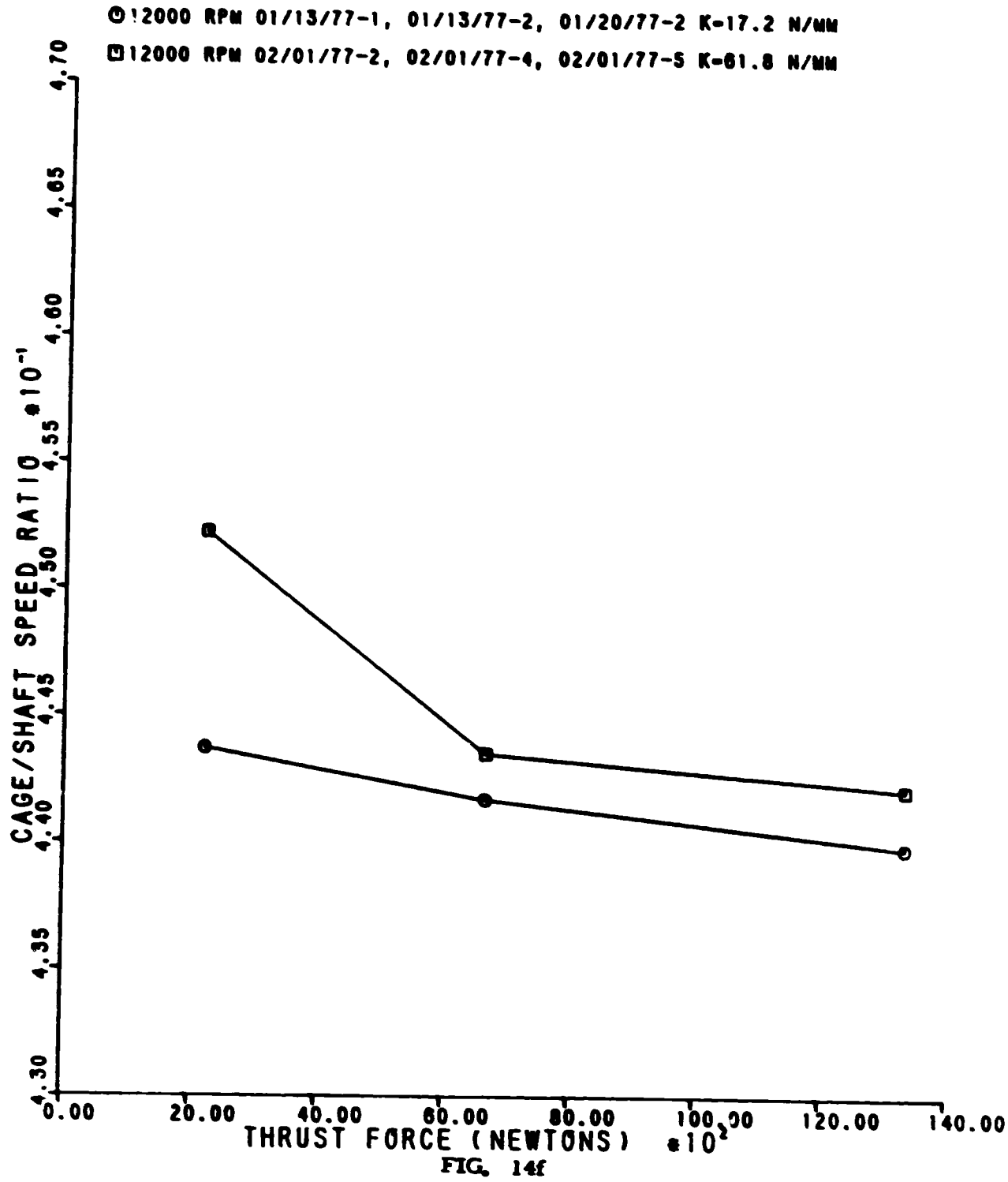


Table 1
Test Bearing Specifications

	<u>P/N 506110</u>	<u>P/N 506111</u>
Raceway Curvatures	52% Inner and Outer	52% Inner and Outer
Bearing Contact Angle	24° - 27° **	24° - 27° **
Bearing Mat'l, Races, Balls	CEVM-M-50-(R _c 60 min)	CEVM-M-50 (R _c 60 min)
Cage Mat'l	AMS-6415 (R _c 28-33)	AMS-6415 (R _c 28-33)
Cage Plating	Silver Plate Per AMS 2412	Silver Plate Per AMS 2412
Cage Plating Thickness, inches	.001-.002	.001-.002
Ball & Ring Stabilization Temp.	600°F	600°F
Balls		
Number	20	20
Nominal Dia., inches	0.750	0.750
Allowable Variation in Any Indiv. Ball Dia. & Sphericity, inches	0.000020 max.	0.000020 max.
Internal Radial Clearance*	.0048-.0060***	.0054-.0060 ***
Axial Play inches	.026 max.****	.024 max ****
Diametral Cage Clearance, in.	.016-.026	.019-.025
Bearing Inner Dia., inches	4.33070-4.33045	4.33070-4.33045
Bearing Outer Dia., inches	6.8898-6.8894	6.8898-6.8894
Inner Race Land Dia., inches	5.343 min.	5.334 min.
Outer Race Shoulder Dia., inches	6.077 max.	6.090 max.
Ball Pitch Dia., in.	5.650	5.635
Bearing Width	1.1811-1.1761	1.1811-1.1761

*Same as Total Diametral Clearance

**Measured Under 60 lb Thrust Load

***Measured Under 33 lb Radial Load

****Measured Under 22 lb Thrust Load

Table 2
SPEED, LOAD, AND SPRING CONSTANTS

Figure 6 4000 RPM Nominal Shaft Speed			Figure 7 8000 RPM Nominal Shaft Speed			Figure 8 12000 RPM Nominal Shaft Speed		
Spring Constant	Load	N/mm	Spring Constant	Load	N/mm	Spring Constant	Load	N/mm
6a	4.73	360	80 Radial	7a	4.73	360	80 Radial	-
6a	17.2	360	80 Radial	7a	17.2	360	80 Radial	-
6a	61.8	360	80 Radial	7a	61.8	360	80 Radial	6a
6d	4.73	667	150 Radial	7b	4.73	667	150 Radial	-
6d	17.2	667	150 Radial	7b	17.2	667	150 Radial	-
6b	61.8	667	150 Radial	7b	61.8	667	150 Radial	6b
6e	4.73	1330	300 Radial	7c	4.73	1330	300 Radial	-
6e	17.2	1330	300 Radial	7c	17.2	1330	300 Radial	-
6c	61.8	1330	300 Radial	7c	61.8	1330	300 Radial	6c
6d	4.73	4450	1000 Radial	7d	4.73	4450	1000 Radial	6c
6d	17.2	4450	1000 Radial	7d	17.2	4450	1000 Radial	6c
6d	61.8	4450	1000 Radial	7d	61.8	4450	1000 Radial	6d
6e	4.73	2220	500 Thrust	7e	4.73	2220	500 Thrust	6d
6e	17.2	2220	500 Thrust	7e	17.2	2220	500 Thrust	6d
-	-	-	-	7e	61.8	2220	500 Thrust	-
6f	4.73	6670	1500 Thrust	7f	4.73	6670	1500 Thrust	6e
6f	17.2	6670	1500 Thrust	7f	17.2	6670	1500 Thrust	-
-	-	-	-	7f	61.8	6670	1500 Thrust	-
6g	4.73	13350	3000 Thrust	7g	4.73	13350	3000 Thrust	6f
6g	17.2	13350	3000 Thrust	7g	17.2	13350	3000 Thrust	-
-	-	-	-	7g	61.8	13350	3000 Thrust	6g

Table 3
SPRING CONSTANTS AND BEARINGS USED

<u>Date Installed in Machine</u>		<u>Spring Constant</u> <u>N/mm</u>	<u>Lb/in</u>	<u>Bearing</u>
June	1976	1.49	8.51	PWA 506110
	August 18, 1976	4.73	27.0	PWA 506111
	Jan. 12, 1977	17.2	98.2	PWA 506110
	Jan. 28, 1977	61.8	353.0	PWA 506110

Table 4

CALCULATED NUMBER OF SHAFT REVOLUTIONS BETWEEN PHOTOGRAPHS

$\Delta\theta_0$ rev	$W_s = (\Delta\theta_0) \frac{16 \times 60}{.441}$	$\Delta\theta_s$ rev	$W_s = (\Delta\theta_s) \frac{16 \times 60}{(-.559)}$
0 to 1	0 to 2,177 rpm	0 to -1	0 to 1,717 rpm
1 to 2	2,177 to 4,354	-1 to -2	1,717 to 3,435
2 to 3	4,354 to 6,531	-2 to -3	3,435 to 5,152
3 to 4	6,531 to 8,707	-3 to -4	5,152 to 6,869
4 to 5	8,707 to 10,884	-5 to -6	6,869 to 8,587
5 to 6	10,884 to 13,061	-6 to -7	8,587 to 10,304
		-7 to -8	10,304 to 12,021

*For a cage to shaft speed ratio of 0.441

Appendix I

```

0001      DIMENSION R(300,6),ANGLE(300),FORCE(300),ANGL(300)
0002      DIMENSION LINE1(8),LINE2(8),LINE3(6),LINE4(8)
0003      DIMENSION LINES(4),FRM(360)
0004      DIMENSION XLB(20),YLB(20)
0005      INTEGER R,ANGLE
0006      ICN=0
0007      IC=0
0008      READ(5,30) S,AK,A
0009      30  FCRPAT(2F10.0,I2)
0010      WRITE(6,31) S,AK
0011      31  FCRMAT(1H1,8HNCTCH = ,F6.0,7H AK = ,F6.4)
0012      WRITE(6,24)
0013      23  FORMAT(5X,110HZR1,ZR2,ZR3,ZR4,ZR2-ZR1,ZR3)
0014      1ZR1 ZR4-ZR1 ZR3-ZR2 ZR4-ZR3 ZR4-ZR2
0015      ZUR1=0.
0016      ZUR2=0.
0017      ZUR3=0.
0018      ZUR4=0.
0019      ZU1=0.
0020      ZU2=0.
0021      ZU3=0.
0022      ZU4=0.
0023      ZU5=0.
0024      ZL6=0.
0025      CO 21 I=1,N
0026      READ(5,11)IZR1,IZR2,IZR3,IZR4
0027      11  FCRMAT(2X,I4,6X,I4,6X,I4,6X,I4)
0028      ZR1=IZR1
0029      ZR2=IZR2
0030      ZR3=IZR3
0031      ZR4=IZR4
0032      Z1=ZR2-ZR1
0033      Z2=ZR3-ZR1
0034      Z3=ZR4-ZR1
0035      Z4=ZR3-ZR2
0036      Z5=ZR4-ZR3
0037      Z6=ZR4-ZR2
0038      WRITE(6,24)ZR1,ZR2,ZR3,ZR4,Z1,Z2,Z3,Z4,Z5,Z6
0039      24  FORMAT(11F10.6)
0040      ZUR1=ZUR1/FLOAT(N)
0041      ZUR2=ZUR2/FLOAT(N)
0042      ZUR3=ZUR3/FLOAT(N)
0043      ZUR4=ZUR4/FLOAT(N)
0044      ZU1=ZU1/FLOAT(N)
0045      ZU2=ZU2/Z2
0046      ZU3=ZU3/Z3
0047      ZU4=ZU4/Z4
0048      ZU5=ZU5/Z5
0049      ZU6=ZU6/Z6
0050      21  CONTINUE
0051      AZR1=ZUR1/FLOAT(N)
0052      AZR2=ZUR2/FLOAT(N)
0053      AZR3=ZUR3/FLOAT(N)
0054      AZR4=ZUR4/FLOAT(N)
0055      AZ1=ZU1/FLOAT(N)
0056      AZ2=ZU2/FLOAT(N)
0057      AZ3=ZU3/FLOAT(N)
0058      AZ4=ZU4/FLOAT(N)
0059      AZ5=ZU5/FLOAT(N)
0060      AZ6=ZU6/FLOAT(N)
0061      F1=S/AZ3
0062      SCZ1=AZ1*F1
0063      SCZ2=AZ2*F1
0064      SCZ3=AZ3*F1
0065      SCZ4=AZ4*F1
0066      SCZ5=AZ5*F1
0067      SCZ6=AZ6*F1
0068      WRITE(6,25)AZR1,AZR2,AZR3,AZR4,AZ1,AZ2,AZ3,AZ4,AZ5,AZ6
0069      25  FCRPAT(1H0,11F10.3)
0070      WRITE(6,32)F1,AZ3
0071      32  FCRMAT(1H0,8HFACTCR = ,F10.4,5X,8HNCTCH = ,F6.0)
0072      WRITE(6,25)SGZ1,SGZ2,SGZ3,SGZ4,SGZ5,SGZ6
0073      READ(5,33)LINE3,LINE1,LINES
0074      33  FCRMAT(6A4,6A4,6A4)
0075      READ(5,34)LINE2,LINE4
0076      34  FCRMAT(6A4,6A4)

```

REPRODUCIBILITY OF THE
ORIGINAL PAGE IS POOR

I FORTRAN(2.3)/MASTER INTEGER WORD SIZE = 1 , * OPTION IS OFF , C OPTION IS

```

N 0377      WRITE(6,33) LINE3,LINE1
N 0378      WRITE(6,34) LINE2,LINE4
N 0379      WRITE(6,35) LINE5
L 0380      WRITE(6,26)
L 0381      26 FCRPAT(1H0," R1   R2   R3   R4   R2-R1   R3-R1   R4-
N 0382          1R1  R3-R2  R4-R3  R4-R2  ANGLE D3-Z3  04-24")*
N 0383          SU03=0.
N 0384          SU04=0.
L 0385      1001 IC=IC+1
N 0386      READ(5,18)R(IC,1),R(IC,2),R(IC,3),R(IC,4),ANGLE(IC)
N 0387      18 FORMAT(1X,I4,6X,I4,6X,I4,6X,I4,6X,I3)
N 0388      IF4IFEOF461,EO,-1,CO TO 50
L 0389      ANGL(IC)=ANGLE(IC)
L 0390      C1=R(IC,2)-R(IC,1)
N 0391      C2=R(IC,3)-R(IC,1)
N 0392      C3=R(IC,4)-R(IC,1)
N 0393      C4=R(IC,3)-R(IC,2)
L 0394      C5=R(IC,4)-R(IC,3)
N 0395      C6=F(IC,4)-R(IC,2)
N 0396      C7=D3-A23
N 0397      D8=D4-A24
L 0398      ELD03=SU03+D3
L 0399      EUD04=SU04+D4
P 6100      GO TO 1001
N 0101      50 CONTINUE
C 6102      IO=IC-1
L 6103      AC3=SU03/FLOAT(IC)
A 6104      AD4=SU04/FLOAT(IC)
C 6105      F2=S/AD3
N 6106      WRITE(6,35)F2,AD3,AD4
L 6107      35 FORMAT(1H0,SHFACTCR = ,F10.4,5X,EMNOTCH = ,F6.0,5X,6MPIN = ,F6.0)
L 6108      WRITE(6,26)
N 6109      20 FCRPAT(1H," SCD1  SCD2  SCD3  SCD4  SCD5  SCD6  DI1  DI2
1  D13  D14  AVER  SOEV  POLNCS  NEWTON  ANGLE D3-AE3  [6-864])
C 6110      I=0
C 6111      XFORLB=0.
C 6112      YFORLB=0.
C 6113      ICOUNT=0
C 6114      SECTOR=18.
C 6115      CG 51 IC=1,IO
L 6116      G1=R(IC,2)-R(IC,1)
C 6117      G2=R(IC,3)-R(IC,1)
C 6118      G3=R(IC,4)-R(IC,1)
C 6119      G4=R(IC,3)-R(IC,2)
L 6120      G5=R(IC,4)-R(IC,3)
L 6121      G6=R(IC,6)-R(IC,2)
C 6122      G7=D3-AD3
C 6123      C8=D4-AD4
L 6124      SCD1=D1*F2
L 6125      SCD2=D2*F2
L 6126      SCD3=D3*F2
L 6127      SCD4=D4*F2
L 6128      SCD5=D5*F2
L 6129      SCD6=D6*F2
L 6130      C1      =(SCD1-SCD2)
C 6131      C2      =(SCD2-SCD3)
L 6132      C3      =(SCD5-SCD6)
L 6133      C4      =(SCD6-SCD1)
L 6134      AD=(D11+D12+D13+D14)/4.
L 6135      SOEV=SQRT((D11-AC1)*(D11-AD)+(D12-AD)*(D12-AD)+(D13-AD)*(D13-AD)+)
L 6136      (D14-AD)*(D14-AD))/3.
L 6137      IC14-AC1)*(D14-AC1)/3.)
L 6138      FORCE(IC)=AD*AF*4.448
L 6139      FCRLB=AD*AK
L 6140      ANGLER=ANGLE(IC)
L 6141      IF (ANGLER.LE.SECTOR) GO TO 100
I=I+1
L 6142      XLB(I)=XFCRLB/FLOAT(ICOUNT)
L 6143      YLB(I)=YFCRLB/FLOAT(ICOUNT)
L 6144      SECTOR=SECTOR+18.
L 6145      XFORLB=0.
L 6146      YFORLB=0.
L 6147      ICOUNT=0
L 6148      100 RANGLE=ANGLE(IC)*.017453
L 6149      XFORLE=(FCRLB*CCS(RANGLE))+XFCRLB
L 6150      YFORLE=(FCRLB*SIN(RANGLE))+YFCRLB
L 6151      ICOUNT=ICOUNT+1
L 6152

```

```

LN 0153      WRITE(6,22) SCD1,SCD2,SCD3,SCD4,SCD5,SCD6,C11,D12,C13,C14,A0,SDEV,
LN 0154      1FCRL8, FORCE(IC), ANGL(IC), DF7.0, E9
LN 0155      22 FORMAT(1H ,6F7.2,6F6.2,2F7.2,F5.0,2F8.0)
LN 0156      51 CONTINUE
LN 0157      WRITE(6,33) LINE3,LINE1
LN 0158      WRITE(6,34) LINE2,LINE4
LN 0159      WRITE(6,33) LINE5
LN 0160      TOTALX=0.
LN 0161      TOTALY=0.
LN 0162      SECTOR=0.
LN 0163      WRITE(6,101)
LN 0164      101 FORMAT(1H0,'SECTCR * FERGES * FCRCES')
LN 0165      CO 1G2 I=1,20
LN 0166      SECTOR=SECTOR+16.
LN 0167      WRITE(6,103) SECTCR,XLB(I),YLB(I)
LN 0168      103 FORMAT(1H0,F5.0,3X,F7.2,2X,F7.2)
LN 0169      TOTALX=TOTALX+XLB(I)
LN 0170      TOTALY=TOTALY+YLB(I)
LN 0171      102 CONTINUE
LN 0172      THETA=CATAN(TOTALX/TOTALY)+57.297
LN 0173      FCRCE1=SQRT((TOTALX**2+TOTALY**2))
LN 0174      WRITE(6,104) THETA,FCRCE1
LN 0175      104 FORMAT(1H0,'ANGLE=',F5.0,3X,'FCRCE=',F7.2)
LN 0176      CALL PLCT
LN 0177      CALL FLOT(1.5,5.5,-3)
LN 0178      CALL FACTCP(.9)
LN 0179      ANGL(IC)=0.
LN 0180      ANGL(IC+1)=60.
LN 0181      CALL AXIS(0.,0.,15) HANGLE (DEGREES),-15.0E..0..0.,E0. )
LN 0182      FORCE(IC)=0.
LN 0183      FORCE(IC+1)=5.
LN 0184      CALL AXIS(0.,-5.,15) HFORCE (NEWTONS),-15.13.03.66.-25..5.1
LN 0185      CALL SYMBCL(-.6,-4.57,-10,1.05H-5.08 -4.00 -3.00 -2.00
LN 0186      1-1.68 0.00 1.08 2.00 3.08 4.00 5.00
LN 0187      2 .90..1051
LN 0188      CALL SYMBCL(-.75,-1.06,-14,15) HFORCE (POUNCS),-90..151
LN 0189      CALL SYMBCL(0.3,4.5,0.1 ,LINE1,0.0,32)
LN 0190      CALL SYMBCL(0.3,4.2,0.1 ,LINE2,0.0,32)
LN 0191      CALL SYMBCL(0.3,3.9,0.1 ,LINE3,0.0,24)
LN 0192      CALL SYMBCL(0.3,3.6,0.1 ,LINE4,0.0,32)
LN 0193      CALL SYMBCL(0.3,3.3,0.1 ,LINE5,0.0,16)
LN 0194      CALL PLOT(-.5,-4.45,3)
LN 0195      CALL PLOT(-.5,4.45,3)
LN 0196      CALL PLOT(-.5,-4.45,3)
LN 0197      CALL PLOT(-.5,-4.45,2)
LN 0198      CALL PLCT(-.56,-3.56,3)
LN 0199      CALL FLOT(-.5,-3.56,2)
LN 0200      CALL FLOT(-.5,-2.56,3)
LN 0201      CALL PLOT(-.5,-2.67,2)
LN 0202      CALL PLOT(-.56,-1.78,3)
LN 0203      CALL FLOT(-.5,-1.78,2)
LN 0204      CALL FLOT(-.5,-0.89,3)
LN 0205      CALL FLCT(-.5,-0.89,2)
LN 0206      CALL FLCT(-.56,0.0,3)
LN 0207      CALL FLOT(-.5,0.0,2)
LN 0208      CALL FLCT(-.56,0.0,3)
LN 0209      CALL FLOT(-.5,0.0,2)
LN 0210      CALL PLOT(-.56,1.78,3)
LN 0211      CALL FLOT(-.5,1.78,2)
LN 0212      CALL FLOT(-.56,2.67,3)
LN 0213      CALL FLOT(-.5,2.67,2)
LN 0214      CALL FLOT(-.56,3.56,3)
LN 0215      CALL FLOT(-.5,3.56,2)
LN 0216      CALL FLOT(-.56,4.45,3)
LN 0217      CALL FLOT(-.5,4.45,2)
LN 0218      NFTS=IC-1
LN 0219      CALL LINE(ANGL,FCRCE,NFTS,1,1,2)
LN 0220      CALL FLOT(0.,0.,559)
LN 0221      END

```

RECORDED ON 11/11/74
ORIGINAL PAGE IS 105

USASI-FCA16A DIAGNOSTIC RESULTS FOR FTM.MAIN

NO ERRORS
ALIB,CALCCMF,ALX-LIBRARY

LEO

B/E

END

DATE

FILMED

OCT 12 1977